Ameloblastin Functions in Enamel, Periodontium and Long Bone

BY

XUANYU LU
B.D.S., Jilin University, Changchun, 2007.7
M.S., Jilin University, Changchun, 2009.7

THESIS

Submitted as partial fulfillment of the requirements
for the degree of Doctor of Philosophy in Oral Science
in the Graduate College of the
University of Illinois at Chicago, 2013

Chicago, Illinois

Defense Committee:

Dr. Xianghong Luan, Chair and Advisor, Department of Oral Biology
Dr. Thomas G.H. Diekwisch, Department of Oral Biology
Dr. Anne George, Department of Oral Biology
Dr. Anakarina B. Bedran-Russo, Department of Restorative Dentistry
Dr. Xiubei Liao, Department of Biochemistry and Molecular Genetics

I dedicate this to my little sister, Yuru Lu, who passed away when she was 12-years-old; she will stay forever in our hearts. And I also dedicate my work to my beloved parents, without their love and support I would not be where I am today.

ACKNOWLEDGMENTS

I would like to thank my mentors, Drs. Xianghong Luan and Thomas G.H. Diekwisch for their unconditional and generous support and encouragement. I am very grateful to Dr. Luan for her valuable and timely help and guidance during my 5 years' Ph.D. training. I express gratitude to Dr. Diekwisch and Dr. Yoshihiro Ito for their valuable insights for this project. I would also like to thank my thesis committee members, Drs. Anne George, Anakarina B. Bedran-Russo and Xiubei Liao for taking time to be on my thesis defense committee and for their advice and support. I thank MOST program directors Drs. Phillip T. Marucha, Luisa DiPietro, and program coordinator Katherine Long for their guidance and support during my Ph.D. training. Also I would like to thank all my lab members for their support and advice.

Last, but not least, I would like to express my gratitude to the entire faculty, staff and students in Department of Oral Biology and MOST program. All the helpful discussions in the seminars helped me improve my experimental design and techniques.

This research was support by NIDCR grant DE18057 and DE19155 to XL., DE13378 and DE18900 to T.G.H.D..

XL

TABLE OF CONTENTS

TABLE OF CONTENTS (continued)

TABLE OF CONTENTS (continued)

CHAPTER PAGE

LIST OF TABLES

LIST OF FIGURES

LIST OF FIGURES (continued)

FIGURE PAGE

LIST OF ABBREVATIONS

AI	Amelogenesis imperfecta
AKT	Protein Kinase B
ALP	Alkaline phosphatase
AMBN	Ameloblastin
AMELX	Amelogenin
AMTN	Amelotin
BMD	Bone mineral density
BMMCs	Bone marrow monocytes/macrophages
BMP	Bone morphogenetic protein
BMSCs	Bone marrow stromal cells
BSA	Bovine serum albumin
BV/TV	Bone volume/total volume
CATK	Cathepsin K
CD	Cluster of differentiation
CFU	Colony forming unit
CFU-ALP	CFU-alkaline phosphatase
CFU-F	CFU-fibroblasts
CFU-Ob	CFU-osteoblasts
Cg.Ar./Ps.Cl.Ar.%	Cartilage area/periosteal callus area
CH	Chondrogenesis
Col 1A1	Collagen 1 alpha 1
Cr.Th.	Cortical thickness
DGEA	Asp-Gly-Glu-Ala
DMP1	Dentin matrix protein 1
DSPP	Dentin sialophosphoprotein
ECM	Extracellular matrix
ELISA	Enzyme linked immunosorbent assay
EMD	Enamel matrix derivative
ENAM	Enamelin
ERK	Extracellular signal-regulated kinases
ERM	Epithelial rests of malassez
FGF	Fibroblast growth factor
FN	Fibronectin
GAPDH	Glyceraldehyde 3-phosphate dehydrogenase
GH	Growth hormone
GP	Growth plate
H&E	Hematoxylin and eosin stain
HERS	Hertwig's epithelial root sheath cells
HET	Heterozygous

LIST OF ABBREVATIONS (continued)

HOMO	Homozygous
IBSP	Integrin-binding sialoprotein
Ig	Immunoglobulin
IGF	Insulin like growth factor
IHH	Indian hedgehog
IL	Interleukin
K14	Keratin 14
MAR	Bone mineral apposition rate
M-CSF (CSF-1)	Macrophage Colony-Stimulating Factor
Md.Ar./Ps.Cl.Ar.%	Mineralized area/periosteal callus area
MEPE	Matrix extracellular phosphoglycoprotein
MMP	Matrix metalloproteinase
MSX	Human muscle segment homebox
MTT	3-(4,5-Dimethylthiazol-2-Yl)-2,5-Diphenyltetrazolium Bromide
No. Ob./bone area	Number of osteoblast/bone area
OC	Osteoclastogenesis
OCN	Osteocalcin
ODAM	Odontogenic, ameloblast associated
OG	Osteogenesis
OPN	Osteopontin
OSX	Osterix
p27	cyclin-dependent kinase inhibiter 1B
PBS	Phosphate buffered saline
PCR	Polymerase chain reaction
PDL	Periodontal ligament
PI3K	Phosphoinositide 3-kinase
PN	Postnatal
POC	Primary ossification center
PTH	Parathyroid Hormone
PVDF	polyvinylidenedifluoride
RANK	Receptor Activator of Nuclear Factor Kappa B
RANKL	Receptor Activator of Nuclear Factor Kappa B Ligand
RGD	Arg-Gly-Asp
Rho A	Ras homolog gene family, member A
RUNX2	Runt-related transcription factor 2
SCPP	Secretory calcium-binding phosphoprotein
SD	Standard deviation
SEM	Scanning electron microscopy
SIBLING	Small integrin-binding ligand, N-linked glycoproteins

LIST OF ABBREVATIONS (continued)

siRNA	Small interfering RNA
SOC	Secondary centers of ossification
SPARC	Secreted protein, acidic, cysteine-rich
SPARCL1	SPARC-like 1 protein
Tb. Nb.	Trabecular number
Tb. Sep.	Trabecular seperation
Tb. Th.	Trabecular thickness
TEM	Transmission electron microscopy
TG	Transgenic
TGFβ1	Transforming growth factor, beta 1
TRAP	Tartrate-resistant acid phosphatase
VCAM1	Vascular cell adhesion molecule 1
VN	Vitronectin
VTKG	Val-Thr-Lys-Gly
Wnt	Wingless-type MMTV integration site family
WT	Wild-type
α	alpha
β	beta
μ	Micro
μCT	Micro-computed tomographic

SUMMARY

Though first introduced as a protein of the developing enamel matrix, there is increasing evidence that the secretory calcium-binding phosphoprotein (SCPP) family member ameloblastin (AMBN), first known as an adhesion molecule, is localized in other tissues such as bone, where it plays significant roles associated with mineral metabolism. Here we expanded the knowledge of AMBN functions in the enamel, periodontium and long bone.

To study the effect of AMBN in enamel formation, we overexpressed AMBN using a keratin 14 (K14) promoter and removed amelogenin (AMELX) from the genetic background by crossbreeding with AMELX null (*amelx*$^{-/-}$) mice. Enamel coverings of *amelx*$^{-/-}$ mice and of the squamate *Iguana iguana* were used for comparison. Scanning electron microscopic analysis documented that AMBN transgenic (AMBN TG) × *amelx*$^{-/-}$ mouse molars were covered by a 5 μm thin 'enameloid' layer resembling the thin enamel of the *Iguana* squamate. Transmission electron microscopy revealed that the enamel of developing AMBN TG × *amelx*$^{-/-}$ mouse molars contained short (approximately 70 nm) and randomly oriented crystals, while WT controls, AMBN overexpressors, and *amelx*$^{-/-}$ null mice all featured elongated and parallel oriented crystals measuring between 300 and 600 nm in average length. These studies illustrate that AMBN promotes the growth of a crystalline enamel layer with short and randomly oriented crystals, but lacks the ability to facilitate the formation of long and parallel oriented apatite crystals.

To investigate AMBN function in the periodontium, we characterized the phenotype of the mandibular bone of AMBN overexpressor. Transgenic mice with 5-fold elevated AMBN levels in mandibles suffered from root cementum resorption and delamination. In an *in vitro* model of osteoclastogenesis, AMBN modulated osteoclast differentiation from bone marrow derived

monocytes (BMMCs), and dramatically increased osteoclast numbers and resorption pits. Furthermore, AMBN more than doubled BMMCs adhesion, accelerated cell spreading, and promoted podosome belt and actin ring formation. These effects were associated with elevated ERK1/2 and AKT phosphorylation as well as higher expression of osteoclast activation related genes. Blocking integrin α2β1 and ERK 1/2 pathways alleviated the effects of AMBN on osteoclast differentiation. Loading mechanic force on lower first molar to trigger orthodontic tooth movement, AMBN overexpressor displayed accelerated tooth movement with increased osteoclasts in PDL. These data indicate that AMBN increases osteoclast number and differentiation as well as mineralized tissue resorption by regulating cell adhesion and actin cytoskeleton polymerization, initiating integrin-dependent extracellular matrix signaling cascades and enhancing osteoclastogenesis.

Previous in vitro studies have indicated that AMBN is involved in osteogenesis. Here we have hypothesized that AMBN is important for timely long bone development as well as fracture repair. Our studies have employed an ameloblastin-deficient mouse model ($AMBN^{\Delta 5\text{-}6}$), which expresses a truncated AMBN protein. Long bone growth in these mice was delayed during the first 6 months of postnatal development, as revealed by X-ray analysis. Micro-computed tomography documented decreases in BV/TV ratio, trabecular number, and both trabecular and cortical thickness, which corresponded to the changes in femur biomechanical parameters such as reduced stiffness, maximum force, and energy to failure. Histomorphometric analysis demonstrated that AMBN mutation resulted in a shortened growth plate and less proliferating cells in the tibia. *In vitro* primary cell culture studies indicated that bone marrow stromal cells (BMSCs) isolated from AMBN mutant had defects in cell proliferation and differentiation

potential, resulting in a reduction in the number of colony-forming units, ALP-positive colonies and mineralized nodule formation. PCR array and qRT-PCR analyses demonstrated down-regulation of several osteogenic-related growth factors, including IGF1 and BMP7, in AMBN-deficient BMSCs. These data indicate that AMBN is involved in long bone formation and that AMBN mutation affects BMSCs cell function.

Together, our data indicate that AMBN is not only involved in tooth amelogenesis, but also functions outside of enamel in periodontal tissue homeostasis and long bone development and fracture healing.

I. INTRODUCTION

A. Background

A.1. SCPP gene family

The mammals have three principal mineralized tissues: enamel, dentin and bone, which form on an extracellular matrix (ECM) proteins encoded by members of the secretory calcium-binding phosphoprotein (SCPP) gene family and other proteins (*1, 2*). The SCPPs are secreted proteins directly associated with calcium ions, and most have many calcium-binding phosphorserine residues (*2, 3*). This SCPP family comprise some saliva proteins, milk caseins, small integrin-binding ligands, N-linked glycoproteins (SIBLING) and enamel matrix proteins (*4*). In humans, DSPP (dentin sialophosphoprotein), DMP1 (dentin matrix protein 1), IBSP (integrin-binding sialoprotein), MEPE (matrix extracellular phosphorglycoprotein) and SPP1 (secreted phosphoprotein 1) belong to SIBLING group referred to as dentin/bone, based on the localization patterns of their coded proteins (*3, 5*). The enamel SCPPs subfamily includes AMEL (amelogenin), AMBN (ameloblastin), ENAM (enamelin), AMTN (amelotin) and ODAM (odontogenic, ameloblast associated), are all involved in enamel formation (*6*). In mammals, all SCPP genes are located in two clusters on the chromosome 4, with exception of AMEL which is located on chromosomes X and Y.

A.2. AMELX and AMBN function in enamel formation

Amelogenin, the major structure protein of the enamel organic matrix, constitutes more than 90% of the enamel's protein content. In humans, the amelogenin gene exist on both X and Y chromosomes (*7*). In male, both the X and Y chromosome-derived amelogenin are expressed, but the protein from the X-chromosome predominates (*8*).

AMEL's function in enamel formation has been demonstrated in human mutation diseases

and *Amelx* knock out animal models. Specific mutations in the *Amelx* gene have been shown to be associated with amelogenesis imperfect (AI), which is manifested by a thin surface layer of mineral lacking a typical rod pattern (*9, 10*). Further, *Amelx* null mice exhibits a dramatic enamel phenotype, similar to that associated with AI in human enamel (*11*). Amelogenin is secreted in a variety of isoforms, the major one having a molecular weight around 25 kDa , and in humans equates to a 175 amino acid product (*12*). Conservation is particularly obvious among the 50 residues in the N-terminal and 20 residues in the C-terminal (*13*). Conservation of the amino acid sequence often implies important physiologic relevance. The supra molecular assembly of AMEL into ‘nanospheres’ after its secretion has been assumed to be critical for the function of this structural protein during enamel formation (*14*). The nanospheres, about 20 nm in diameter, that are thought to regulate crystal spacing (*15, 16*).

Ameloblastin is the second most abundant protein in enamel, constituting about 5% of the total protein present in the organic matrix. The human AMBN gene has been localized to chromosome 4q21 and contains 13 exons (*17, 18*). Most AMBN expression occurs at the secretory stage and diminishes at the maturation stage (*19*). AMBN protein has an apparent molecular weight of 65-70 kDa, is rich in proline, glycine, and leucine (*17, 20*), and includes one or two sulfated O-linked glycosylation (*21*). Based on immunolocalization studies of ameloblastin N-terminal cleavage products appearing in the sheath or inter-prismatic space in porcine enamel, AMBN has been hypothesized to be involved in the control of the prismatic structure of enamel (*22*). The AMBN C-terminal proteolytic products have high affinity for calcium ions, indicating their possible involvement in controlling mineralization (*21*). Furthermore, several animal models have been generated to illustrate the function of AMBN in amelogenesis. Over-expression of AMBN in mice significantly alters enamel crystal habit and

enamel rod morphology in a fashion resembling AI (*23*). Moreover, there is lack of enamel formation in the AMBN knockout mouse, since the ameloblasts detached from the surface of the developing tooth which indicate AMBN is a cell adhesion molecule that facilitates the attachment of ameloblasts the enamel matrix (*19*). No human AMBN mutations outside of apparent polymorphisms have been identified in AI kindred, presumably because its pattern of inheritance is autosomal recessive and occurs only rarely (*24*).

A.3. Origin of the SCPP-associated enamel proteins, a view from evolution

Duplication and diversification of ancestral genes encoding mineralized tissues bone, dentin and enamel were crucial events in vertebrate evolution *(25*). Enamel was identified in early jawless vertebrates, about 500 million years ago (*2*). This suggests the enamel matrix proteins have at least the same age. Taking advantage of gene sequencing techniques, the sequences SCPP genes were aligned and analyzed phylogenetically. The most recent and major enamel protein, AMEL, is believed to have evolved from a gene ancestral to ENAM and AMBN by duplication and translocation onto a chromosomal region that belongs to the X-Y chromosomes of placental mammals (*2, 3, 26*).

In early evolution, SPARC (secreted protein, acidic, cysteine-rich), a common ancestor of SCPP genes, duplicated into SPARCL1 (SPARC-like 1 protein).During successive rounds of genome and gene duplication, SPARCL1 and its descendants were copied several times on the same chromosome, giving rise to two clusters: the ameloblast-expressed/milk/saliva protein gene cluster and the bone/dentin protein gene cluster, SIBLINGs. The ENAM ancestor duplicated from an SCPP ancestor and one ENAM copy was duplicated again, giving rise to the ancestors of AMBN/AMEL and of AMTN/ODAM. After its duplication from AMBN, AMEL was translocated to the X-Y chromosomes. In short, there were at least five duplication events that

took place from SPARC to AMEL in enamel mineralization genes (*6*): SPARC -> SPARCL -> SCPP ancestor ->ENAM -> AMBN -> AMEL. This continuous evolution of enamel proteins appears to correspond to a gradual increase in enamel complexity during the evolution of vertebrates with the emergence of enamel prisms during the reptilian mammalian transition (*27*, *28*).

A.4. Osteoclasts origination, adhesion and differentiation.

Bone is a dynamic tissue which is maintained and remodeled by the actions of osteoclasts, osteoblasts and osteocytes. Osteoclasts are bone-resorbing cells derived from hematopoietic precursors of the monocyte macrophage lineage (*29*). These cells are formed through the differentiation and fusion of mononuclear phagocyte precursors in the presence of macrophage colony-stimulating factor (M-CSF) and receptor activator of NFκB ligand (RANKL) which subsequently activates RANK on the surface of hematopoietic precursor cells (*30*). Osteoclast activity is normally closely integrated with that of bone-forming osteoblasts, to enable the continual removal and replacement of bone that occurs throughout the life. Both CSF-1 and RANKL are essential factors for osteoclasts to survive, proliferate and differentiate required to induce the expression of the osteoclast lineage specific genes, including tartrate-resistant acid phosphatase (TRAP), cathepsin K (CATK), calcitonin receptor and the β3-integrin, and lead to the development of mature osteoclasts (*31*).

From a clinical perspective, changes in osteoclast number or activity have dramatic effects on the life of an organism: osteoclast hyperactivity results in osteoporosis, while osteoclast defects cause increased bone density in individuals suffering from osteopetrosis (*32*). Changes in osteoclast physiology not only affect the entire skeletal system but also the jaws and teeth, where inflammatory or pro-inflammatory cytokines cause root resorption as a result of orthodontic

treatment (*33*, *34*) or bone resorption and associated tooth loss as a result of periodontal disease (*35*, *36*). The intricate balance between bone resorption and apposition is exemplified during physiological tooth movement where bone resorption at movement-direction alveolar bone walls and bone apposition on the contralateral side, and plays roles in the continuous maintenance of the attachment apparatus.

Osteoclastic bone resorption consists of multiple steps: the proliferation of osteoclast progenitors, differentiation of progenitors into mononuclear prefusion osteoclasts, fusion of osteoclasts into multinucleated osteoclasts, and migration of osteoclasts to the resorption site (*37*). After circulatory hematopoietic monocytes/marcrophages attaching to bone specific resorption sites, they undergo osteoclastic differentiation and polarize to create a tight sealing zone closely attached to the bone surface with a ruffled border, highly convoluted membrane that faces the resorbing surface (*38*). The contact of osteoclasts with the apatitic bone surface activates small GTPases of the Rho family (*39, 40*), which in turn induces osteoclast spreading, podosome formation and the formation of the sealing zone (*41*, *42*, *43*). The initial attachment of osteoclasts to bone matrix is mediated by integrins of heterodimeric adhesion receptors (*37*). So far five integrins have been identified in osteoclasts. They are αvβ3 (a classical vitronectin receptor), αvβ5, α2β1 (collagen/laminin receptor), and αvβ1, which binds to a variety of extracellular matrix proteins, including vitronectin (VN), collagen, osteopontin (OPN), bone sialoprotein, and fibronectin (FN) (*44, 45*), and integrins α9β1 (*46*). The interactions between these integrins and bone matrix are functionally important for osteoclast activation. They induce an integrin conformation change leading to the so-called outside-in signaling, which in turn triggers a number of intracellular events, including cytoskeletal remodeling (*47*). For example, αvβ3 activates several pathways involving phosphatidyl inositol kinases, c-Src tyrosine kinase,

PYK2/FAK, p130Cas, PTP-PEST, c-Cbl, WASP and Arp2/3 (*48, 49*). Integrin α2β1 mediated matrix remodeling requires tyrosine kinase-ERK1/2 signaling (*50*).

A.5. AMBN function as an adhesion molecule in the periodontium.

While first discovered in ameloblasts and considered as an enamel specific protein (*17*), AMBN is also expressed by odontoblasts (*51, 52*), osteoblasts (*53*), cementoblasts (*54*) and epithelial rests of malassez (ERM) in the periodontium (*55*).AMBN also increased proliferation in periodontal ligament cells (*56*) and osteoblasts (*57*). Hertwig's epithelial root sheath (HERS) cells express AMBN, whereas other enamel proteins including amelogenin, enamelin, and tufterin are eliminated in the tooth root development process (*58*). Interrupting AMBN expression by small interfering RNA (siRNA) during the tooth root development period reduces proliferation of HERS cells and cases shorter roots (*59*). It may be assumed that AMBN is related to tooth root formation.

At the beginning, *in vivo* studies have demonstrated that AMBN is a cell adhesion molecule, although it lacks the RGD integrin-binding motif. Mutation of AMBN results in detachment of ameloblasts from the developing enamel matrix and a loss of cell polarity in an AMBN null mouse model (*60*). *In vitro* studies clarify the effect of AMBN on cell adhesion and proliferation involved with RhoA and p27 (*61*).

Based on protein informatics analysis, AMBN contains a DGEA motif located on exon 11, which is a potential integrin-binding site of collagen I (*62*), and a thrombospondin-like cell adhesion motif, VTKG (*63*). Several AMBN interaction partners on osteoblasts have been identified. Sonoda et al. demonstrated that AMBN contains several heparin-binding domains, which might be responsible for the interaction of AMBN with the surface of dental epithelial cells (*64*). Beyeler et al. identified a fibronectin interaction site in the AMBN, narrowed down to

a sequence of 13 amino acid residues derived from exon 7 (*65*). Iizuka et al. demonstrated that AMBN interaction with CD63 and integrinα2β1 regulates osteogenic differentiation (*66*). Further studies discovered that AMBN greatly enhances the attachment of periodontal cells through the small GTPase RhoA, while AMBN reduces periodontal cell proliferation through the kinase inhibitor p27 (*61*).These results suggest that AMBN is important for the attachment and maturation of periodontal ligament cells.

A.6. Endochondral bone development

Bones in different parts of skeleton develop through two distinct process, intra- membranous ossification and endochondral ossification. Intramembranous ossification, which occurs in the flat bones of the skull, involves direct differentiation of embryonic mesenchymal cells into the bone-forming osteoblasts. In contrast, endochondral ossification, which occurs in the remainder of the skeleton, involves the replacement of the cartilage model by bone tissue (*32*, *67*).

Endochondral bone formation begins with the condensation of mesenchymal cells which is a prerequisite for subsequent chondrogenesis differentiation in the embryonic stage (*68*). Cells in the core of the condensations differentiate into chondrocytes that secrete a cartilage matrix rich in type II,IX, and XI collagen and specific proteoglycans (*69*). When development proceeds, a predetermined program of chondrocyte differentiation ensues in the central diaphysis, leading to chondrocyte hypertrophy. The hypertrophic chondrocytes express collagen X and direct the mineralizaion of the surrounding matrix, while signaling to adjacent perichondrial cells to direct their differentiation in to osteoblasts, and also to stimulate the invasion of blood vessels. Capillaries invade the perichondrium surrounding the future diaphysis and transform it into the periosteum, whereas osteoblastic cells differentiate, mature, and secrete collagen I and other bone-specific molecules, including osteocalcin (OCN), alkaline phosphatase (ALP), integrin-

binding sialoprotein (IBSP) and etc (*32*). Matrix mineralization, in turn, is followed by vascular invasion from vessels originating in the periosteal collar that allows for the migration of osteoblast precursor cells into the primary ossification center. These cells transform into mature osteoblasts and initiate new bone formation on the degrading matrix scaffolding.

Primary ossification center (POC) serves as a continual source of cartilage conversion to bone and linear growth of the long bone during development and postnatally (*70*). In late fetal life and early childhood, secondary centers of ossification (SOC) appear within the cartilaginous epiphyses by a mechanism very similar to that used in the formation of the primary center (*71*). Cartilage is retained at the growth plate (GP), extending the full width of the bone and separating epiphysis from diaphysis (*72*). Cessation of growth occurs at the end of puberty, when growth plates are replaced by bone.

A.7. Regulation of osteogenic differentiation of MSCs

Mesenchymal cells are a major cell population responsible for bone formation both at embrynic and postnatal stages. The MSCs (mesenchymal stem cells) are multipotent stem cells that can differentiate into a variety of cell types, including osteoblasts, chondrocytes, and adipocytes, as well as into other nonmesodermic cells (*73, 74*). During bone formation, the differentiation of osteoblasts from their mesenchymal progenitors is regulated by transcription factors (such as RUNX2, OSX, MSX2 and etc), and some specific extracellular signals (BMPs, WNT and IGF will be mentioned here)

Runt-related transcription factor 2 (RUNX2), also named Cbfa1, is the major transcription factor regulating osteoblast commitment and osteogenic differentiation of BMSCs (*75, 76*). Deletion of *Runx2* in mice resulted in lack of bone formation and the skeleton comprised only chondrocytes and cartilage (*77, 78*). RUNX2 mutation-related haploinsufficiency in mice (*78*)

and humans leads to the cleidocranial dysplasia phenotype (*79-81*). RUNX2 is the earliest osteoblast differentiation marker currently known, its expression during development and after birth is high in osteoblasts (*77*).

Osterix (OSX), another zinc finger protein that belongs to the SP family of transcription factors, acts downstream of Runx2 and its absence causes a lack formation of osteoblasts (*82*). OSX not only plays a role in embryonic osteoblast differentiation, but is also critical for postnatal osteoblast and osteocyte formation and function (*83*). Kurata et al. recorded that *Osx* overexpression was capable of initiating osteogenesis, shown by early marker expression, but failed to generate terminally differentiated osteoblasts (*84*)

The muscle segment homeobox factor (MSX) also play roles in osteoblast differentiation. For example, a mutation in *Msx2* underlies Boston-type craniosynostosis (*85*), whereas MSX2 inactivation in mice delays skull ossification, an outcome associated with decreased *Runx2* expression (*86, 87*). Enhancing expression of *Msx2* keeps osteoblast precursors transiently in a proliferative state, delaying osteoblast differentiation, resulting in an increase in the osteoblast pool and ultimately in an increase in bone growth (*88, 89*).

The extracellular singles, including systemic hormones, such as parathyroid hormone (PTH), or other local growth factors, including bone morphogenetic proteins (BMPs) family, WNT and insulin-like growth factors (IGFs) regulates osteogenic differentiation of MSC (*90, 91*).

BMPs belong to the TGFβ1 superfamily, with more than 30 members identified in mammals (*92-94*). Many of these signaling proteins, mostly notably BMP2, BMP6, BMP7, and BMP9, are inducers of osteogenesis both *in vitro* and *in vivo* (*94, 95*).Genetic studies have uncovered important roles for BMP2, BMP4 and BMP7 in promoting osteoblast differentiation (*96*). In the absence of BMP2 during bone fracture healing, mesenchymal progenitors at the repair site do not

differentiate, leading to a failed healing response (*97*). BMP7 is capable of inducing differentiation of stem cells into osteoblasts and induction of endochondral bone formation at bone defect sites (*98*). Since 2001, implantation of rhBMP7 has been licensed in Europe as a treatment for long bone non-unions alternative to the use of autologous bone (*99*).

The Wnt/β-catenin signaling pathway also plays a critical role in osteoblastic cell differentiation and bone formation. Mutations in Wnt receptors leading to alterations in Wnt signaling result in profound changes in bone mass (*100*). Deletions of *Wnt* or *β-catenin* result in absent osteogenesis and increased osteoclastogenesis, whereas expression of a stable form of β-catenin, shielded from degradation, in the skeleton results in osteopetrosis because of enhanced osteogenesis and impaired osteoclastogenesis and bone resorption (*101, 102*).

Insulin like growth factor (IGF) is the most abundant growth factors present in skeletal tissue. Systemically IGF-I is synthesized by the liver, where its synthesis is growth hormone (GH) dependent (*103*). But locally, IGF-I plays an important role in the autocrine and paracrine regulation of cell metabolism in a variety of tissues, including cartilage and bone (*104, 105*). Transgenic mice expressing IGF-I under the control of the osteocalcin promoter exhibit increases in trabecular bone secondary to an increase in bone formation (*106*). Inactivation of *Igf1, Igf2* or *Igf1r* in mice causes growth arrest because of failed chondrocyte proliferation and maturation (*107*). IGF1 plays a pivotal role in longitudinal bone growth, because *Igf1* gene deletion results in dwarfism in mice (*107, 108*) and extreme short stature in humans (*109*).

Besides the growth factors mentioned above, some other molecules also important for osteogeneic differentiation, such as FGFs, NOTCH and IHH molecules, please follow the reviews for more details (*71, 93, 95, 110*).

A.8. AMBN and osteogenesis

The function of AMBN in osteogenesis could be illustrated by clinical application of the Emdogain (Enamel matrix derivative, EMD), which is a protein extract purified from porcine enamel, to obtain periodontal regeneration (*111-113*). EMD is composed mainly of amelogenin (90%) and other non-amelogenin proteins including AMBN. The presence of AMBN degradation products, particularly the N-terminal 13-17 kDa fragment commonly known as sheath proteins, in EMD may play a role in osteogenic differentiation, cementum formation, and bone growth (*114*). Some *in vitro* studies suggest AMBN could function as a growth factor or signaling molecule to promote PDL cell proliferation and differentiation in the periodontal regeneration (*56, 115, 116*). This is also supported by the bioinformatics analysis of AMBN protein showing that it has a structure with an internal organization similar to other known signaling molecules (*117-119*).

Besides its function in enamel biomineralization, AMBN is also expressed during the development of mesenchymal dental hard tissues (*120*), during trauma-induced reparative dentin formation (*121*), during embryonic and post-natal stages of craniofacial bone formation (*53*) and during mouse calvarial development (*122*). In rat craniofacial bone of intramembranous ossification, AMBN mRNA and protein were detected in the superficial layer of the condensed vascularized connective tissue and in the cell layer covering the surface of newly formed woven bone. In endochondral ossification, the protein was found in the extracellular matrix of the cartilage templates and in the perichondrium (*53*). Most recently, it has been demonstrated that AMBN plays a crucial role in the regulation of cranial bone growth and suture close via *Msx2* suppression and proliferation inhibition (*123*).

The ameloblastin null mice transcript truncated mRNA missing exon 5 and 6, so called

AMBN$^{\Delta 5\text{-}6}$ mutant (*124*). These mice not only showed enamel defects as predicted, but also exhibited a more porous interdental bone and generally reduced thickness of the alveolar bone process. Furthermore, both *in vivo* and *in vitro* experiments have revealed that AMBN induces hard tissue regeneration, by influencing differentiation and growth of mesenchymal cells at the healing site (*114, 115, 125*). Recombinant AMBN enhanced the proliferation of mesenchymal stem cells and osteoblasts, as well as the differentiation of osteoblast precursor cells by stimulating IL-6 and IL-8 (*125*). To specifically locate ameloblastin in cellular levels, scholars proved AMBN mRNA and protein expression in primary osteoblasts, chondrocytes and osteoclast (*57*). Specially, *Ambn* is expressed in mesenchymal stem cells and its gene upstream region contains structural elements, many of which could be related directly to bone formation, regulating transcriptional activity in a stromal cell line derived from bone marrow (*126*). The mechanism studies verified that AMBN function as a promoting factor for osteogenic differentiation via interaction between CD63 and integrin β1 by inhibiting Src kinase.

B. Hypothesis of the study

AMBN functions as a cell adhesion molecule as well as matrix protein, and modulates mineralized tissue formation.

B.1. AMBN enrichment in the enamel matrix without AMELX affects enamel crystal structure and results in prismless enamel resembling reptilian tooth covering.

B.2. AMBN modulates osteoclast adhesion and activation in the periodontium through the integrin/ERK pathway.

B.3. AMBN mutant mice display a skeletal bone defect phenotype associated with impaired BMSC proliferation and differentiation.

C. Specific aims of the study

C.1. To determine how AMBN affects enamel matrix formation and enamel crystal growth.

In this aim, we have crossed AMBN TG overexpressor with amelx$^{-/-}$ null mice and characterized enamel features of AMBN TG × amelx$^{-/-}$ mice using SEM and TEM to evaluate the enamel crystal structure which was compared with that of *lguana.*

C.2. To decipher the pathways by which AMBN modulates osteoclastogenesis.

Here we used AMBN overexpression mice as an *in vivo* model to determine the effect of AMBN on periodontal development. In addition, we applied BMMCs culture systerm to examine role of AMBN protein in osteoclast cell adhesion and RANKL-stimulated osteoclastogenesis *in vitro,* and decipher the pathways by which AMBN modulates osteoclastogenesis.

C.3. To determine the function of AMBN in long bone formation.

In the last aim, we characterized the bone defect phenotype of the femurs and tibias from AMBN$^{\Delta 5\text{-}6}$ mutant mice during the development stage, assessed proliferation and osteogenic, osteoclastogenic and chondrogenic differentiation abilities of primary BMSCs isolated from AMBN$^{\Delta 5\text{-}6}$ mutant mice in *ex vivo,* and identified specific candidate genes related to bone loss phenotype and impaired differentiation potential of BMSC in AMBN$^{\Delta 5\text{-}6}$mutants.

II. MATERIALS AND METHODS

1. AMBN transgenic and knockout animal models and genotyping

Transgenic constructs were generated using the human K14 cassette construct (a generous gift from Dr Elaine Fuchs, Rockefeller University) to overexpress the mouse *Ambn* coding region (Fig. 1). The1,269-bp *Ambn* coding region with a *Bam* HI site at the 3′ end and a *Xho* I site at the 5′ end was amplified by the PCR. The *Ambn* gene was inserted between the β-globin intron and the K14 poly-A signal. A β-globin intron was used to ensure that the transgenes were transcribed properly. The transgenic fragments were freed from the construct by digesting the constructs with *Sac* I and *Hin*d III, gel purified, and microinjected into mouse zygotes. In total, six independent lines were generated. Germline transmission was determined by PCR analysis of genomic DNA obtained from tail biopsies. The Qiagen multiplex PCR kit (Qiagen, Valencia, CA, USA) was used for PCR, which was performed using a set of specific primers for K14 promoters displayed in Table III. PCR products were analyzed on a 2.0% agarose gel. Offspring mice carrying the *Ambn* transgene (AMBN TG) were mated with AMELX null mice ($amelx^{-/-}$) *(24)*. F1 offspring positive for the transgene and heterozygous for AMELX ($amelx^{+/-}$) were mated, yielding an F2 generation that was then genotyped by tail biopsies. Altogether, four groups were generated: wild-type (WT), AMBN transgenic overexpression (AMBN TG), AMELX null ($amelx^{-/-}$), and AMELX null crossed with AMBN transgenic overexpression (AMBNTG × $amelx^{-/-}$).

The original AMBN knockout mouse model was created and obtained from Dr. Yamada (*60*). The null allele was generated by disrupting expression of full-length AMBN in exon 5 and 6. The mouse model is referred to as $AMBN^{\Delta 5\text{-}6}$ mutant (*124*). We backcrossed AMBN mutated mice with C57BL/6 for 10 generations to create genomic homogenized heterozygous breeders.

The AMBN wild-type (WT), heterozygous mutant ($AMBN^{HET}$) and homozygous mutant ($AMBN^{\Delta 5\text{-}6}$) generated by the 1 male and 2 female mating approach for heterozygote-heterozygote crossing. Genotyping was done by PCR analysis of genomic DNA extracted from mouse tail clips, using neomycin primer (R2) to detect the targeted allele, and F1 and R1 primers to detect the wild type allele (Table III). All experimental protocols and animal handling were approved by Committee on the Ethics of Animal Experiments of the University of Illinois at Chicago (permit number: 11-077)

2. Protein extraction and Western Blot analysis

Mandibular molar root/bone tissues from the transgenic and control animals on postnatal days 3, 6, 10, 15 and 20 or cultured cells were collected. Long bone sample derived from the femur and tibia from C57BL/6 mice on postnatal day 1, 3, 7, 10, 15, 20, 30 and 3 month. Equal amounts of protein extracts in a lysis buffer containing 100 mM TrisHCl pH 9.0, 200 mM KCl, 25 mM EDTA, 36 mM $MgCl_2$, 2% deoxycholic acid and 10% DTT v/v were subjected to SDS–polyacrylamide gel electrophoresis, and the separated proteins were transferred to a PVDF membrane (Immobilon P, Millipore). The membrane was incubated with anti-AMBN, AMELX, anti-RhoA, AKT, pan-AKT, pho-ERK, ERK, β-actin, β-tubulin, NFATc1 or c-Fos primary antibodies (Abcam). Immune complexes were detected with peroxidase-conjugated secondary antibody (Molecular Probes, Carlsbad, CA) and enhanced by chemiluminescence reagents (Pierce Biotechnology, Rockford, IL). The expression amounts of protein were compared after normalization against β-actin or β-tubulin as an internal calibrator in each lane.

3. Scanning electron microscopy

For studying of enamel structure, scanning electron microscopy were conducted. Three female 30-day postnatal mice from each group (WT, AMBN TG, amel$^{-/-}$, and AMBN TG × amel$^{-/-}$) were sacrificed according to the University of Illinois at Chicago (UIC) Animal Care Guidelines. Lower mandibles were isolated, fixed in 4% paraformaldehyde, dehydrated in 70% ethanol and in 100% ethanol, and then hemisected in the saggital plane using an EXAKT sawing device (Exakt Technologies, Oklahoma City, OK, U.S.A.). The enamel surface was etched in EDTA for 5 min, rinsed thoroughly, and dried overnight. To evaluate tooth root surface, molars from mandibles of 35-day-old wild-type (WT) and AMBN transgenic (TG) mice were extracted and dehydrated in a series of ethanol, air dried. Samples were coated with gold and palladium and then examined using a JEOL JSM-6320F scanning electron microscope (JEOL USA, Inc, Peabody, MA, USA).

4. Transmission electron microscopy

For transmission electron microscopy (TEM) studies to enamel crystal, three, 3-day postnatal mice from each group (WT, AMBN TG, amelx$^{-/-}$, and AMBN TG × amelx$^{-/-}$) were sacrificed. Then, the lower molars of these mice were dissected under a dissecting microscope. Molar samples were fixed in 2% [volume by volume (v/v)] glutaraldehyde and 2% (v/v) paraformaldehyde in 0.1 M cacodylate buffer for 2–4 h, and postfixed in 2% (v/v) osmium tetroxide (OsO_4) in cacodylate buffer, at pH 8. Subsequently, samples were dehydrated in a series of graded ethanols and embedded in EMBed 812 epoxy resin (EMS, Hatfield, PA, USA) following transitioning in propylene oxide. For TEM, five representative samples from each group were selected and ultrathin sections were cut and floated on a trough presaturated with

hydroxyapatite to slow the rate of possible mineral dissolution. The floating time of the sections on water was minimized. The sections were then examined using a JEOL 1220 TEM microscope (JEOL USA, Inc, Peabody, MA, USA). Digital micrographs were recorded from five representative areas of each section at × 30,000 magnification, and crystal length was analyzed using ANOVA.

5. Whole mount X-gal and alizarin red staining

For whole mount X-gal staining, mandibles from *LacZ* transgenic mice at postnatal day 35 were fixed with 4% paraformaldehyde in PBS at 4 °C overnight. The samples were then incubated in the dark with a staining buffer containing 0.05 mM $K_3Fe(CN)_6$, 0.05 mM $K_4Fe(CN)_6$, 1 mM $MgCl_2$, and 1 mg/ml X-gal at 37 °C for 7 h.

For whole mount alizarin red staining, mandibles from wild type (WT) and *Ambn* transgenic mice at postnatal day 35 were fixed, dehydrated and then stained with saturated alizarin red S (Sigma, St Louis, MO) in 0.5% potassium hydroxide (KOH).

Whole embryos for alcian blue/alizarin red skeletal staining were prepared as described previously(*123*). All embryos including WT, $AMBN^{HET}$ and $AMBN^{\Delta 5\text{-}6}$ at embryonic day 18.5 were fixed and dehydrated with 70%, 100% ethanol and acetone. The samples were stained with saturated alcian blue (Sigma, St Louis, MO) in 95% ethanol for 2 days, destained with 95% ethanol, and rehydrated. Subsequently, samples were then stained with saturated alizarin red S (Sigma) in 0.5% potassium hydroxide (KOH) solution for 2 days, destained in 0.5% KOH solution until all soft connective tissue turned clear and then stored in 80% glycerol.

6. Tissue processing

Mandibles from WT, *Ambn* or *LacZ* transgenic mice were dissected and fixed with 4% paraformaldehyde in PBS at 4 °C overnight. For long bone development analysis of AMBN mutant during postnatal stage, AMBN mutant littermate mice were euthanized at 1.5, 2, 3, 4 and 6 months old. For undecalcified ground sections, tissues were dehydrated, embedded in Technovit 7200 (Exakt Inc., Oklahoma, OK) and prepared into 10 μm sections for subsequent von Kossa staining. For decalcified paraffin sections, samples were demineralized in EDTA, and processed for paraffin sections. Sections were subjected to H&E staining, Villanueva staining, TRAP staining, *in situ* hybridization or immunohistochemistry describing as follow.

7. Micro-computed tomographic (μ-CT) and bone histomorphometry analysis

To visualize mineralized tissues in mandible of AMBN overexpressor, 6-week-old WT and AMBN transgenic tissue blocks were analyzed using microcomputed tomography (micro-CT). For this purpose, 3D X-ray CT images were acquired using a high resolution scanner (Viva CT 40 Scanco Medical AG, Brüttisellen, Switzerland) in 10μm resolution as described in previous (*127*). For long bone development analysis during postnatal stage, AMBN mutant littermate mice were euthanized at 1.5, 2, 3, 4 and 6 months old. The femurs from male and female group at each time point were collected and fixed. X-ray images scanned by FIXATRON (FAXITRON BIOPTICS, LLC, AZ). Samples from 2 and 4 months old male and female littermates were performed bone histomorphometry analysis. The distal femoral metaphyses were scanned with a Scanco40 μ-CT . The following parameters were estimated: bone volume/ total volume (BV/TV, %), trabecular thickness (Tb.Th., mm), trabecular number (Tb. Nb. , mm), trabecular separation (Tb. Sep. , mm), cortical thickness (Cr. Th. , mm) and bone mineral density (BMD,

gHA/cm^3) (*127*). Quantitative histomorphometry of stained ground and paraffin sections were performed in distal half of femur. Images were acquired by Leica DMRX microscope (Leica).

To study the dynamic bone modeling, 6-week-old AMBN$^{\Delta 5\text{-}6}$ littermates were used for bone fluoresces labeling. Tetracycline hydrochloride (Sigma) (25mg/kg) injection was followed by the same dose of calcein 5 days later, and animals were euthanized 2 day after that. The femurs were collected then underwent un-decalcified ground sections preparation. Bone histomorphometry analysis was conducted by Image J software.

8. *In situ* hybridization

In situ hybridization analysis was performed using a Digoxingenin (DIG)-labeled probe. Briefly, deparaffinized and rehydrated sections were treated with Proteinase K and then hybridized with a hybridization solution containing DIG-labeled AMBN antisense or sense RNA probe at 65 °C for 16 h. Sections were then washed at high stringency, blocked and incubated with anti-DIG-Alkaline Phosphatase antibody (Roche, Mannheim, Germany). The localization of AMBN mRNA was revealed using the NBT/BCIP substrate

9. Immunohistochemistry

Sections were deparaffinized, rehydrated and treated with 3% peroxide and methanol for 10 mins followed by a brief incubation in 10 mM sodium citrate buffer with 0.05% Tween 20 at pH 6.0 for antigen retrieval. After blocking, sections were first incubated with affinity purified polyclonal anti-AMBN, anti-IGF1 and anti-BMP7 antibodies at a dilution of 1:200 at 4 °C overnight, and then with anti-rabbit secondary antibody (Abcam, Cambridge, MA) at a dilution of 1:500. Protein expression was detected with a Histomouse Broad Spectrum AEC or DAB kit

(Invitrogen, Carlsbad, CA) under a light microscope.

To verify AMBN and K14 co-localization, fluorescent immunohistochemistry was performed using rabbit anti-AMBN or mouse anti-K14 antibodies (Abcam). The samples were incubated overnight at 4 °C with primary antibodies and then with secondary FITC-conjugated anti-rabbit IgG antibody or Texas Red-conjugated anti-mouse antibody (Invitrogen). Immunoreactivity was observed under a fluorescence microscope. As a negative control, non-immune rabbit serum was used instead of the primary antibody.

10. von Kossa staining

Ground sections were stained with 5% silver nitrate for 1 h under UV exposure and then de-stained with 5% sodium thiosulfate. Counter staining with was conducted 1% fast red solution.

11. TRAP staining

Osteoclasts were visualized using a tartrate resistant acid phosphatase (TRAP) staining procedure. For this procedure, either fixed cells or de-paraffinized sections were incubated in acetate buffered solution containing naphthol AS-MX phosphate, Fast Garnet GBC salt, and tartrate solution (0.67 mol/l) (Sigma, St. Louis/MO) for 60 min in 37°C, and then counterstained with hematoxylin.

12. Safarin O staining

The paraffin sections were stained with hematoxylin working solution after deparaffinezed and rehydrated. The slides were stained with 0.05% fast green solution for 5 minutes and rinse

quickly with 1% acetic acid for 10 seconds. Subsequently, slides were stained in 0.1% safranin O solution for 5 minutes and then dehydrated and mounted.

13. Alcian blue staining

After deparaffinized and hydrated, slides were stained in 1% alcian blue solution for 30 minutes, and then counterstained in nuclear fast red solution for 5 minutes. Dehydrated and mounted slide for observation.

14. Serum biochemistry

Mouse blood samples were collected following euthanization via heart puncture from 2 and 4 month-old littermate WT, $AMBN^{HET}$ and $AMBN^{\Delta 5\text{-}6}$ mutant animals. Blood was allowed to clot for at least 1 hour at 4°C, centrifuged for 10 minutes×3,000 rpm, and supernatant (serum) was collected. Centrifugation was repeated for 10 minutes×2,500 rpm and the resulting serum layer was used for serum test or stored at −80°C until further use. For serum calcium (Ca), phosphorous (P) and alkaline phosphatase (ALP) activity measurement, the samples were analyzed by an automated chemical analyzer (Johnson and Johnson VT350) in UIC BRL facility. Serum tartrate-resistant acid phosphatase (TRAP) concentration was measured by mouse TRAP assay ELISA kit (IDS, Scottsdale, AZ) following the manual instructions.

15. Biomechanical testing

The femurs from male AMBN mutant littermates (n=4-5 each group) were used for femur 3-point bend tests as described previously (*128, 129*). Fresh isolated femur samples were fixed in 70% ethanol and frozen in -20°C for later using. On the day of testing, the femurs were thawed

and rehydrated with 1×PBS for 3 hours. Three-point bending was performed with a support span of 6.0 mm. The bones were loaded at the midshaft of the femur, perpendicular to the long axis of the bone, with the load applied in the anterior to posterior direction. Samples were tested to failure at a deflection rate of 5 mm/min using a custom anvil (*128*). Bending force-deflection curves were constructed and analyzed for stiffness (N/mm) and maximum force to failure (N). The energy to failure (N*mm) was calculated from the classical equations of beam theory for a simply supported beam with a central concentrated load.

16. AMBN protein expression and purification

The mouse *Ambn* coding region was amplified by PCR with a 5'Nde1 site and a 3'BamH1 site. The PCR products were inserted in the pET-28 expression vector (Novagen, Madison, WI) which was transformed into BE21 cells. The expression of recombinant mouse AMBN (rmAMBN) was induced with IPTG at a concentration of 1mM at 32 °C for 4 h. Protein purification was performed used Ni-NTA agarose (Qiagen).

17. CFU-F, CFU-ALP and CFU-Ob assays

For colony forming efficiency (CFU-F) assay, Bone marrow stromal cells (BMSCs) were flushed from 4-week old WT, $AMBN^{HET}$ and $AMBN^{\Delta 5\text{-}6}$ littermates. The cell suspensions were filtered using a 70 μm strainer and passed through 16- and 20- gauge needles to break down cell aggregates. Then the cell suspensions were filtered through a 40 μm cell strainer (Becton-Dickinson, Franklin Lakes, NJ) in order to obtain singly cells. The red blood cells were lysed using 0.1% Acetic Acid. Nucleated cells were plated in 35 mm dishes at 0.5×10^5 or 1×10^5 cells/well in complete MesenCult medium (STEMCELL Technologies, Vancouver ,

Canada) with duplicated cultures. On day 14 the cultures were fixed and stained with ALP, after counted ALP+ colonies, the culture dishes were subject to Giemsa (STEMCELL Technologies) staining. An ALP+ colony was defined as a colony that was positive for ALP activity and contained at least 20 cells which were observed under dissecting microscope. For the CFU-Ob assay, MesenCult medium was switched to osteogenic medium at 14 days for an additional 7 days then analyzed for mineralized matrix by alizarin red staining. An alizarin red positive colony was defined as a CFU-Ob that reacted to alizarin red staining and contained at least 20 cells. We determined the colony-forming efficiency by quantifying the number of colonies per 10^5marrow cell plated.

18. Osteoclast differentiation induction and blocking

To study the AMBN function in osteoclastogenesis *in vitro,* Bone marrow cells were isolated from 5-week old CD1 mice by flushing femurs and tibias with PBS and cultured in α-MEM with 10% FBS, antibiotics and M-CSF (10 ng/ml, R&D systems, Minneapolis, MN) for 1 day. Non-adherent cells were collected and further cultured for 4 days in the presence of M-CSF (10ng/ml). Adherent cells were used as bone marrow monocytes/macrophages (BMMCs). To induce osteoclast differentiation, BMMCs were cultured with M-CSF (10 ng/ml) and RANKL (50 ng/ml, R&D Systems) for 5 days. The differentiated BMMCs were subjected to TRAP staining, actin ring formation and bone resorption analyses. Same method was applied to compare the BMMCs osteoclastic differentiation potential between AMBN mutant littermate mice.

To block osteoclast differentiation, an anti-α2β1 integrin antibody (10 μg/ml, Millipore, Billerica, MA) was used to neutralize the integrin receptors. In addition, PI3K inhibitor

LY294002 (10 μM, Sigma) and the ERK1/2 inhibitor UO126 (10 μM, Sigma) were applied to inhibit PI3K and MER/ERK pathways.

19. Primary mouse bone marrow stromal cell culture

Bone marrow stromal cells(BMSCs) were isolated from femur and tibia of 4-week-old WT, $AMBN^{HET}$ and $AMBN^{\Delta 5\text{-}6}$ mutant mice following the protocol described previously (*130*), and cultured at 2×10^6 nucleatedcells per 10-cm^2 well in α-minimal essential medium (α-MEM) supplemented with 15% FBS (GIBCO, Grand Island, NY). After cells reached confluence, they were cultured in the presence of 10^{-7} M dexamethasone (Sigma-Aldrich,St. Louis, MO), 10 mM β-glycerol phosphate and 50 μM ascorbate-2-phosphate to induce osteoblastogenic differentiation. The medium was changed every third day until day10 for alkaline phosphatase (ALP) staining using alkaline phosphatase magenta immunohistochemical substrate solution (Sigma-Aldrich, St. Louis, MO,USA), and up to 21 days for mineralization assay by alizarin red staining.

For chondrogenesis differentiation, 1×10^6 MSCs resuspend in 5 mL of the pre-warmed completed STEMPRO® Chondrogenesis Differentiation media (GIBCO, Grand Island, NY) in 15 mL centrifuge tube. Centrifuge the cells at 200 g for 5 minutes at room temperature. Loosen the cap of the tube to allow gas exchange and incubate upright at 37° C and 5% CO_2, and refeed cell mass cultures every 3 days. After 21 days cultivation, the chondrogenic pellets were fixed, embeded and processed for Alcain Blue and Safranin O staining.

20. Cell attachment

Adhesion assays were performed using 35 mm untreated culture dishes (Corning, NY). The

dishes were coated with recombinant mouse AMBN (rmAMBN), BSA, or recombinant mouse amelogenin (rmAMEL) proteins at concentrations of 5 or 10 μg/ml at 4 °C overnight, and blocked with 2% denatured BSA at room temperature for 1 h. After washing, 10^6 of BMMCs were seeded into each dish and incubated at 37 °C for 4 h. Nonadherent cells were removed by washing with PBS and the remaining cells were counted under a microscope.

21. F-actin staining

BMMCs were placed in rmAMBN coated 35 mm dishes. To elucidate podosome formation, cells were cultured for 12 h in the coating plate with blocking antibodies or inhibitors. To induce actin ring formation, cells were cultured for 5 days in the presence of M-CSF (10 mg/ml) and RANKL (50 mg/ml). The cultured cells were fixed with 4% paraformaldehyde in PBS, permeabilized with 0.1% Triton-100, and then stained with rhodamine- or FITC-conjugated phalloidin (Sigma). Flourescent images were captured under a Leica DMRX fluorescent microscope.

22. Bone resorption assay

BioCoat Osteologic MultiTest Slides (BD Biosciences, San Jose, CA) were coated with rmAMBN (10 μg/ml). 2×10^3 of BMMCs were seeded into each well and cultured for 5 days with M-CSF (10 ng/ml) and RANKL (50 ng/ml). The cells were removed with 6% NaOCl and each slice was washed with distilled water, air dried and examined for resorption pits.

23. Flowcytometry assay

4-week-old male $AMBN^{\Delta 5\text{-}6}$ and C57BL6 wild-type mice were sacrificed by CO_2. The

femurs and tibias were dissected and bone marrow was flushed out by a fine gauge needle with PBS. Single-cell suspensions were obtained by pipetting and filtering with 40 μm cell strainer. Red blood cells were lysed from the collected bone marrow cells with red blood cell lysis buffer (eBioscience, San Diego).Bone marrow nucleated cells were then resuspended at 2×10^6 cells/ml in PBS with 1%FBS. The cells were incubated for 30 minutes at 4°Cin dark with a fluorescently conjugated anti-mouse monoclonal antibody against CD105 and CD106 (eBioscience, San Diego), and the corresponding isotype control IgGs. All analyses were done on CyAn ADP analyzer (Beckman Coulter) at UIC RRC core facility.

24. RT^2 profiler PCR array assay and quantitative RT-PCR

After been treated with osteogenic medium for 7 days, total RNA was isolated from BMSCs by RNeasy Plus Mini Kit (QIAGEN, Maryland) according to the manufacturer's instructions. Two micrograms of total extracted RNA was applied toward genomic DNA elimination and cDNA generation with RT^2 First Strand Kit (QIANGEN, Maryland). Specimens were analyzed using the mouse pathway-focused osteogenesis PCR array (QIANGEN). Briefly, the cDNA samples of the specimens from BMSCs of AMBN WT and $AMBN^{\Delta 5\text{-}6}$ mutants were added to the RT^2 qPCR master mix containing SYBR Green and reference dyes. The above mixture was then aliquoted across the PCR array template (QIAGEN) which contained 84 mouse osteogenesis pathway-specific genes plus controls. The real-time PCR analysis was carried out using an ABI 7000 sequence detector (Applied Biosystems, Foster, USA). Relative gene expression values were analyzed using the Superarray web-based software package performing all $2^{-\Delta\Delta Ct}$ based fold-change calculations, which sets change of at least 2-fold as the "cutoff" value for the transcripts being differentially expressed in the experimental groups. To confirm the genes

expression we identified by RT^2 PCR array, we performed RT-real-time PCR using sequence-specific SYBR green primers (Table III) and ABI 7000 detection system. GAPDH was used as endogenous control. Relative expression level were calculated by $2^{-\Delta\Delta Ct}$ method mentioned previously.

25. BrdU staining and cell proliferation assay

3-week-old $AMBN^{WT}$, $AMBN^{HET}$ and $AMBN^{\Delta 5\text{-}6}$ littermates were injected with BrdU (Sigma) (100mg/kg) intraperitoneally 1 hour prior to euthanization to label the proliferating chondrocytes in growth plate. Tibias and femurs were dissected and processed for paraffin sections subsequent to demineralization. The sections were stained with BrdU staining kit (Invitrogen). Cell proliferation assay was performed by MTT assay. Before termination of culture, cells were incubated in MTT solution (2mg/ml of MTT in αMEM with 5% FBS) for 4 hours. To quantify proliferative activity, the MTT stained cells were lysed in HCL/Isopropanol and absorbance was detected at 450 nm with background substraction.

26. Tooth movement treatment

6-week-old male AMBN TG and WT mice were used in tooth movement experiment. Anesthesia was accomplished using Ketamine (100 mg/kg) and Xylazine (5 mg/kg). In order to create lateral movement, the expansion wire placed on the mandibular incisor was fixed by composite resin to provide sufficient orthodontic force. Mandibular first molars at both sides were horizontally expanded toward buccal side with 20 g. Two genotype groups of 3 mice in each were maintained in tooth expansion for period of 7 day, after which they were sacrificed by CO_2. Mandibles were collected, fixed and decalcified for paraffin based sectioning.

27. Bone fracture healing model

The procedures conducted in this surgical study were approved by the Animal Ethics Committee of Jilin University and were carried out according with the Guidelines for the care and use of laboratory animals. A unilateral left side open transverse tibia fracture with intramedullary needle fixation will be selected as the bone fracture model in this study (*131*). Two-month old male mice will be anesthetized with ketamine (100mg/kg) by intraperitoneal injection. An electric hair shaver will be used to make the operation field free of covering fur. Surgeries will be then performed under aseptic conditions. A 1.5 cm long skin incision was made along the antero-medial surface of the tibia. At the medial side of the patellar ligament, a 27 gage syringe needle will be inserted into the bone marrow cavity of the tibia through the tibial plateau, by which a pin canal was well established and the marrow cavity was suitable enlarged. The needle is then removed, and a No.11 surgical blade was used to transect the diaphysis of the tibia at the middle point of the diaphysis shaft, following by selecting and inserting a syringe needle varying from 25 to 27 gages, whichever fits the bone marrow cavity well to stimulate fixation of the intramedullary needle. The distal tip of the syringe needle was ensured to reach the narrowest point of the marrow cavity of tibia. The periosterum remained intact and soft tissues will be well protected and the fibula will be carefully preserved to be unabridged. The pin beyond the cortex of the tibial plateau will be cut off within 2mm by a wire-cutter. A 4.0 silk suture will be used to close the wound and buprenorphine will be administrated by intraperitoneal injection for pain relief for the first three days after the operation Both AMBN$^{\Delta 5\text{-}6}$ mutant and control mice were sacrificed post-operatively by time points day 7, 14, 21 and 28 day to obtain tibial samples from the operation side. During the procedure, callus tissue was carefully protected and the intramedullary needle was removed. Samples harvested will be analyzed by X-ray, micro-CT and

histology.

28. Statistical analysis

Quantitative data were presented as means ± SD and compared with analysis of one way ANOVA. The difference between groups was considered statistically significant at $p< 0.05$.

III. RESULTS

A. AMBN-rich enamel matrix favors short and randomly oriented apatite crystals

A.1. Generation of mutant mice expressing an AMBN-enriched enamel matrix that lacks AMELX

Four different mouse models were used to determine the effect of AMBN on enamel crystal growth: (i) an AMBN-overexpressing mouse in which the *Ambn* gene was driven by a K14 promoter (AMBN TG), (ii) an AMBN-overexpressing mouse crossed with an *Amelx* null mouse to remove the AMEL background in the developing enamel matrix (AMBN TG × amelx$^{-/-}$), (iii) an *Amelx* null mouse as a control for the loss of AMELX (amelx$^{-/-}$), and (iv) a wild-type control of the same strain (WT; FVB) (Fig. 1). Western blot analysis using our anti-AMBN IgG on mouse molar extracts revealed elevated levels of AMBN expression in AMBN TG mice as well as in AMBN TG × amelx$^{-/-}$ mice, while the expression levels of AMBN in WT mice and amelx$^{-/-}$ mice were relatively lower (Fig. 1B). Specifically, AMBN protein levels in AMBN overexpressors were 6.5-fold higher compared with wild-type controls, and AMBN protein expression in AMBN TG × amelx$^{-/-}$ mice was 2.78-fold higher than in amelx$^{-/-}$ mice and 8.56-fold higher than in WT controls, as revealed by densitometry (Fig. 1B, C). The levels of AMELX protein in a second set of western blot results, using AMELX as the primary antibody, demonstrated that neither amelx$^{-/-}$ mice nor the AMBN TG × amelx$^{-/-}$ tested positive for AMELX, while AMELX was present in WT and AMBN TG mice (Fig. 1C). Together, these results indicate that we have generated a mouse model (AMBN TG × amelx$^{-/-}$) with an enamel matrix enriched in AMBN and lacking AMELX.

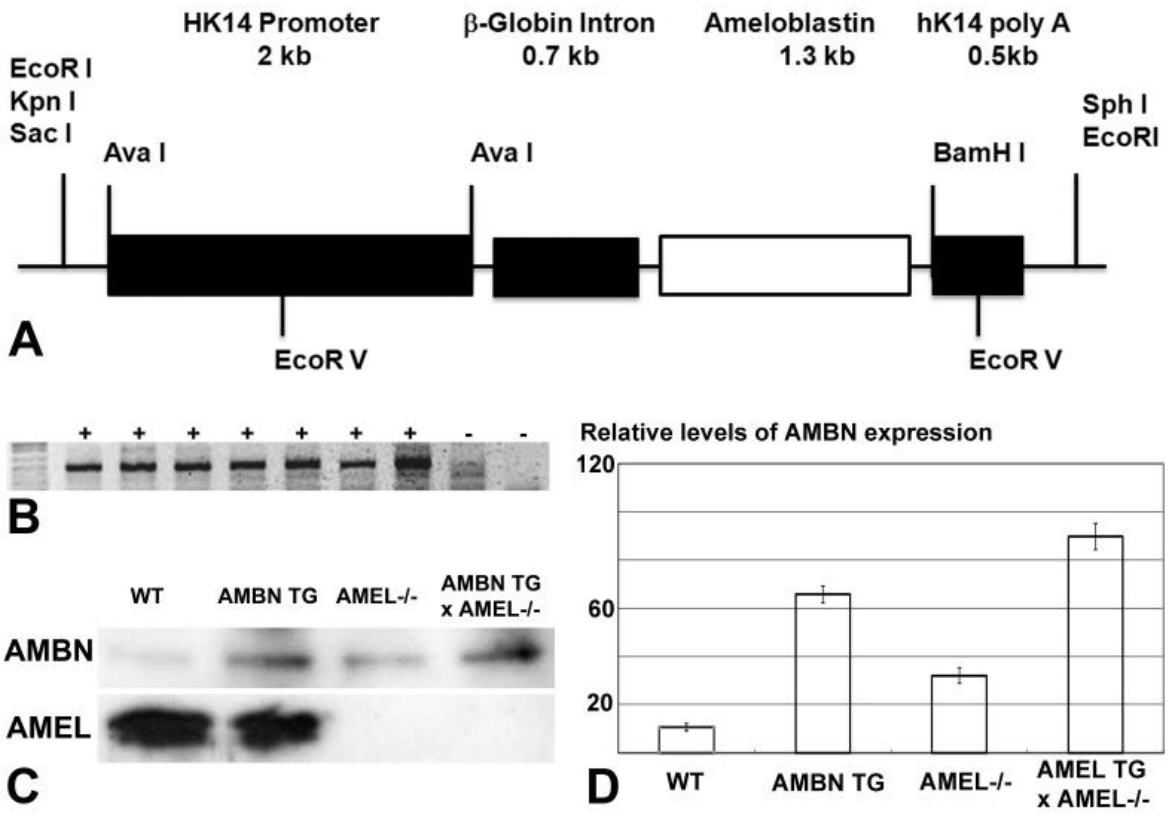

Figure 1. Generation of mutant mice expressing an ameloblastin (AMBN)-enriched enamel matrix. (A) Construct used for the generation of AMBN overexpressing mice using a keratin 14 (K14) promoter to drive the AMBN transgene. (B) PCR genotyping results for the identification of offspring carrying the AMBN transgene. (C) Western blot comparison of AMBN and amelogenin (AMELX) expression among the following groups of mice: wild-type (WT); AMBN overexpressor (AMBN TG); AMELX null (amelx$^{-/-}$); and AMBN overexpressor crossed with AMELX null (AMBN TG × amelx $^{-/-}$). (D) Densitometry evaluation of relative levels of AMBN expression. Values represent mean ± SD. h = human.

A.2. SEM of wild-type and AMBN-enriched enamel matrix

Scanning electron microscopy was performed to compare the developing enamel of WT, AMBN TG, amelx$^{-/-}$, and AMBN TG × amelx$^{-/-}$ mice. Compared with the enamel of WT mice and AMBN TG mice, the enamel thickness of amelx$^{-/-}$ mice and AMBN TG × amelx$^{-/-}$ mice was reduced by approximately 10-fold and elaborate prism patterns were replaced by simple pyramids formed by individual crystals (Fig. 2). Moreover, there was a highly significant decrease in enamel prism diameter between WT controls and AMBN TG overexpressors, from 2.38 ± 0.51 to 1.32 ± 0.34 μm ($p < 0.05$) (Fig. 2).

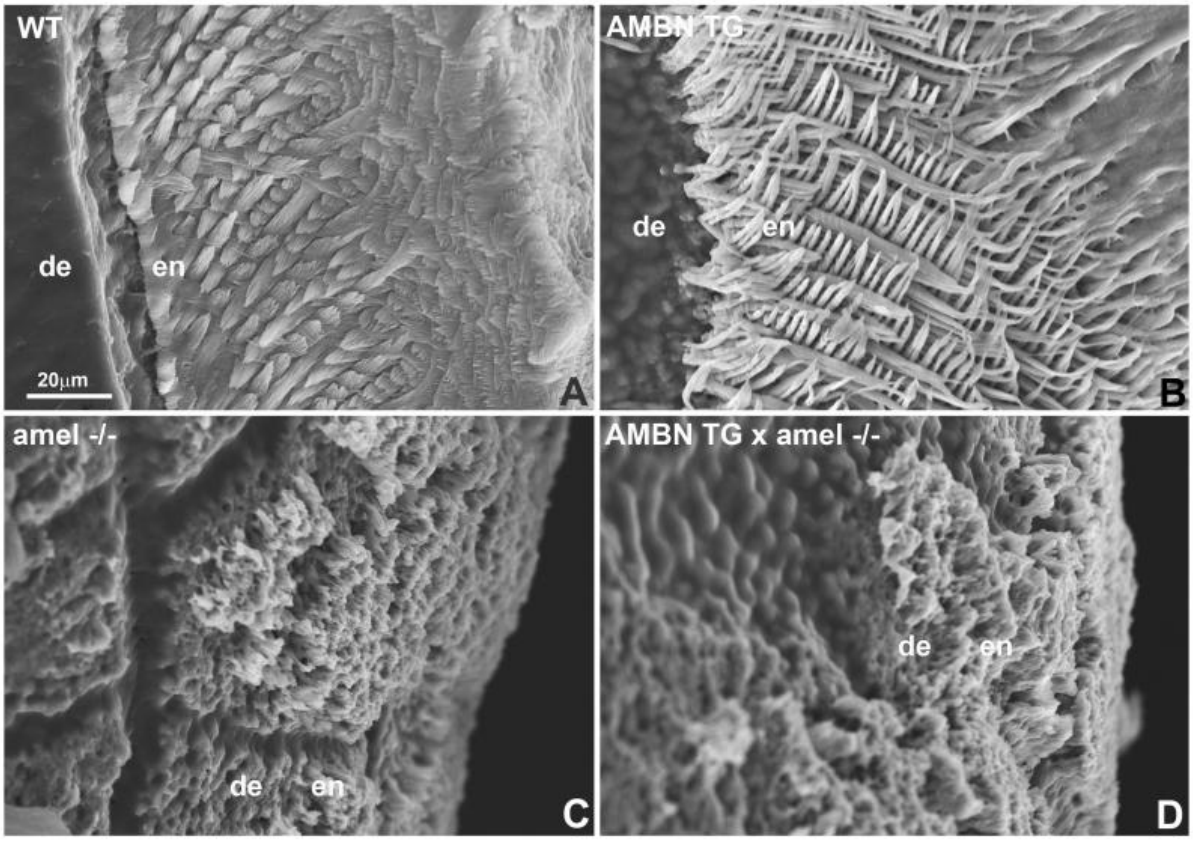

Figure 2. Scanning electron microscopy images of etched mouse first mandibular molar distal slope enamel. Samples were from (A) wild-type mice (WT), (B) ameloblastin over-expressor mice (AMBN TG), (C) amelogenin null mice (amelx $^{-/-}$), and (D) AMBN overexpressor mice crossed with AMELX null mice (AMBN TG × amelx $^{-/-}$). de, dentin; en, enamel.

.

A.3. Comparison between *Iguana* enamel and mouse enamel lacking AMELX

Scanning electron micrographs of *Iguana iguana* tooth crowns revealed a partial covering of the tip of the *Iguana* tooth crown with a thin layer of short enamel crystal patches (Fig. 3). At high magnification, *Iguana* enamel was organized into short and thin enamel crystal bundles, oriented perpendicularly to the enamel surface, comparable in morphology to those found on the enamel surface of amelx$^{-/-}$ mice and AMBN TG × amelx$^{-/-}$ mice (Fig. 3).

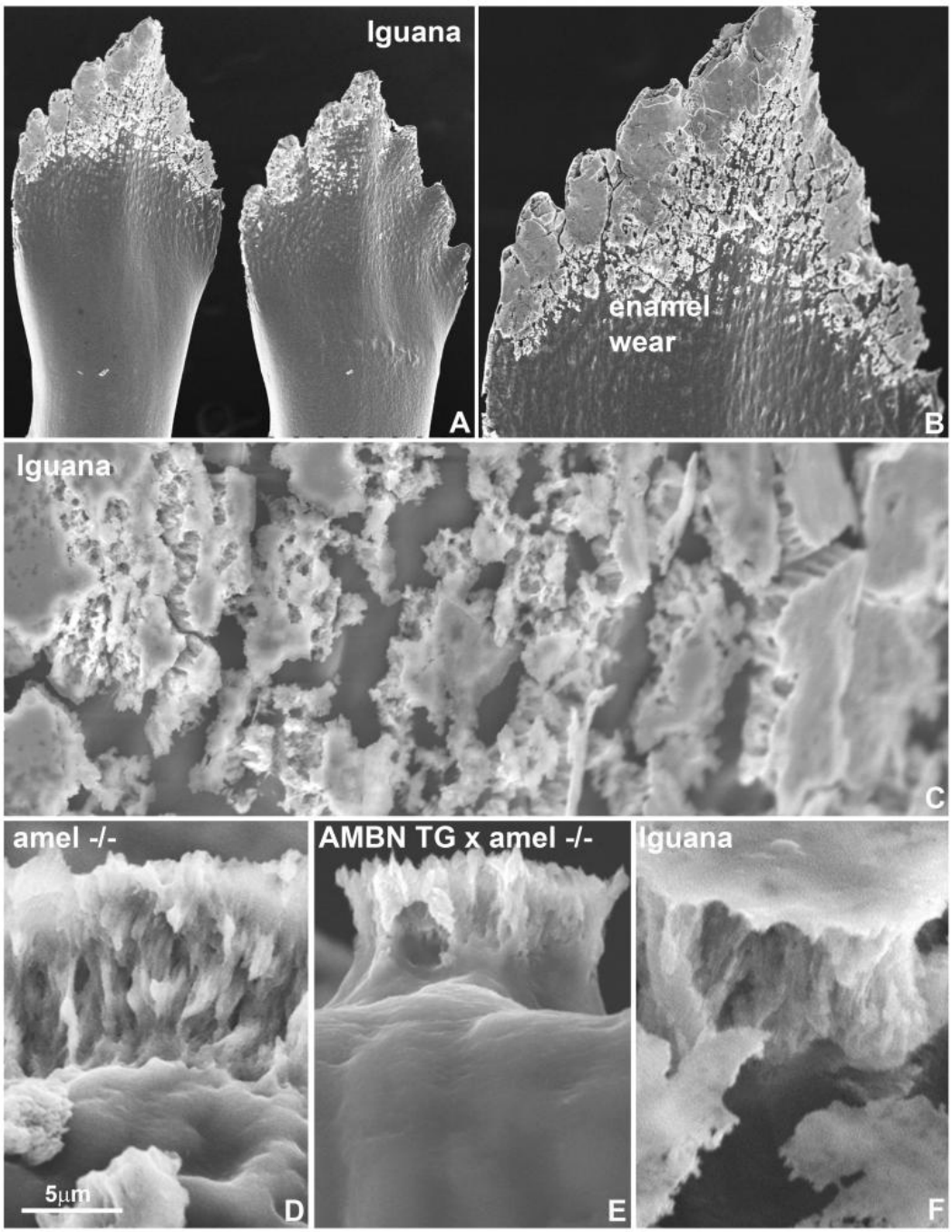

Figure 3. Comparison of scanning electron microscopy images of *Iguana* enamel and mutant mouse enamel. (A–C) Scanning electron microscopy images of *Iguana iguana* tooth crowns. Note the pronounced wear pattern on *Iguana* enamel surfaces (B) and the presence of a thin layer of short enamel crystal patches (C). Scanning electron microscopy images taken tangentially to the crown surface of the enamel of amelogenin null mice (amelx$^{-/-}$) (D), ameloblastin overexpressor mice crossed with AMELX null mice (AMBN TG × amelx $^{-/-}$) (E), and *Iguana* (F). Bar = 5 μm.

A.4. Comparison, by TEM, between enamel crystal structure and organization from WT and AMBN TG mice

Enamel crystals from AMBN TG × amelx$^{-/-}$ mice were short and randomly oriented compared with enamel crystals from WT, amelx$^{-/-}$, and AMBN TG mice (Fig. 4). Crystals from AMBN TG × amel$^{-/-}$ mice measured 72.2 ± 22.9 nm (and were therefore similar to *Iguana* crystals, which measured 73.5 ± 11.2 nm), whereas all three control groups were found to have significantly longer crystals: 322.5 ± 92.1 nm in the WT mice, 542.3 ± 143.2 nm in the AMBN TG mice, and 336.5 ± 69.1 nm in the amelx$^{-/-}$ mice. Differences in crystal dimension between WT mice and AMBN TG mice were significant ($p < 0.05$); and differences in crystal dimension were highly significant ($p < 0.01$) between WT mice and AMBN TG × amel$^{-/-}$ mice and between WT mice and *Iguana*. At high magnification, the short and randomly oriented enamel crystals in the AMBN TG matrix resembled those in the enamel matrix of the *Iguana* (Fig. 4).

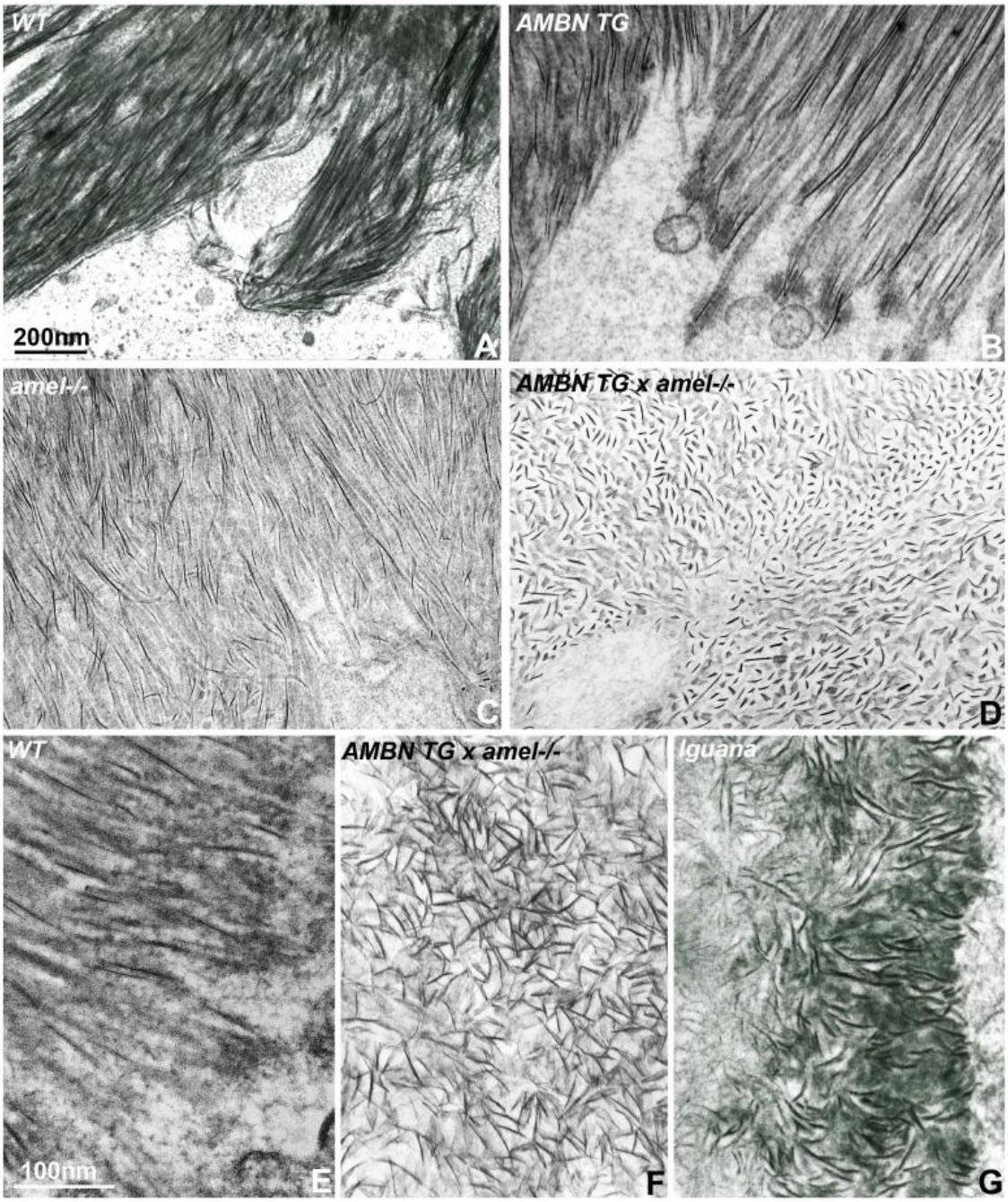

Figure 4. Transmission electron microscopy images of enamel crystal organization following transgenic modulation of the enamel matrix ameloblastin content in first mandibular molars of 3 d postnatal mice. (A) Wild-type mice (WT) (B), AMBN overexpressor mice (AMBN TG), (C) amelogenin null mice (amelx$^{-/-}$), and (D) AMBN overexpressor mice crossed with AMEL null mice (AMBN TG × amelx $^{-/-}$). Bar = 200 nm for (A)–(D). Comparison between high-magnification electron micrographs of WT mouse enamel (E), AMBN TG × amelx $^{-/-}$ enamel (F), and *Iguana iguana* enamel (G). Bar = 100 nm for (E)–(G).

B. AMBN modulates osteoclastogenesis through the integrin/ERK pathway

B.1. AMBN is expressed in Hertwig's Epithelial Root Sheet (HERS) and in the periodontal ligament of mouse molar teeth

Our interest in AMBN in the periodontium was peaked by a dramatic increase in AMBN expression in the Epithelial Rests of Malassaz (ERM) during tooth movement or after mechanical injury of cementum (*55, 132*). As a first step to understand AMBN function in the periodontal ligament, the temporo-spatial expression pattern of AMBN was mapped during tooth development. Using in situ hybridization analysis, AMBN mRNA was prominently localized in ameloblasts and HERS (Fig. 5A) as well as ERM (Fig. 5D). ERM were identified as islands of cuboidal cells aligned parallel to the root surface in the midst of elongated periodontal ligament fibroblasts. Lower levels of mRNA were also detected in odontoblasts and dental pulp on postnatal day 12 (Fig. 5). AMBN mRNA was substantially enhanced in AMBN transgenic (TG) mice (Fig. 5 B). No signal was detected in the control, in which *Ambn* sense RNA was used as a probe (Fig. 5 C).

As a second step in our analysis of AMBN expression and function in periodontal tissues AMBN overexpressing transgenic mice driven by the human K14 promoter (*133*) were generated. To verify overexpression of the K14-driven transgene in HERS and ERM, a K14-LacZ transgenic mouse model was also created. Whole mount X-gal staining demonstrated the localization of the transgene in HERS and ERM cells (Fig. 5E). Immunohistochemistry analysis revealed distinct staining for AMBN protein in ERM cells and surrounding periodontal ligament of postnatal day 35 WT and TG mice, and ERM staining intensity was higher in TG mice than in WT counterparts (Figs. 5 F, G). Our immunohistochemical data indicated that AMBN protein expression in ERM cells was higher than in surrounding periodontal ligament cells, especially

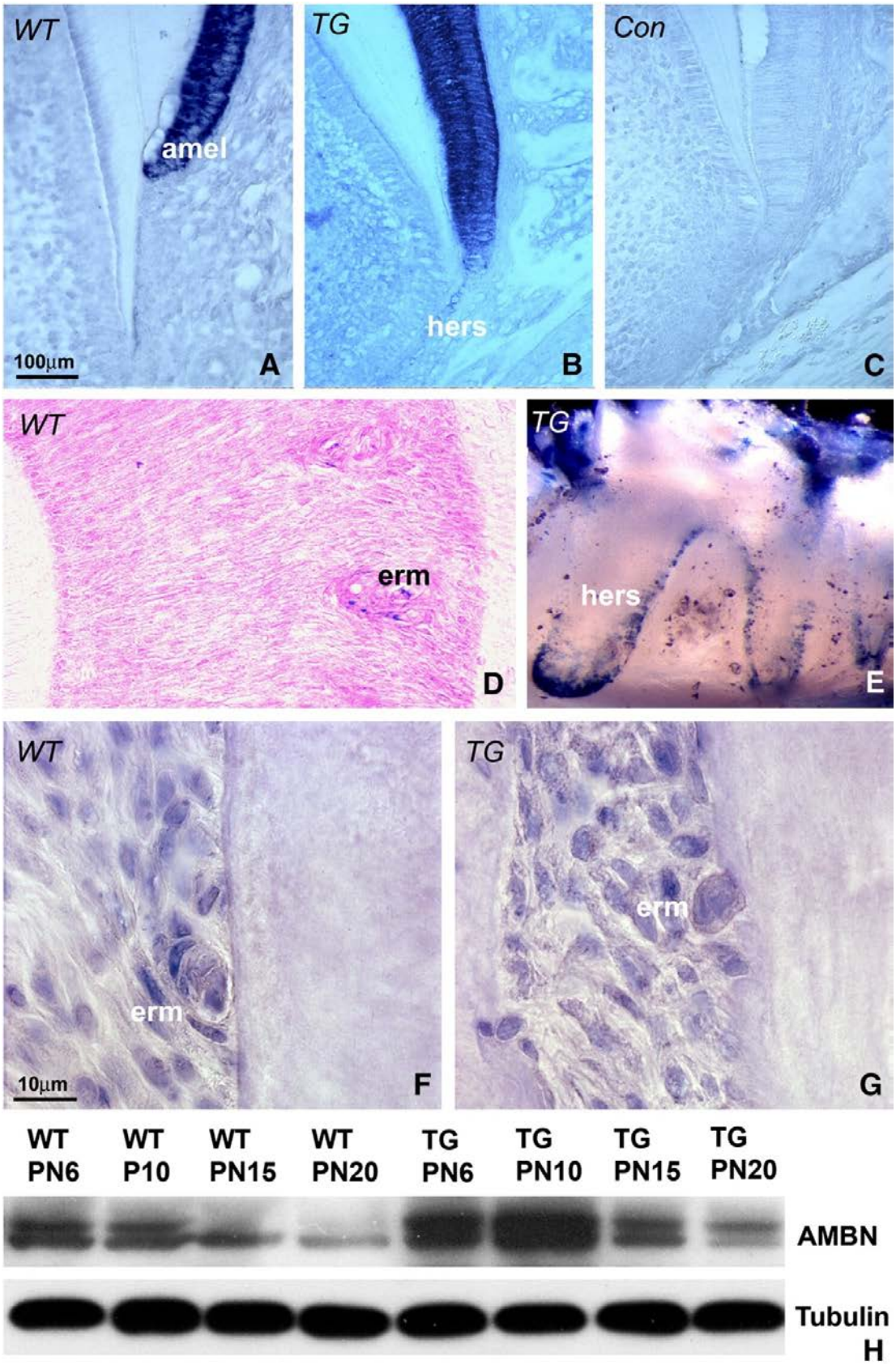
WT
amel
100μm
A
TG
hers
B
Con
C
WT
erm
D
TG
hers
E
WT
erm
10μm
F
TG
erm
G
WT PN6
WT P10
WT PN15
WT PN20
TG PN6
TG PN10
TG PN15
TG PN20
AMBN
Tubulin
H

Figure 5. AMBN expression in postnatal developing molar teeth. (A–D) *Ambn* mRNA *in situ* hybridization analysis in mouse molars. Paraffin sections of 12 day postnatal wild-type (A) transgenic (B), and 35 day postnatal WT (D) mouse molars were hybridized against mouse antisense AMBN coding region, and the sense AMBN served as a control (C). (E) X-gal staining of oral epithelial cells and ERM/HERS (blue color) in LacZ transgenic mice. (F and G) Immunohistochemistry analysis of AMBN protein expression in PN 35 mouse molars. Immunoreactivity for the AMBN protein was visible as brown staining in the periodontal ligament and at higher levels in ERM. (H) Changes in AMBN expression in transgenic (TG) and wild-type (WT) molars as revealed by Western blot. Mouse molars from postnatal day 6 (PN6), day 10 (PN10), day 15 (PN15) and day 20 (PN20) were used for analysis. Molecular weights of the expressed AMBN proteins are 55 and 50 kDa. β-Tubulin was applied as a protein loading control. *amel* = ameloblasts, *hers* = Hertwig's Epithelial Root Sheath, *erm* = epithelial rests of Malassez.

in AMBN overexpressing mice. To quantify the expression of AMBN in developing mouse teeth, protein was extracted from molars and surrounding tissues at subsequent stages of periodontal development (postnatal days 6–20). Western blot analysis revealed two bands corresponding to the AMBN protein, one with a higher molecular weight at 55 kDa and a second with a lower molecular weight at 50 kDa (Fig. 5 H). The expression of AMBN gradually decreased from PN6 to PN20 in WT and TG mice (Fig. 5 H). Furthermore, densitometry analysis on Western blots revealed that on postnatal day 10, AMBN was five times higher expressed in AMBN overexpressing mice than in WT controls.

Immunofluorescence-based comparison of AMBN and K14 localization in 10 days postnatal developing tooth roots demonstrated co-localization of both proteins in HERS cells (Fig. 6 A–D). There were strings of small patches of overlapping AMBN/K14 labeling along the HERS cell membrane (Fig. 6 D). Cultured alveolar bone osteoblasts stained for both AMBN and K14 (Fig. 6 E–H). There was an intense intracellular AMBN labeling in the periphery of the nuclear envelope (Fig. 6 E).

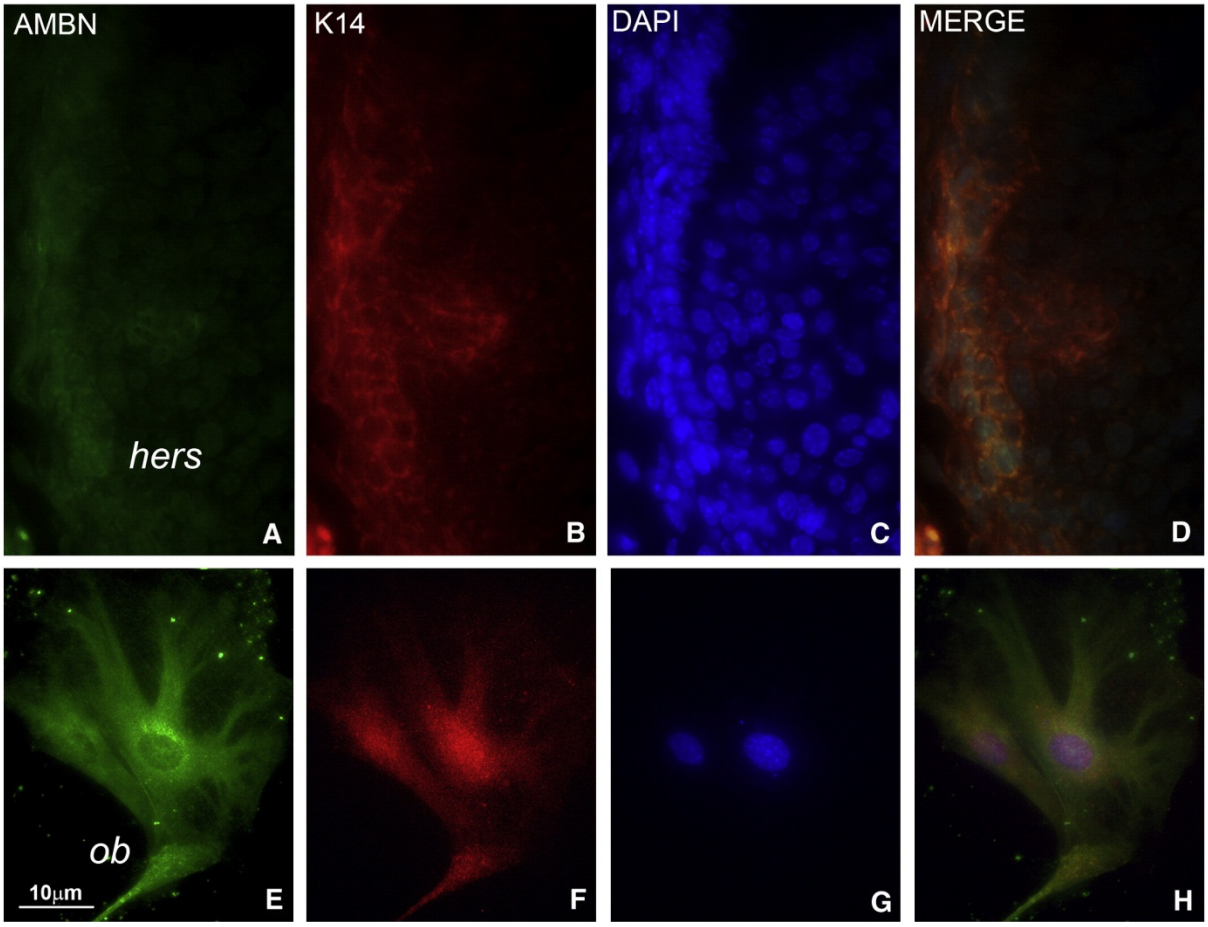

Figure 6. Co-localization of AMBN and Keratin 14 in Hertwig's Epithelial Root Sheath and in alveolar bone osteoblasts. (A–D) AMBN (A), Keratin 14 (B), and DAPI (C) triple fluorescent staining in Hertwig's Epithelial Root Sheath (hers). (D) is an overlay image. Hertwig's root sheath is the bilayered epithelium on the left side of the image. Green fluorescence for AMBN and red fluorescence for K14 were detected in HERS cells (A, B). Note the strong yellow label in patches along the HERS cell membrane indicating presence of both AMBN and K14 (D). (E–H) AMBN (E), Keratin 14 (F), and DAPI (G) triple fluorescent staining in alveolar bone osteoblasts (ob). (H) is an overlay image. Alveolar bone osteoblasts were stained for both AMBN (green label, E) and K14 (red label, F). Note the intense reaction for AMBN in the periphery of the nuclear envelope (E). *hers* = Hertwig's Epithelial Root Sheath, *ob* = alveolar bone osteoblasts.

B.2. AMBN overexpression induces alveolar bone loss and tooth root resorption

Enamel of AMBN transgenic mice featured a dull surface and yellowish color (Fig. 7 B), indicating that our AMBN overexpression model was associated with an enamel defect. Whole mount alizarin red staining revealed that the AMBN overexpressor suffered from significant bone loss at the crest of the alveolar bone as well as an increase in the periodontal ligament thickness (Fig. 7 B). Alveolar bone loss was most prominent at the crest of the first root of the first molar (Fig. 7 B). Micro-CT analysis revealed a reduction in alveolar bone wall thickness when comparing TG to WT counterparts (Fig. 7 D versus Fig. 7 C). Scanning electron microscopy revealed a smooth root surface in the control molars (Fig. 7 E) compared to a relatively rougher surface with root resorption lacunae on the AMBN over-expressing molar roots (Fig. 7 F). Micro-CT 3D-images of the molar-region dentoalveolar complex of wild-type ((Fig. 7 G) and AMBN transgenic mice (Fig. 7 H) revealed widened alveolar crypts, roughened alveolar bone surfaces, and reduced interradicular spaces in AMBN overexpressors (Figs. 7 H versus G). The bone morphometric comparison demonstrated significantly reduced trabecular bone volume (BV/TV), bone mass density (BMD), trabecular number, and trabecular thickness ($p < 0.05$) in AMBN transgenic versus WT mice (Fig. 7 I). The approximately 10% reduction in trabecular bone volume and bone mass dentistry as a result of AMBN gain of function was a sizable and significant ($p < 0.05$) effect. In contrast, bone surface/volume ratio (BS/BV) increased slightly and significantly ($p < 0.05$) in AMBN overexpressors, while trabecular separation increased as well, but the difference was not significant (Fig. 7 I).

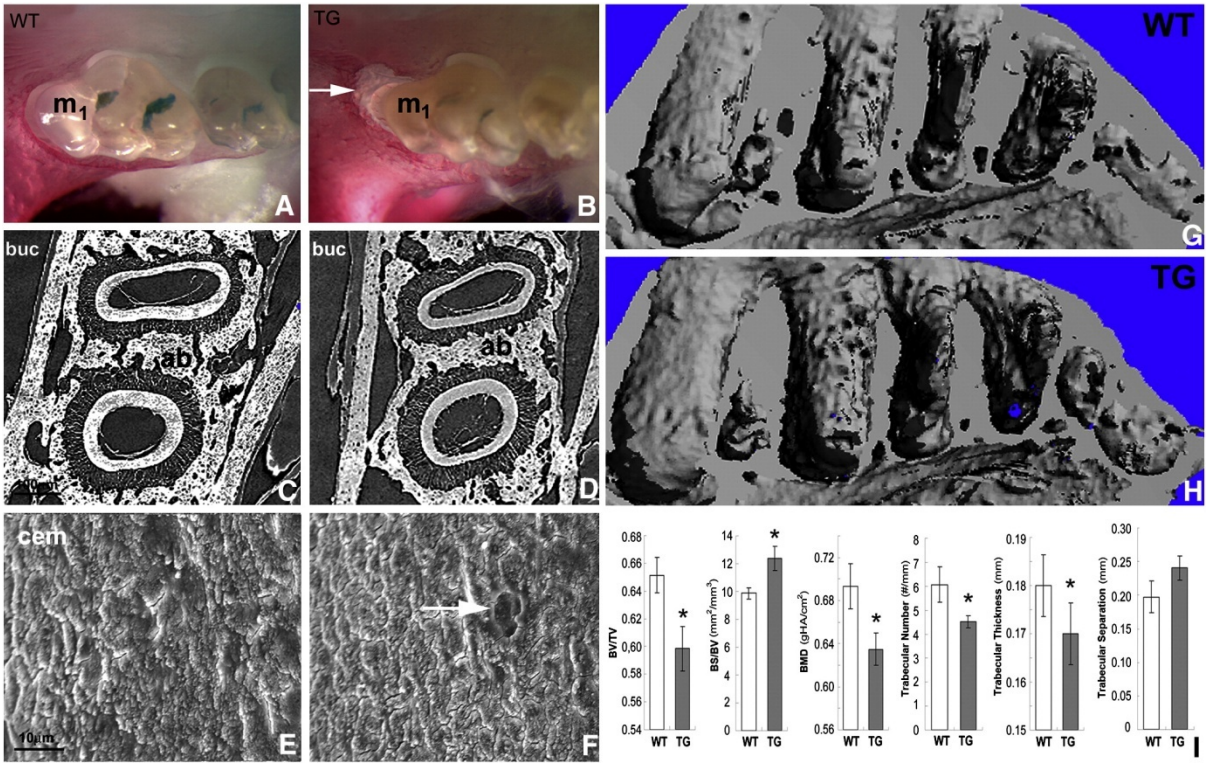

Figure 7. Bone loss and root resorption in AMBN overexpressor molars. (A, B) Whole-mount alizerin red staining of mandibles from AMBN transgenic (TG) and wild-type (WT) mice at 35 days postnatal. First molars are marked M1. Note the significant bone loss at the crest of the alveolar bone (arrow) as well as the increase in periodontal ligament width in AMBN transgenic mice as compared to wild-type controls. (C, D) Micro-CT comparison of root sections of WT and TG mice. (E, F) Scanning electron microscopy images of molar teeth of 35 days old WT and AMBN transgenic mice. The arrow indicates a resorption pit on the TG molar root. (G, H) 3D μ-CT image reconstruction of the molar-region dentoalveolar complex of wild-type (G) and AMBN transgenic mice at age 42 days postnatal (H). Note the widened alveolar crypts, roughened alveolar bone surfaces, and reduced interradicular spaces in AMBN overexpressors (H versus G). Morphometric comparison between AMBN transgenic and WT mice. The following parameters were compared (3 samples per group, from left to right): trabecular bone volume fraction (BV/TV), surface/volume ratio (BS/BV), bone mass density (BMD), trabecular number, trabecular thickness, and trabecular separation. All but the trabecular separation were significantly different ($p < 0.05$) between both groups. * = $p < 0.05$.

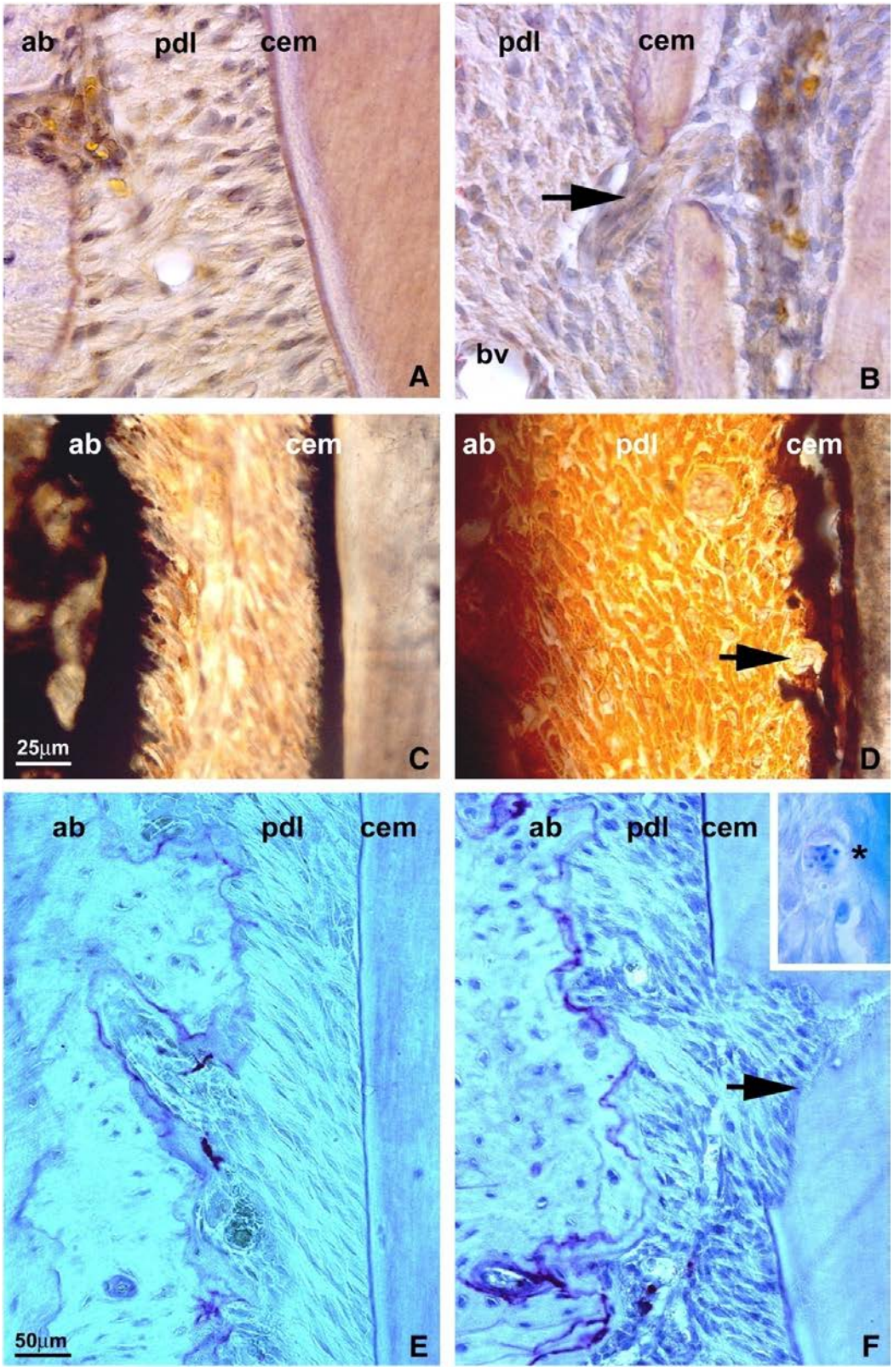
ab
pdl
cem
A
pdl
cem
bv
B
ab
cem
25μm
C
ab
pdl
cem
D
ab
pdl
cem
50μm
E
ab
pdl
cem
*
F

Figure 8. Changes in osteoclast activity in the periodontal ligament of AMBN overexpressor mice. (A, B) Representative histological sections of molars from WT (A) and AMBN overexpressor (B) postnatal day 35 mice. The arrow points to a perforated mineralized tissue layer in AMBN TG mice that was sufficiently disrupted to allow periodontal fiber insertions between dental pulp and ligament. (C–D) von Kossa staining of mouse molar roots sectioned through the acellularcementum region of the cervical roots of WT (C) and AMBN overexpressor (D) mice on postnatal day 35. There were de-laminations of acellularcementum in Ambn overexpressing mice (cem) and giant cells on the root surface of AMBN mutant mice (arrow). (E, F) TRAP staining of molar sections of WT (E) and AMBN overexpressor (F) mice. Arrows indicate osteoclast activity. The inset in (F) illustrates the presence of cementoclasts on the root surface of postnatal day 15 AMBN TG mice (asterisk marking cementoblast and adjacent lacuna of tooth surface). These were not found in WT mice. *ab* = alveolar bone, *pdl* = periodontal ligament, *cem* = cementum, *bv* = blood vessel.

B.3. AMBN overexpression is associated with increased osteoclast/cementoclast activity

Villanueva's Osteochrome staining of ultrathin ground sections demonstrated an acellularcementum layer featuring a homogeneous structural integration with the underlying root dentin in controls (Fig. 8 A). A number of layers displayed metachromatic colorations, and transitions occurred gradually between each layer (Fig. 8 A). In *Ambn* over-expressing transgenic mice, the junction between acellularcementum and dentin was disrupted (Fig. 8 B). There was an open channel between periodontal ligament and dental pulp with a group of periodontal fibroblasts crossing in between (Fig. 8 B). Von Kossa staining of WT mouse molars at PN 35 revealed a dark brown and intact acellular cementum surface (Fig. 8 C), while acellular cementum was de-laminated from the root surface in *Ambn* over-expressing mice (Fig. 8 D). In addition, a few giant cells were attached on the surface of the acellular cementum (Fig. 8 D). In tandem with increased root resorption, TRAP staining of molar root sections indicated higher osteoclast activity in the periodontal ligament of AMBN overexpressors (Fig. 8 F) than in that of WT mice (Fig. 8 E). Resorption areas in PN 35 AMBN overexpressors were explained by multiple cementoclasts present on the surfaces of PN 15 AMBN overexpressor molar roots (Fig. 8 F, insert), and cementoclasts were absent on WT PN 15 controls (not shown).

B.4. AMBN modulates RANKL-stimulated osteoclastogenesis *in vitro*

Our findings in AMBN overexpressing mice indicated that increased AMBN levels were associated with enhanced osteoclast activity and mineralized tissue resorption. To determine the role of AMBN on mineralized tissue dynamics *in vivo*, studies were designed to test AMBN's function as an extracellular matrix mediator in osteoclasts and their precursors. In these studies, the interaction between cells and AMBN was mimicked in an *in vitro* model system, in which untreated culture dishes were coated with AMBN at two different concentrations. The effect of AMBN on RANKL induced osteoclast differentiation was evaluated after BMMCs were subjected to BSA- or AMBN-coated cell culture plates or calcium-phosphate substrate, and cultured in the presence of RANKL (50 ng/ml) and CSF-1 (10 ng/ml) for 5 days. The number of multi-nuclear and TRAP-positive osteoclasts was increased by 3.45-fold upon AMBN treatment (Figs. 9 A, B and E). In addition to its effect on osteoclast size and number, AMBN also had significant impact on bone resorbing activity as determined by the number and area of resorption pits on Biocoat-treated culture dishes (Figs. 9 C, D), resulting in 4.7-fold higher pit numbers and 4.01-fold increased resorption pit area following AMBN treatment (Figs. 9 F, G).

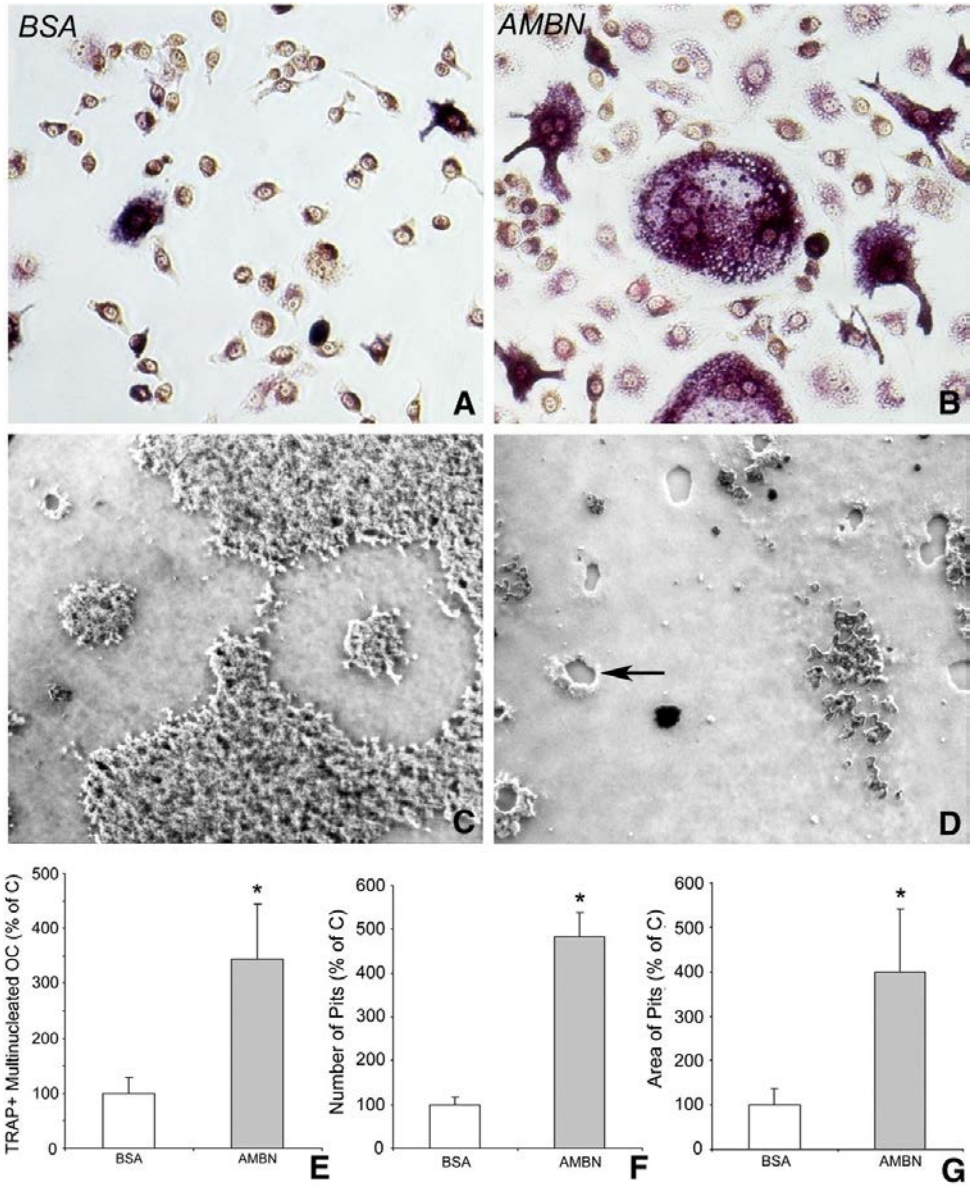

Figure 9. AMBN modulation on osteoclast differentiation *in vitro*. Osteoclast formation was induced from BMMCs cultured on BSA or AMBN coated culture dishes or calcium-phosphate substrate with CSF-1 (10 ng/ml) and RANKL (50 ng/ml) for 5 days. (A and B) TRAP staining showed a pink cytoplasm in multinucleated cells, indicative of mature osteoclasts. (E) Comparison of TRAP-positive/multinucleated cell density between treatment groups. Data are presented as mean ± SD for four different cultures. (C and D) Effect of AMBN on the ability of differentiated osteoclasts to form resorption pits. The phase contrast microscopy images showed a comparison between AMBN and BSA treated bone matrix (Biocoat™) subjected to BMMCs and osteoclast induction conditions. Note the presence of resorption pits (arrow) in the AMBN treated group. (F and G) The number and area of resorption pits in the AMBN treatment group are presented as percentage of the control group. * = $p < 0.05$.

B.5. AMBN enhances BMMC adhesion and induces adhesion-dependent phosphorylation of ERK and AKT

Previous studies have highlighted the role of AMBN as an extracellular adhesion molecule (*60*). We therefore hypothesized that AMBN might exert its effects on osteoclastogenesis and mineral homeostasis through cell adhesion related mechanisms. In support of this concept, AMBN treatment significantly enhanced adhesion of both Raw cells (data not shown) and BMMCs (Fig. 10 A), and this effect was dosage-dependent (Fig. 10 A). Both BSA and recombinant mouse amelogenin (rmAMEL, another enamel matrix protein) were used as controls and did not affect cell adhesion (Fig. 10 A).

Adhesion of cells to ECM initiates signaling pathways which lead cellular spreading and polarization. Potential intermediaries that might modulate the effect of AMBN on BMMCs include extracellular-signal-regulated kinases (ERK) and phosphatidylinositol 3-kinases (PI3K), both of which have been implicated in the regulation of cell adhesion and osteoclastogenesis and act as second messengers (*134*, *135*). To determine whether AMBN affects ERK and PI3K pathways, ERK1/2 and AKT phosphorylation was examined by Western blot. Our study indicated that AMBN treatment enhanced ERK 1/2 and AKT phosphorylation 15 min after cell seeding. The level of ERK1/2 phosphorylation was 1.6-fold and AKT phosphorylation was 2.3-fold higher in the AMBN treated group than in the BSA group (Fig. 10 B, $p < 0.05$). Fold increase in ERK1/2 phosphorylation was calculated from the sum of the bands detectable on the Western blot and from three independent experiments.

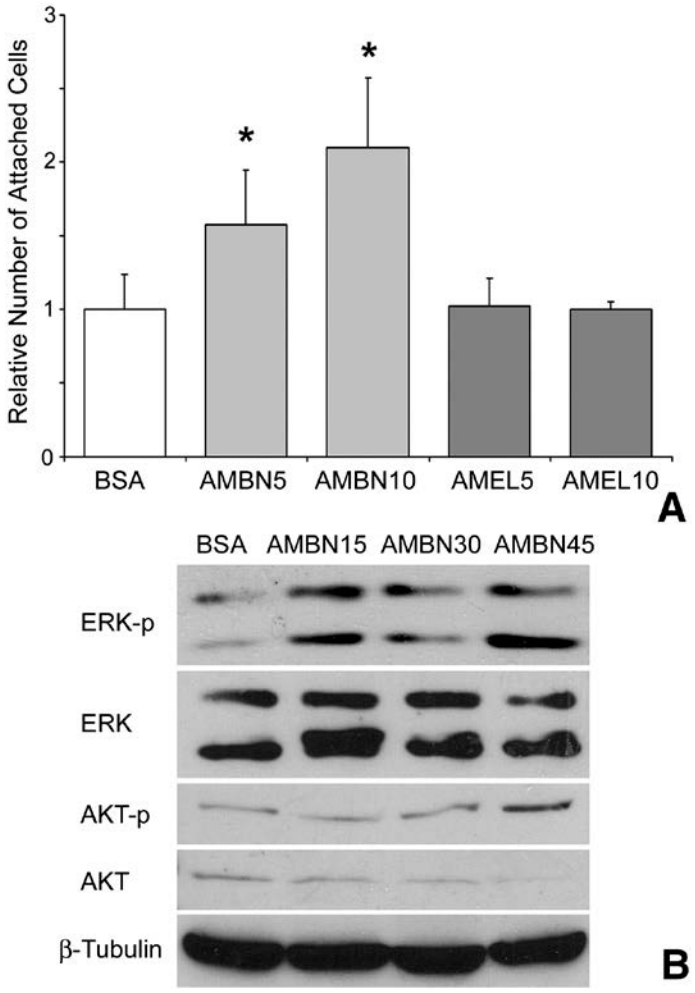

Figure 10. Role of AMBN in BMMC adhesion. BMMCs were seeded onto culture plates that were coated with AMBN or AMEL at two different concentrations, and blocked with BSA. (A) Adhesion of BMMCs on BSA, AMBN or AMEL coated plates. The number of attached cells was counted after 4 h of culture. AMBN5/AMEL5 contained 5 μg/ml and AMBN10/AMEL10 contained 10 μg/ml of the recombinant AMBN or AMEL in the coating solution used to coat the plates. (B) Western blot analysis of the effect of AMBN on adhesion-dependent phosphorylation of key extracellular matrix signaling molecules, ERK and AKT, in BMMCs. The Western blot compares BSA and AMBN treatments after 15 (AMBN15), 30 (AMBN30) and 45 (AMBN45) min of incubation. * $p < 0.05$.

B.6. AMBN regulates osteoclast podosome and actin ring formation and is involved in α2β1 and MER pathways

To illustrate cytoskeletal changes as a result of AMBN treatment, BMMCs were cultured in the presence of either AMBN or BSA. Following culture, F-actin was stained using rhodamine-phalloidin. After seeding for 12 h, BMMCs were still rounded in the BSA control culture (Figs. 11 A, B), while cells had adhered to and spread on the AMBN-coated substrate (Figs. 11 E, F). Individual dot-like structures (podosomes) appeared at the cell periphery of AMBN-treated BMMCs and these podosomes were connected with each other through actin fibers (Figs. 11 E, F).

Adhesive interaction between cells and ECM proteins is mediated by cell surface receptor integrins. It has been reported that the rodent AMBN protein contains a potential α2β1 integrin binding domain and a thrombospondin cell adhesion motif (*19*). To determine whether integrins participate in AMBN-mediated cell adhesion and subsequent spreading, an anti-α2β1 integrin antibody (10 μg/ml) was used to neutralize the integrin receptors. In addition, we used the ERK1/2 inhibitor U0126 and the PI3K inhibitor LY294002 to inhibit ERK and PI3K pathways to determine their involvement in the effect of AMBN on osteoclasts. In comparison to AMBN-treated BMMCs, the integrin α2β1 antibody did not block BMMC spreading, but reduced the number of podosomes (Figs. 11 I, J). Application of the ERK inhibitor U0126 and the PI3K inhibitor LY294002 to AMBN-treated BMMCs resulted in a loss of podosomes and F-actin reorganization (Figs. 11 M, N, Q, and R).

Coating of culture substrates with AMBN resulted in a significant 3.3-fold increase in osteoclast actin ring diameter compared to osteoclasts on BSA-coated controls (Figs. 11 C, S, $p < 0.05$). In addition, AMBN-treated BMMCs exhibited more and larger sealing zones than BSA-

treated cells (Fig. 11 G). Treatment with anti-α2β1 integrin antibody in addition to AMBN coating did not affect the actin ring diameter (Figs. 11 K, S), while treatment with the ERK-inhibitor U0126 resulted in a reduction of actin ring size compared to the AMBN coated group (Figs. 11 O, S). Moreover, the number of multi-nuclear and TRAP-positive osteoclasts was increased by 3.75-fold upon AMBN treatment (Figs. 11 H, T, $p < 0.05$). The antibody against integrin α2β1 and the ERK-inhibitor U0126 partially inhibited AMBN-associated osteoclast activation (Figs. 11 K, O and T), with multinuclear osteoclast numbers reduced to 53% after anti-α2β1 integrin antibody block and 40% after application of U0126 (Fig. 11 T) as compared to the AMBN treated group only.

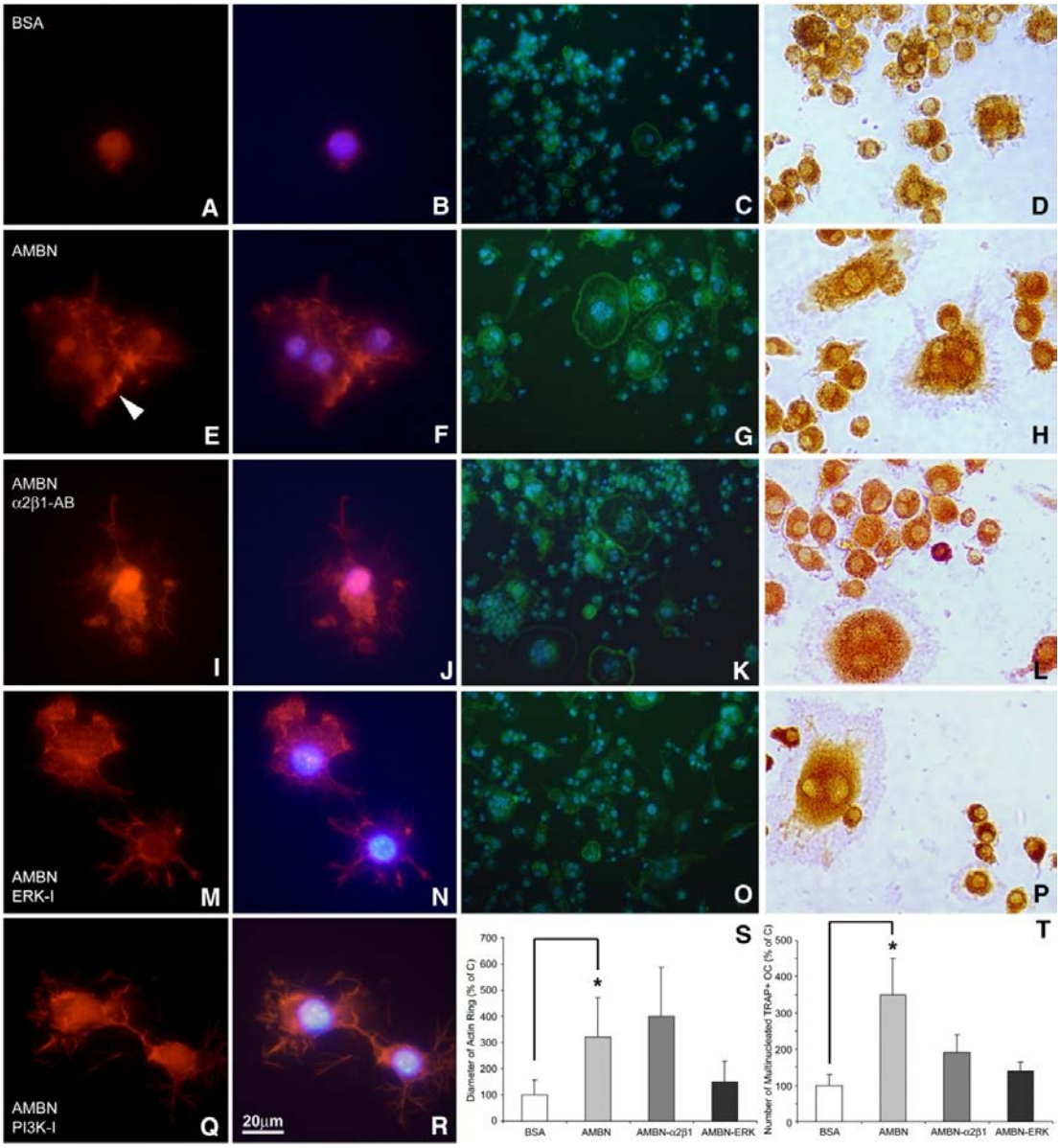

Figure 11. Involvement of α2β1 integrins and ERK1/2 in AMBN-modulated formation of podosome and actin ring. (A, B, E, F, I, J, M, N, Q, R) Fluorescent images of BMMCs cultured on dishes treated with either BSA (A and B), AMBN (E and F), AMBN plus α2β1 integrin antibody (I and J), AMBN plus ERK inhibitor (M and N), or AMBN plus PI3K inhibitor (Q and R). Cells were stained with the actin-filament stain rhodamine-phalloidin (A, E, I, M, Q) and nuclei were counterstained with DAPI (B, F, J, N, R). Following AMBN treatment, BMMCs displayed podosome-like structures (arrowhead). (C, G, K, O) FITC-phalloidin staining indicated actin ring formation characteristic of osteoclasts. Multiple nuclei were visualized in osteoclasts with actin rings using DAPI (D, H, L, P), TRAP staining showed a pink cytoplasm in multinucleated cells, indicative of mature osteoclasts. (S and T) Comparison of actin ring diameter and TRAP-positive/multinucleated cell density between treatment groups. Data are presented as mean ± SD for four different cultures. * = $p < 0.05$.

B.7. AMBN upregulates osteoclast activation-related protein expression through α2β1 and MER pathways

RhoA activity is required to induce integrin clustering and focal complex formation (*136*, *137*). To assess whether AMBN-mediated adhesion of BMMCs stimulated RhoA activity, RhoA expression levels in response to AMBN treatment were examined using Western blot analysis. After 4 h of cell seeding, there was RhoA expression in AMBN-treated cells was 2.2-fold increase compared to BSA-treated cells (Fig. 12, $p < 0.05$). Two inhibitors of adhesion molecules/pathways, α2β1 antibody and UO126, inhibited the effect of AMBN on RhoA expression, with RhoA returning to control levels when AMBN was used in combination with adhesion inhibitory agents (Fig. 12). To determine whether AMBN affects RANKL-stimulated expression of osteoclastogenic regulatory genes, NFATc1 and c-FOS expression was determined using Western blots (Fig. 12). AMBN five times increased NFATc1 protein expression and doubled c-FOS expression as revealed by densitometry (Fig. 12, $p < 0.01$). These results further support our hypothesis that AMBN regulates osteoclast differentiation. In addition, the anti-α2β1 integrin antibody and the ERK-inhibitor UO126 efficiently suppressed AMBN-induced NFATc1 expression (Fig. 12).

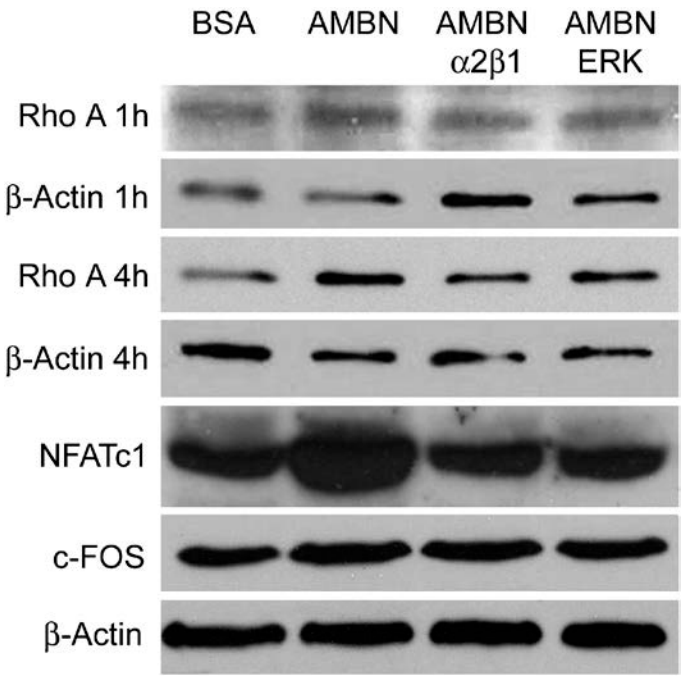

Figure 12. Effect of AMBN on osteoclast activation-related protein expression. BMMCs were seeded onto BSA or AMBN coated culture dishes and incubated for 1 h (Rho A 1 h), 4 h (Rho A 4 h) or 12 h (NFATc1 and c-FOS) in the presence of M-CSF and RANKL. AMBN function was selectively inhibited with anti-α2β1 integrin antibody or ERK inhibitor. Expression of osteoclast activation-related proteins was detected by Western blot. β-Actin served as loading control.

B.8. Overexpressing AMBN accelerates tooth movement with increased osteoclasts in PDL

In order to study clinical application potential of the AMBN protein during periodontal remodelling, a nickel-titanium wire was placed on the mandible incisor to provide orthodontic force to tip the first molar towards the buccal side. The histological analysis revealed that the thickness of alveolar bone wall at buccal side was reduced significantly and alveolar bone became more porous in transgenic mice when compared with wild-type control (Fig.13 A, B). The width of periodontal ligament was decreased on the compression area (Fig.13 A 1, 2, 4 and B, 1, 2, 4) and increased on the tension area (Fig.13, A 3 and B 3) at day 7 after treatment both in AMBN TG and wild-type control. The AMBN TG group exhibited a significant increase in multinucleated osteoclasts cell number with greater bone resorption on the buccal bone surface compared with wild-type mice. Dentin resorption lacuna was also observed in AMBN TG mice. In contrast, the dentin and cementum remained intact in wild type mice.

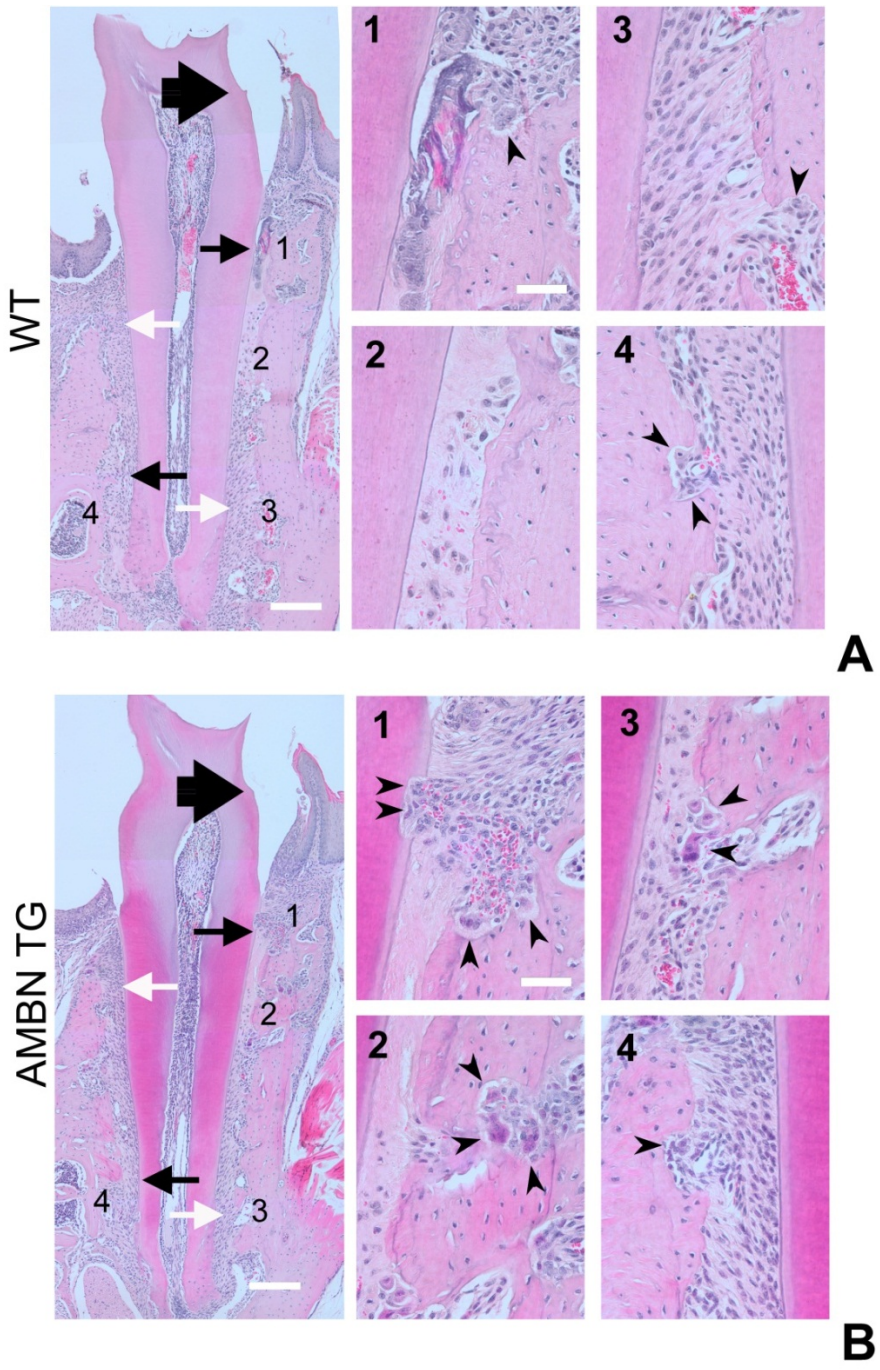

Figure 13. Coronal section of the mouse mesial root of lower first molar after 7 days of mechanical force loading. The lower first molar of WT (A) and AMBN TG (B) animals were loaded with 20g mechanical stress toward the buccal side (large black arrow). The width of PDL was decreased in the compression area (black arrows, higher magnification showed in 1, 2, 4) and increased in the tension area (white arrows, showed in 3). Multinucleated osteoclasts (arrow head) attached on the alveolar bone surface in resorption lacuna. Dentin resorption lacuna was observed in AMBN TG mice in the compression area (B, 1). Bar = 200μm in A and B, bar = 50μm in high magnification.

C. AMBN affects long bone formation

C.1. AMBN is expressed in developing mouse femurs and localized in the growth plate

As the first step to study the effect of AMBN on long bone formation, we isolated total RNAs and proteins from C57BL/6 wild type mouse femurs during postnatal stage from 1day until 3 month. After the total cDNA have been reverse transcripted, the full length of AMBN coding region around 1.2kb were amplified by PCR (Fig.14 A). In the tooth, AMBN mRNA was expressed on postnatal day 1 (PN1) reached the peak on PN10 and dropped on PN15. Compared with control RNA extracts from developing teeth, the amount of AMBN mRNA expression in the femur is about a hundred times lower, as quantified by GAPDH expression. Total proteins from femurs were extracted by guanidine hydrochloride following the protocol (*138, 139*). The AMBN protein was detected by Western Blotting using a rabbit polyclone anti-AMBN antibody (Fig.14 B). As early as PN0, the AMBN full length band around 50kD was detected, and its expression amount maintained until PN21. Eventually, it decreased to almost undetectable level in 3-month-old femurs. Compared with AMBN expression level in mouse molars on PN7 day mouse, the amount of AMBN in femurs was obviously lower. The β-actin was used as protein loading control.

In order to illustrate the spatial expression pattern of AMBN during femur development, we conducted immunohistochemistry analysis. The specificity of the AMBN polyclonal antibody was tested on paraffin sections of PN3 mouse molars based (Fig.14 C *i-ii*). The positive immunoreactivity of AMBN was visible as brown staining in the unmineralized enamel matrix as well as polarized differentiated ameloblasts. Negative controls (Fig.14 C *iii-v*) did not show any positive staining. During femur development, AMBN protein was expressed in the primary ossification center (POC) (Fig.14 C d, i, n, s and x) beneath the subchondral bone and cortical

bone (CB) (Fig.14 C e, j, o, t and y) from PN0 to PN35 during postnatal growth. In addition, AMBN was not expressed in the undifferentiated chondrocytes at the center of distal femur on PN0 (Fig.14 C c). In contrast, AMBN was expressed at the site of initiate mineralization in the secondary ossification center (SOC) (Fig.14 C g) on PN6 and during subsequently development stages (Fig.14 C l, g and v). Interestingly, in the growth plate (GP), AMBN protein was detected in the chondrocytes in the proliferating zone from PN12 to PN35 (Fig. 14 C m, r and w) but not in the resting chondrocytes onPN0 and PN6 (Fig. 14 C c, h).

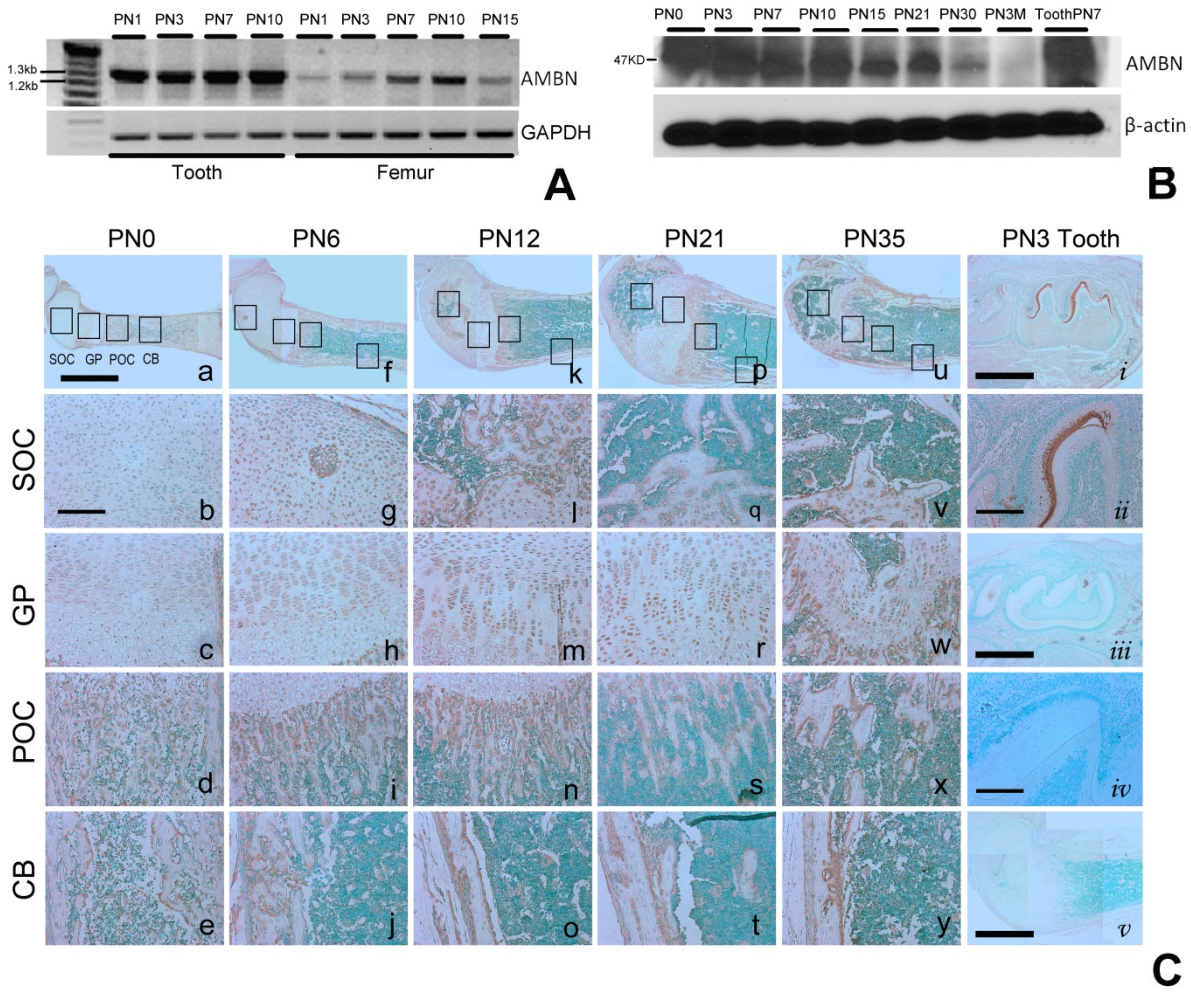

Figure 14. AMBN is expressed in mouse femurs and localized in growth plates during femur development. (A) AMBN mRNA was detected by regular RT-PCR during mouse molar and femur development on postnatal (PN) day 1, 3, 7, 10 and 15. GAPDH was applied as cDNA loading control. (B) Western blot analysis revealed the AMBN protein expressed during mouse femur development at PN day 0, 3, 7, 10, 15, 21, 30 and 3month old age. The β-actin was applied as a protein loading control. (D) Immunohistochemistry analysis of AMBN protein expression in PN0 (a-e), PN6 (f-j), PN12 (k-o), PN21 (p-t), PN35 (u-y) in mouse femur, and PN3 tooth (*i-ii*) with negative control (*iii-v*). Immunoreactivity for the AMBN protein was visible as brown staining in the tissues. The inset boxes in (a, f, k, p and u) from left to right were represent of secondary ossification center (SOC), growth plate (GP), primary ossification center (POC) and cortical bone (CB) respectively. The high magnification images showed below followed the sequence. The specificity of AMBN polyclone antibodies was demonstrated by detecting in PN3 mouse fist morlar (*i-ii*). Negative control conducted by replacing primary antibody to PBS (*iii-v*). Bar=1mm in a, f, k, p, u, *i*, *iii* and *v*. Bar=200μm at b-e, g-h, l-o, q-t, v-y, *ii* and *iv.*

C.2. Two months old AMBN mutant mice had shorter skeletons and lower body weight.

$AMBN^{\Delta 5\text{-}6}$ mutant mice were generated by homologous recombination, replacing exon 5 and 6 with neomycin resistance cassette (Fig.15, A) as described before (*60*). $AMBN^{\Delta 5\text{-}6}$ mutant mice were maintained in C57BL/6 background. The genotype of wild type (WT), AMBN heterozygous ($AMBN^{HET}$) and AMBN homozygous ($AMBN^{\Delta 5\text{-}6}$) mutant mice was confirmed by PCR analysis (Fig.15 B). Both $AMBN^{HET}$ and $AMBN^{\Delta 5\text{-}6}$ had no obvious fertility problems and newborns appeared normal. However, $AMBN^{\Delta 5\text{-}6}$ exhibited smaller skeletons and mild patterning defects with delayed ossification in phalange and metatarsal when E18.5-day-old embryos were examined (Fig.15 C). Adult $AMBN^{\Delta 5\text{-}6}$ mutant mice appeared morphologically normal compared with $AMBN^{HET}$ and WT in 2-month-old, but those mice had smaller litter size when observed externally (Fig.15 D a) or examined under X-ray (Fig.15 D b). Moverover, both male and female $AMBN^{\Delta 5\text{-}6}$ mutant mice displayed lower body weight during the first 16-week period compared with wild type litters (Fig.15 F, G). This lower body weight is not associated with the amount of food intake even though the $AMBN^{\Delta 5\text{-}6}$ mouse demonstrated enamel defects in molars and incisors (*60*, *124*). There was no difference in food intake between 4 weeks old wild-type ad homozygous mutant mice (Fig.15 E).

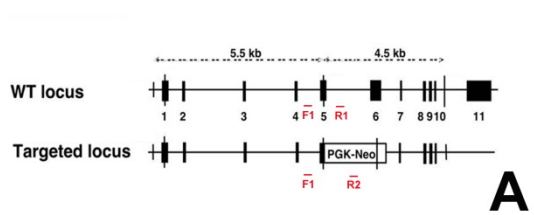
5.5 kb
4.5 kb
WT locus
1 2 3 4 F1 5 R1 6 7 8 9 10 11
Targeted locus
PGK-Neo
F1
R2

A

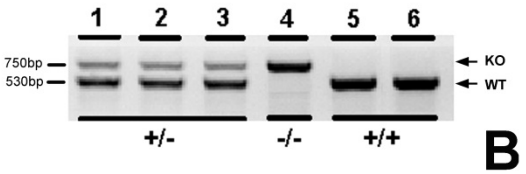
1 2 3 4 5 6
750bp
530bp
KO
WT
+/-
-/-
+/+

B

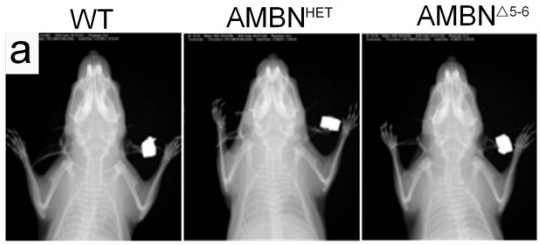
WT
AMBN^HET
AMBN^Δ5-6
a

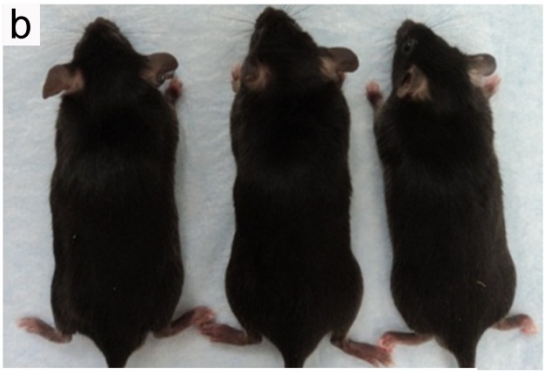
b

D

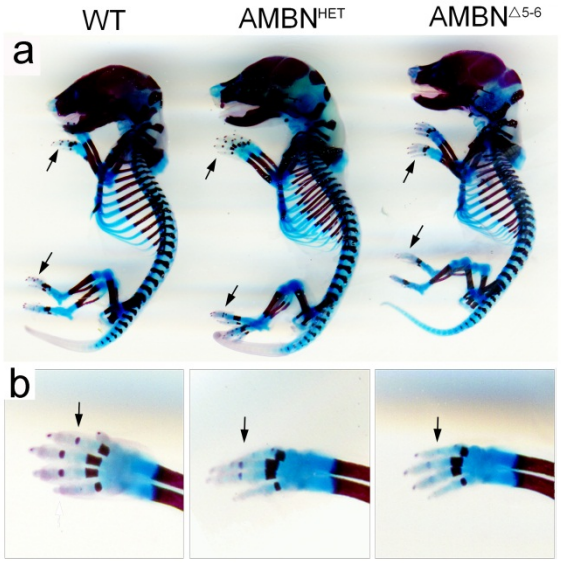
WT
AMBN^HET
AMBN^Δ5-6
a
b

C

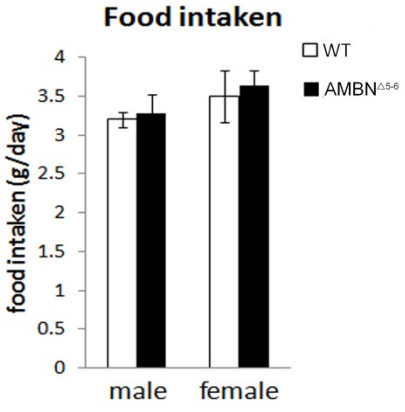
Food intaken
WT
AMBN^Δ5-6
food intaken (g/day)
0
0.5
1
1.5
2
2.5
3
3.5
4
male
female

E

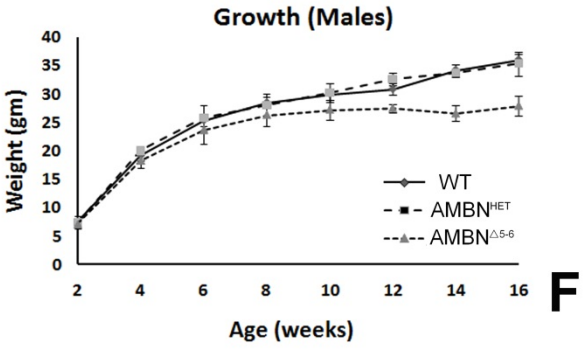
Growth (Males)
Weight (gm)
0
5
10
15
20
25
30
35
40
2
4
6
8
10
12
14
16
Age (weeks)
WT
AMBN^HET
AMBN^Δ5-6

F

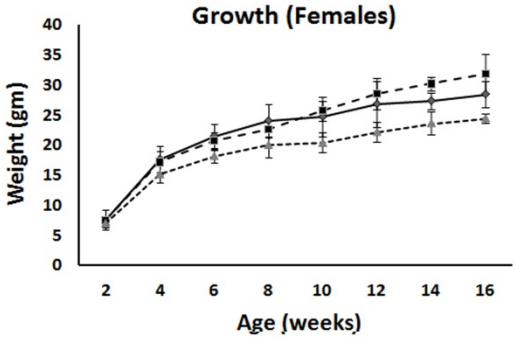
Growth (Females)
Weight (gm)
0
5
10
15
20
25
30
35
40
2
4
6
8
10
12
14
16
Age (weeks)

G

Figure 15. AMBN$^{\Delta 5\text{-}6}$ mutant mice appeared morphologically normal at 2-month-old age but have smaller skeleton and lower body weight. (A) The design of the AMBN$^{\Delta 5\text{-}6}$ target vector was illustrated. The locations of the arrows indicate a primer designed sites for genotyping. (B) Genotype PCR analysis of mouse tail clips from 6-week-old littermate mice derived from AMBN^{HET} breeding parents. (C) Representative images of whole skeleton staining of 18.5-day-old WT, heterozygous and homozygous AMBN mutant embryos. Arrows point to the delayed ossification of the phalange (a) and metatarsal (b). (D) The comparative images of 2-month-old litters of WT, AMBN^{HET} and AMBN$^{\Delta 5\text{-}6}$ mice showed that AMBN homozygous mutant has smaller skeleton in overall gross morphology observed both by X-ray scanning of skeletal structures (upper panel) and exterior examination (lower panel). (E) The amount of food intake of 4-week-old WT mice compared with AMBN mutant mice in male and female group during 24 hours (n=4, NS). (F, G) Graphs of body weight during first 16 weeks growth for male (F) and female (G) of WT (*gray diamond*), heterozygous (*black box*) and homozygous (*gray triangle*) AMBN mutant mice. All experiments mice were maintained in the C57/BL6 background.

C.3. Femur growth was delayed in developing AMBN mutant mice

Based on the smaller skeletons in the 2-month-old litters, femurs were collected to characterize the long bone phenotype in $AMBN^{\Delta 5\text{-}6}$ mutant mice during a 6 month growth period from female and male littermates (Fig.16 A). Femur volume and length were examined and quantified using a FIXATRON X-ray scanning device (Fig.16 B, C In 1.5- and 3-month-old mice, femur length in $AMBN^{\Delta 5\text{-}6}$ mutants was significantly shorter (5-6%, $p < 0.05$) and femurs were less mineralized compared with WT or $AMBN^{HET}$ littermates regardless of male or female groups. However, in 4- and 6-month old, femur length in $AMBN^{\Delta 5\text{-}6}$ mutants almost caught up with wild-type and $AMBN^{HET}$, only displaying minor reduction in size and mineralization. The femurs from $AMBN^{HET}$ did not show a significant difference compared with wild type mice.

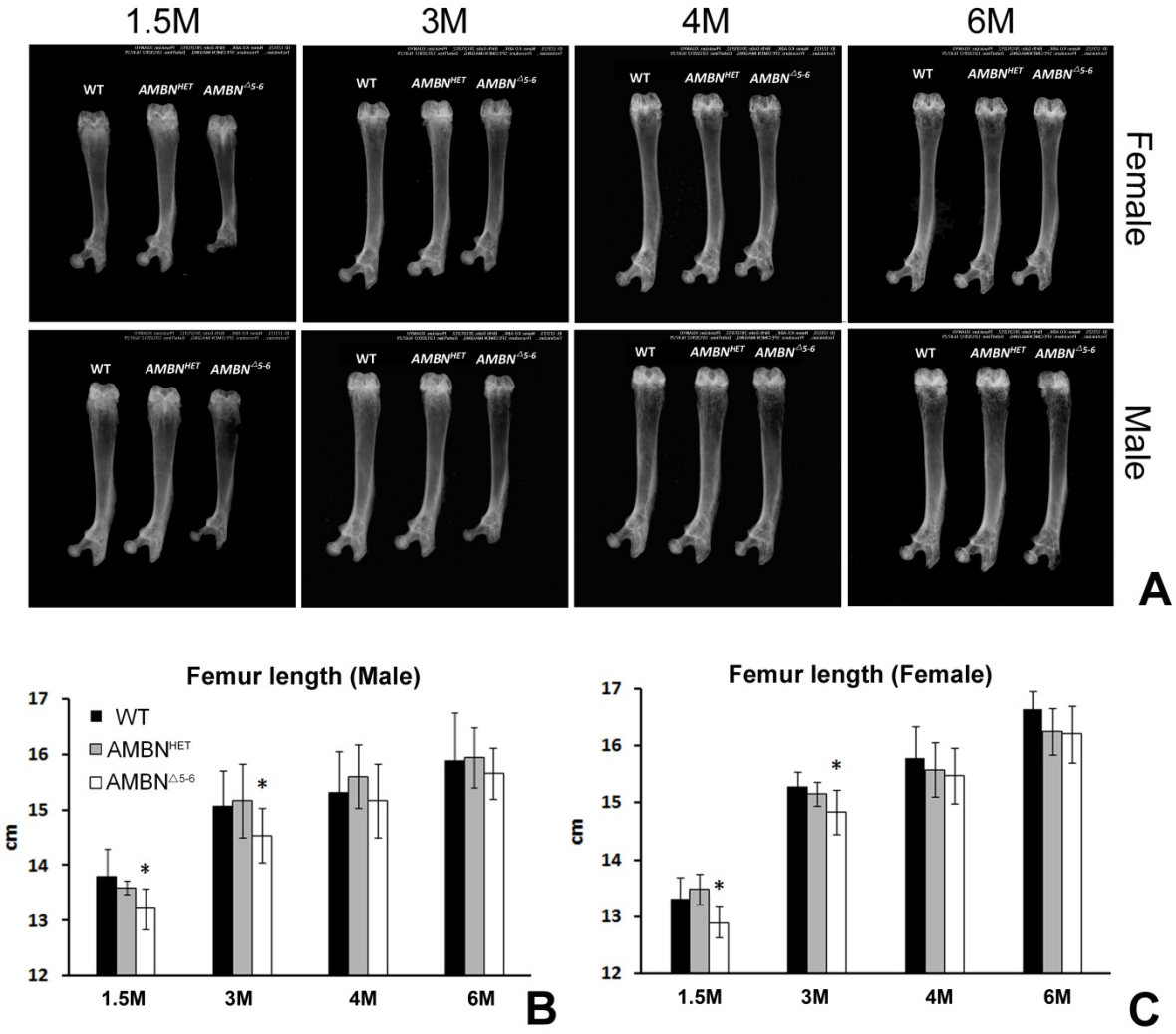

Figure 16. Femur growth was delayed in AMBN mutants during the first 6 month development. (A) Representative image of FAXITRON X-ray analysis of femurs among 1.5-, 3-, 4- and 6-month-old littermate of WT, AMBN^{HET} and AMBN$^{\Delta 5\text{-}6}$ mutant mice in female (upper panel) and male(lower) group, demonstrated decrease in femur length and mineralization density in AMBN$^{\Delta 5\text{-}6}$mice. (B, C) The measurement of the length of femurs in littermates of WT, AMBN^{HET} and AMBN$^{\Delta 5\text{-}6}$ mice in male (B) and female (C) group, revealed delay of AMBN$^{\Delta 5\text{-}6}$delayed femur longitudinal growth during development. Data are presented as mean ±SD. for 4 to 6 mice in each genotype group (* = $p<0.05$ versus wild-type littermates).

C.4. Lower bone mass and reduced bone formation rate in femurs of AMBN mutants

Micro-computed tomographic (μ-CT) scanning was employed to detect micro-structural changes in bone mass. Only femurs from 1.5- and 3-month-old (1.5mo and 3mo) male littermates were collected since both male and female $AMBN^{\Delta 5\text{-}6}$ mutant displayed the same bone defects. The loss in bone mass was more apparent in the trabecular bone with significantly decreased bone volume/total volume (BV/TV) (30% $AMBN^{\Delta 5\text{-}6}$ verse WT) in $AMBN^{\Delta 5\text{-}6}$ mice (Fig.17 A-C).

In addition, bone architecture in $AMBN^{\Delta 5\text{-}6}$ mice deteriorated, as evidenced by a significant decrease in trabecular number (Tb.Nb.) (25% in 1.5mo, 23% in 3mo, $p<0.05$ versus WT) and thickness (Tb.Th.) (18% in 1.5mo, 20% in 3mo, $p<0.05$ versus WT), and a significant increase in the mean separation between individual trabeculae (Tb. Sep.) (30% in 1.5 mo, 33% in 3 mo, $p<0.05$ versus WT) (Fig. 17 C). The cortical thickness (Cr.Th.) in homozygous mutant mice also decreased significantly (20% in 1.5M, 19% in 3M, $p<0.05$ versus WT), but there was no significant difference in bone mineral density (BMD).

Histomorphometry of WT, $AMBN^{HET}$ and $AMBN^{\Delta 5\text{-}6}$ mice was conducted to further characterize the bone phenotype of $AMBN^{\Delta 5\text{-}6}$. H&E and von Kossa staining revealed a low-bone-mass phenotype in AMBN mutant mice (Fig.17 D-G). Bone volume/total volume in the distal femur metaphysic was reduced by more than 50% in 1.5- and 3-month old $AMBN^{\Delta 5\text{-}6}$ mice relative to wild-type littermates (Fig.17 I). The number of osteoblast/bone area (N0. Ob./bone area) also significantly decreased (27% in 1.5-month, 32% in 3-month, $p<0.05$ verse WT) in the AMBN mutants (Fig.17 I). However, there was no significant difference between $AMBN^{HET}$ and wild type mice in terms of bone mass. Dynamic histomorphometry based on fluorescent bone markers showed abundant double tetracycline and calcein labels on the inner cortical bone

surface of wild type mice. In contrast, labels in AMBN$^{\Delta 5\text{-}6}$ mice most frequently formed a single fluorescent line, which was only interrupted sparingly by double labeled stretches with short distance between tetracycline and calcein labels. Accordingly, bone mineral apposition rate (MAR), a parameter of new bone formation, was significantly higher in wild-type than in AMBN mutant mice (Fig.17 H).

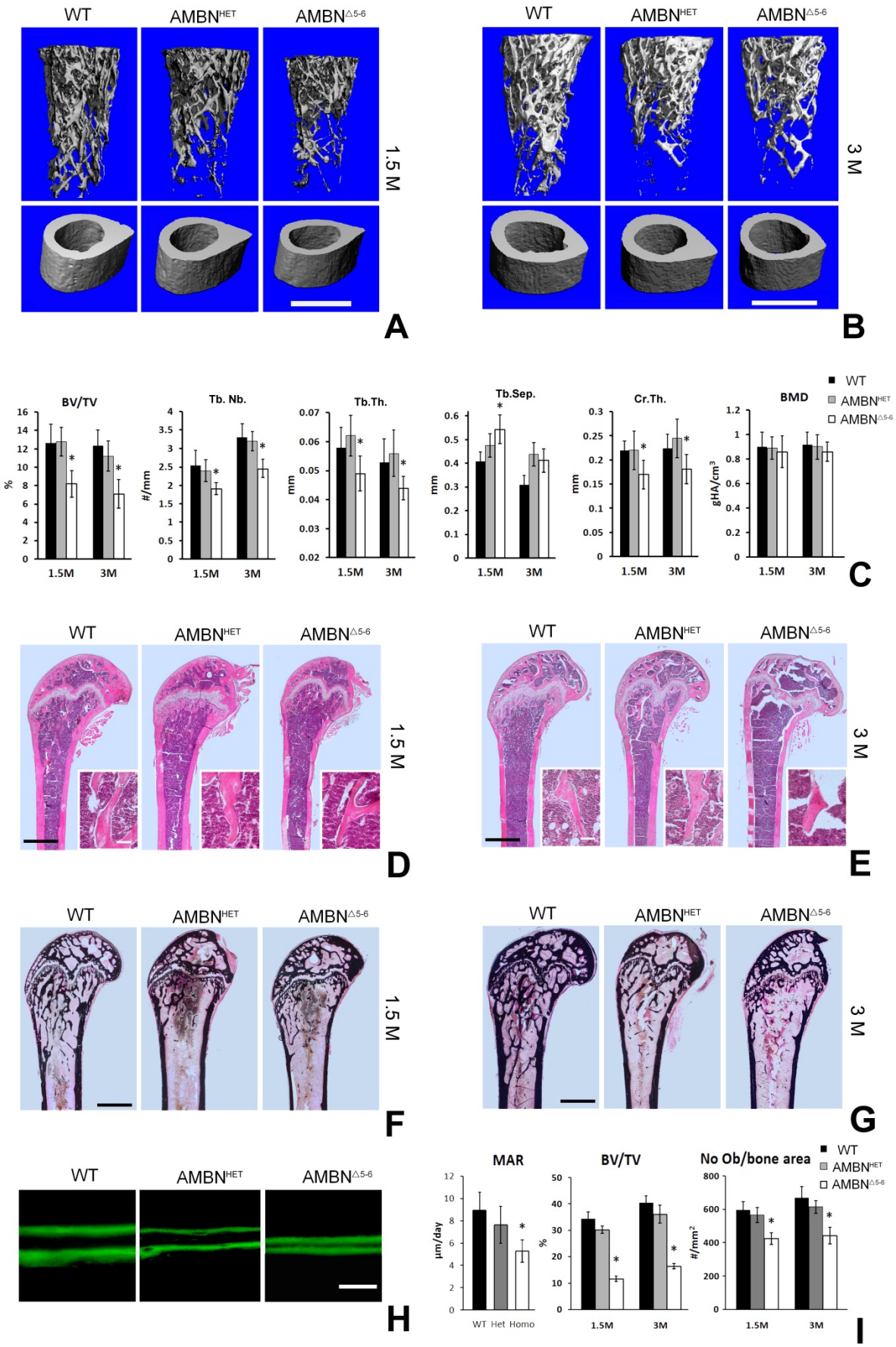
WT
AMBN^HET
AMBN^Δ5-6
1.5 M
3 M
A
B
BV/TV
Tb. Nb.
Tb.Th.
Tb.Sep.
Cr.Th.
BMD
1.5M
3M
C
D
E
F
G
H
MAR
BV/TV
No Ob/bone area
WT Het Homo
I

Figure 17. Quantitative μ-CT and histological analysis of femurs showed decreased bone mass and in AMBN$^{\Delta 5\text{-}6}$ mutant mice. (A, B) Representative images of 3D micro-computed tomographic (μ-CT) reconstruction of the trabecular microstructure in distal femoral metaphysis (upper panel) and middle diaphysis of cortical bone (lower panel) of 1.5- and 3-month old AMBN male littermates. Bar=1mm. (C) Trabecular bone volume/tissue volume (BV/TV), trabecular number (Tb.#), trabecular thickness (Tb.Th.), trabecular separation (Tb.Sp.), cortical thickness (Cr.Th.) and bone mineral density (BMD) were calculated. Data acquired from scanco 40 scanning software. Data are presented as mean ± SD. with 3 mice in each genotype group. * = $p<0.05$ mutant versus WT littermates. (D, E) H&E staining of the distal femurs of 1.5- and 3-month old WT, AMBN^{HET} and AMBN$^{\Delta 5\text{-}6}$ male mice. Bars = 1mm. Insert pictures indicate higher magnification of inset box at trabecular bone region. Bars= 200μm at insert graph. (F, G) The von Kossa and fast red staining of distal femurs of 1.5-month and 3-month old littermates. Bars=1mm. (H) Representative tetracycline and calcein double labeling in 5 days interval. Bar=50μm. (I) Quantitative of mineral apposition rate (MAR) from dynamic bone histomorphometry, 2D histology with distal femur bone volume/ total volume (BV/TV) and number osteoblasts/ bone area (No.Ob./bone area). Data are presented as mean ± SD. with 4-6 mice in each genotype group. Statistical significance was evaluated by one way ANOVA, * = $p<0.05$.

C.5. Change of femur mechanical properties in AMBN mutant mice

Based on our finding that $AMBN^{\Delta 5\text{-}6}$ mutants had lower bone mass in trabecular and reduced cortical bone thickness, we hypothesized that AMBN homozygous mutant mice would be more likely to suffer bone fracture. To address this question, we evaluated femur biomechanical properties using 3-point-bending experiments (Table I). Compared with 2-month-old WT and $AMBN^{HET}$, the $AMBN^{\Delta 5\text{-}6}$ mice showed smaller midshaft total area but without statistical significance. As expected, femur stiffness in homozygous mutant mice was 14% and 10% lower than in WT and $AMBN^{HET}$ mutant mice ($p<0.05$). In addition, the maximum force yield to failure (16% lower than WT, 15% lower than $AMBN^{HET}$, $p<0.05$), maximum stress (10% lower than WT and 8% lower than $AMBN^{HET}$, $p<0.05$) and energy to failure (40% lower than WT and 38% lower than $AMBN^{HET}$, $p<0.05$) were also lower. There was no difference in these parameters between $AMBN^{HET}$ and WT mice.

TABLE I

FEMUR BIOMECHANICAL PROPERTIES IN 2-MONTH-OLD MALE MICE

	WT	**AMBN^{HET}**	**AMBN$^{\Delta 5\text{-}6}$**
Total Area(mm^2)	1.70±0.19	1.67±0.19	1.58±0.13
Stiffness (N/mm)	155.41±13.11	147.03±27.91	135.13±20.00 *****
Maximum force(N)	25.10±4.08	24.49±4.48	21.06±1.28 *****
Maximum stress(Mpa)	14.27±3.01	14.05±2.13	13.42±1.81
Energy to failure(N*mm)	5.25±2.65	5.06±0.88	3.2±1.22 *****

Data are presented as means ± SD from 5 to 6 individual mice. * = P<0.05 AMBN$^{\Delta 5\text{-}6}$ mutant mice verse wild-type control.

C.6. Significant decrease in serum alkaline phosphatase and TRAP activity in AMBN mutant mice

The serum biochemistry markers were analyzed in the 2- and 4-month-old littermates (Table II). Serum calcium and phosphate levels did not show any significant difference between the three genotype groups. However, the serum alkaline phosphatase (ALP) activity significantly decreased in 2- and 4-month old AMBN homozygous mutant mice when compared with WT and $AMBN^{HET}$ ($p<0.05$), which indicates that decreased osteoblast activity leads to lower serum ALP activity. Total serum TRAP enzyme activity, which was measured by ELISA, was significantly reduced in AMBN homozygous mutant when compared with WT or $AMBN^{HET}$ control mice in 2- and 4-month old litters ($p<0.05$). These findings suggests that osteoclast activities is also impaired by lost full length of AMBN.

TABLE II

BIOCHEMICAL ANALYSIS OF SERUM FROM 2- AND 4-MONTH-OLD MICE

		WT	**AMBN^{HET}**	**AMBN$^{\Delta 5\text{-}6}$**
Ca (mg/dl)	**2month**	8.11±2.01	8.04±1.71	8.09±1.87
	4month	9.45±0.2	9.35±0.23	9.41±0.17
P (mg/dl)	**2month**	10.1±1.91	10.21±1.84	10.37±1.59
	4month	11.05±0.2	11.48±2.09	11.35±3.14
ALP (U/L)	**2month**	82.33±6.45	81±7.89	71.5±8.58 *****
	4month	74.66±12.22	72±11.78	62.67±5.03 *****
TRAP (U/L)	**2month**	5.96±2.5	5.96±2.23	3.38±1.49 *****
	4month	3.54±0.98	3.35±1.36	2.7±1.18 *****

Data are presented as means ± SD from 5 to 6 individual mice.* = P<0.05 AMBN$^{\Delta 5\text{-}6}$ verse wild-type.

C.7. Shortened growth plate and reduced chondrocyte proliferation rate during endochondral bone formation in AMBN mutant tibias

Endochondral ossification in the growth plate is predominantly responsible for the longitudinal growth of long bone (*71*). To ask whether AMBN was involved in the endochondral ossification of long bones, 3 weeks old $AMBN^{\Delta 5\text{-}6}$ mice were analyzed for potential developmental defects in the growth plate. As shown in (Fig.18 A), growth plate thickness was significantly decreased in AMBN homozygous mutant mice (29% less than WT and 20% less than $AMBN^{HET}$, $p<0.05$). The decrease in growth plate thickness was due to a relative size reduction of the proliferation and hypertrophic zone in $AMBN^{\Delta 5\text{-}6}$ mice (Fig. 18A). This reduction in the combined proliferation/hypertrophic zone thickness is also evidenced by a slight thinning of the proteoglycan-rich zone as demonstrated by alcian blue staining (Fig. 18 A). Next, we determined chondrocyte proliferation rates in the proliferation zone by 5-bromodeoxyuridine (BrdU) labeling. The numbers and percentage of BrdU-positive cells were significantly decreased between $AMBN^{\Delta 5\text{-}6}$ and WT or $AMBN^{HET}$ mice (Fig.18 A, C). In order to evaluate the secondary ossification center (SOC) at the early postnatal stage, the area of the distal femur epiphysial ossification centers in comparison to the entire epiphyseal area in WT and $AMBN^{\Delta 5\text{-}6}$ littermates on PN10 was determined using image analysis (Fig.18 B). In $AMBN^{\Delta 5\text{-}6}$ mice, the percentage of SOC was 5% decreased compared to WT litters. Taken together, the data show that lack of full length AMBN in the growth plate affects the differentiation and proliferation of growth plate chondrocytes.

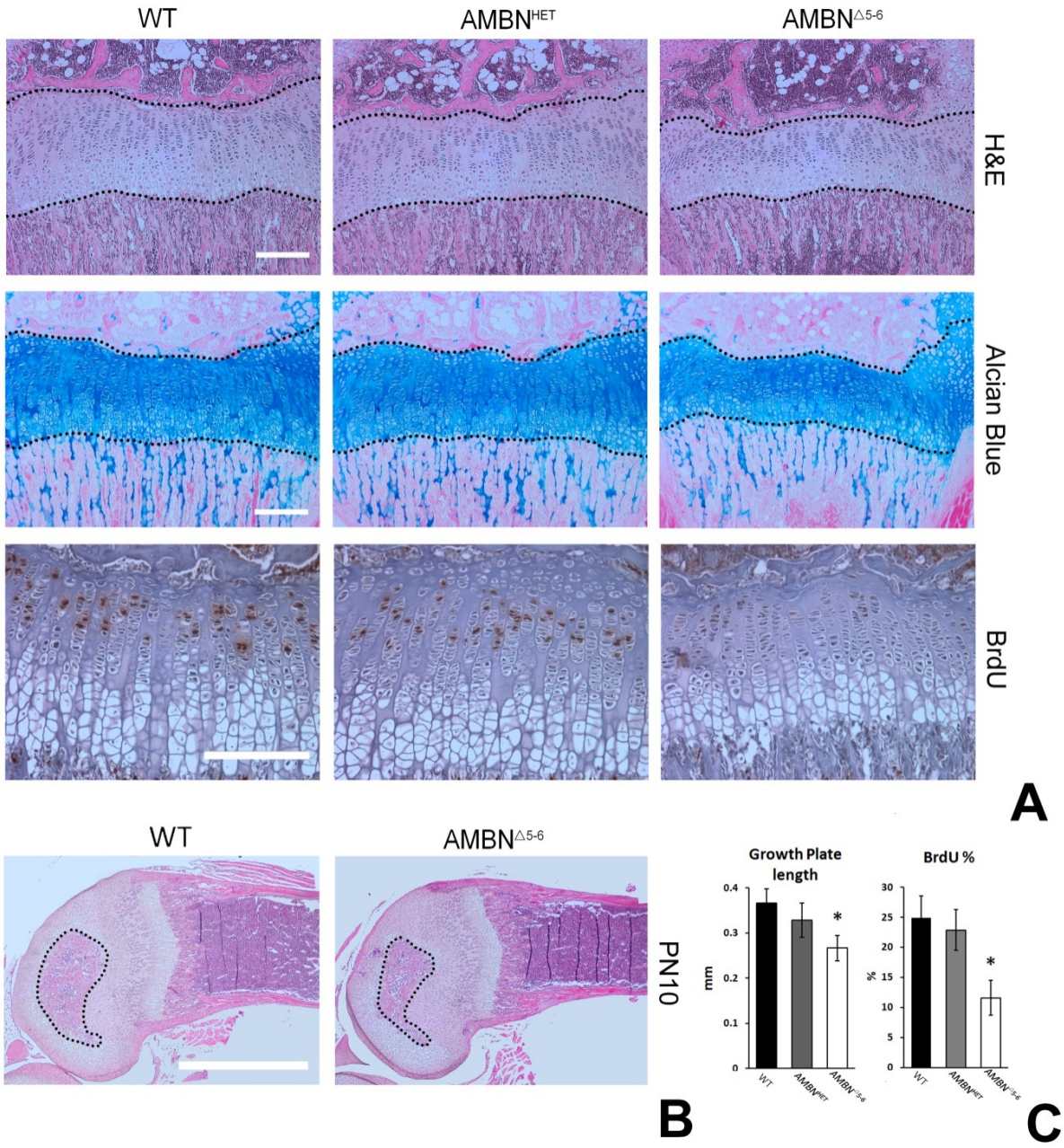

Figure 18. AMBN mutant tibia shows a shortened growth plate and a lowered chondrocyte proliferation rate at 3 weeks postnatal age. (A) Tibia sections from 3-week-old WT, $AMBN^{HET}$ and $AMBN^{\Delta 5\text{-}6}$ litters were stained by H&E (upper panels), alcian blue (middle panels). Immunohistochemistry labeled BrdU-incorporated chondrocytes (lower panels). The broken lines outlined growth plates in the up and middle panels. Bar=200μm. (B) The H&E staining of distal femur sections from postnatal 10day WT and $AMBN^{\Delta 5\text{-}6}$ litters. Bars=1mm. (C) The quantitative analysis of the length of growth plate (left), and the ratio of the number of the BrdU-positive chondrocytes in the proliferation zone of the tibia (right) in 3-week-old WT, $AMBN^{HET}$ and $AMBN^{\Delta 5\text{-}6}$ litters. The results are expressed as the mean ± SD from 3 mice in each group. Statistical significance was evaluated by ANOVA, * = $p<0.05$.

C.8. Bone marrow stromal cells from AMBN mutants displayed impaired proliferation and differentiation potential

Here we have turned to cellular-level studies to explain changes in femur morphogenesis as revealed in our histomorphometric analysis. Previously we have demonstrated that AMBN is expressed in mesenchymal cells (*57, 126*), suggesting that *ex vivo* analysis of BMSCs from AMBN mutant mice may provide a valuable tool to illuminate the function of AMBN during BMSC differentiation and bone formation. Stemness characteristics, proliferative and differentiation capacity of AMBN mutant BMSCs were compared to WT BMSCs using colony forming unit (CFU) assays. These assays revealed that CFU-fibroblast numbers (CFU-F), CFU-alkaline phosphatase positive colonies (CFU-ALP) and CFU-osteoblast numbers (CFU-Ob) were significantly reduced in $AMBN^{\Delta 5\text{-}6}$ mice when compared with WT and $AMBN^{HET}$ mutant controls ($p<0.05$) (Fig.19 A, B). Moreover, both the size of CFU-F colonies and the number of cells within a colony were reduced significantly in cells cultured from AMBN mutant mice (Fig.6 A b). In addition, the area occupied by mineralized matrix as revealed by alizarin red staining was smaller in AMBN homozygous mutant cell populations when compared to controls (Fig.19 A). The reduction in CFU-F formation frequency corresponded with a decrease in CD105 and CD106 (vascular cell adhesion molecule 1, VCAM1) double positive mesenchymal stem cell populations in freshly isolated bone marrow nucleated cells (Fig.19 D). Furthermore, BMSCs from $AMBN^{\Delta 5\text{-}6}$ mutant had a significantly lower growth rate compared with WT controls during 5 days culture as demonstrated using the MTT assay (Fig.19 C). This finding indicated that the number of mesenchymal stem cells in the bone marrow of $AMBN^{\Delta 5\text{-}6}$ mice was reduced, and that $AMBN^{\Delta 5\text{-}6}$ BMSCs displayed impaired proliferation and differentiation potential.

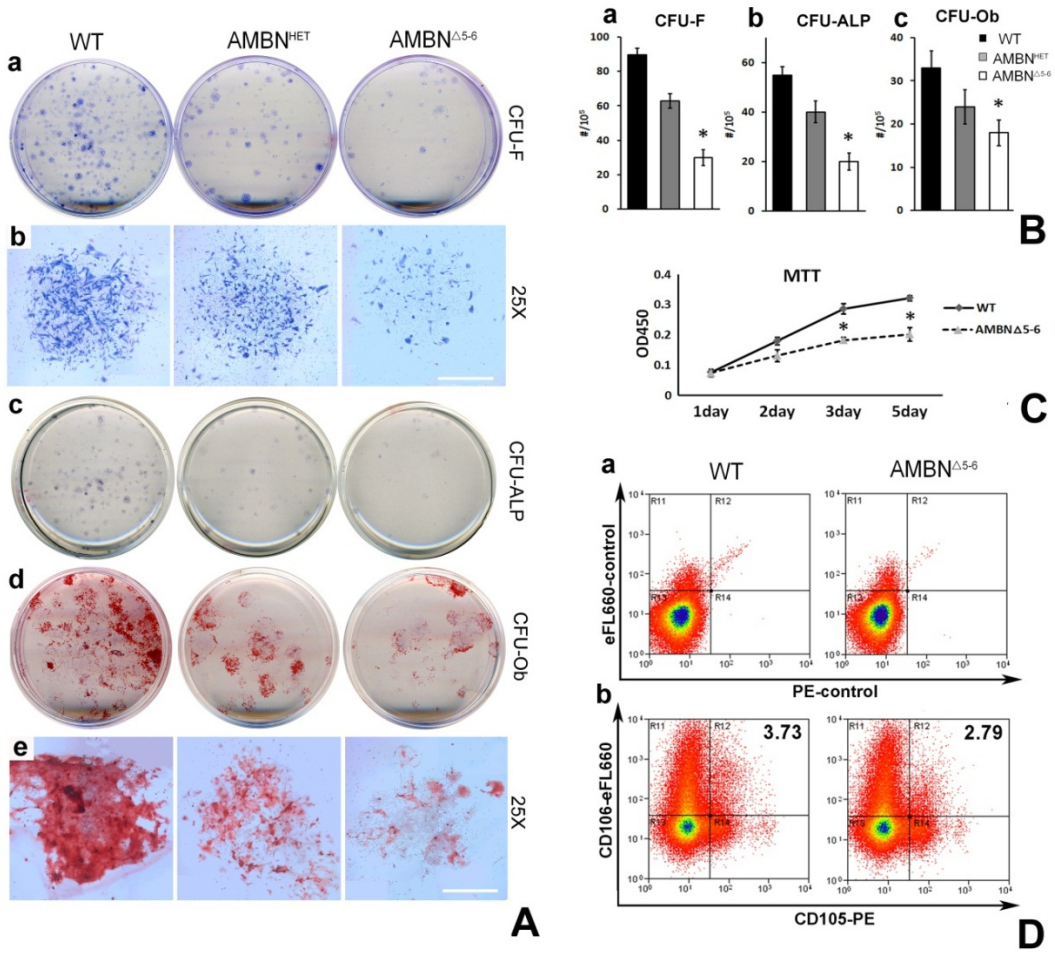

Figure 19. BMSCs from AMBN$^{\Delta 5\text{-}6}$ mice displayed less stem cell populations and impaired proliferation and differentiation potential. (A) Representative plates from colony forming units (CFU) assay of BMSCs between 4-week-old AMBN littermates. The CFU-fibroblasts (CFU-F) (a, b) and CFU-alkaline phosphatase (CFU-ALP) (c) assay were conducted by culturing BMSCs for 14 days. The CFU-osteoblastic units (CFU-Ob) (d, e) were cultured for 14 days then changed in osteogenic medium until 21 days. Representative plates of total CFU-F were stained with Giemsa and the colonies were observed under microscope (b). The CFU-ALP positive colonies stained in the same palate (c). Mineralized colonies were positive stained with Alizarin red (d) and visualized as mineralized colonies under microscope (e). (B) The counts of CFU-F (a), CFU-ALP (b) and CFU-Ob (c) colony numbers of CFU assay after 14 and 21 days culture and differentiation. Data were obtained from duplicate of 4 different animals in each genotype group, and values are presented as means ± SD. * = $p<0.05$ mutant versus WT. (C) The growth rate of BMSC per 96 well by a MTT assay by 1, 2, 3 and 5 days after culture. Data were obtained from triplicate of 3 different samples. Statistic calculated by one way ANOVA and value are presented as means ± SD. * = $p<0.05$ mutant versus WT. (D) Flowcytometry analysis of freshly isolated bone marrow nucleated cells from 1-month-old AMBN homozygous mutant and age match wild-type control mice stained with mAb against CD106 and CD105 markers (b) and isotype control (a) in dot plots. The percentage of the population with the double positive is showed in the (b).

C.9. Effects of AMBN mutation on osteogenic, osteoclastogenic and chondrogenic differentiation of bone marrow cells

Previous studies have documented AMBN expression in BMSCs, osteoblasts (*122*), CD34+ osteoclast cells and chondrocytes (*53, 57*) at levels that were substantially lower than in developing teeth. Thus, to explain the significant effects of AMBN in long bone morphogenesis, we sought to determine AMBN expression levels and patterns during osteogenic (OG) and chondrogenic (CH) differentiation of BMSCs, and osteoclastogenic (OC) differentiation of BMMCs is not clear. To this end, differentiation of primary BMSCs and BMMCs isolated from C57BL/6 wild type mice was induced for 14 days using specific induction media (Fig.20 A). This study documented that relative to GAPDH, *Ambn* mRNA was expressed at low levels during osteogenesis differentiation with an expression peak on day 3 (Fig.20 A). Surprisingly, during osteoclast and chondrocyte lineage differentiation, *Ambn* expression level significantly increased at day 7 after induction and peaked on day 14 (Fig.20 A). These findings together with our immunohistochemical data (Fig. 14) prompted us to speculate that AMBN might play a role during BMSC commitment during osteoclast and chondrocyte lineage differentiation.

To determine how changes in AMBN expression affect osteoblast, osteoclast and chondrocyte lineage differentiation of BMSCs *in vitro*, we examined osteogenic, osteoclastogenic and chondorgenic markers and lineage-specific gene expression. This study documented that ALP activity, matrix mineralization (Fig.20 B) and expression of osteoblast specific genes (*Osx, Runx2, Ibsp and Opn*) were reduced during osteogenic differentiation of AMBN mutant BMSCs compared with wild type control (Fig.20 C). The role of AMBN in osteoclastogenesis was investigated after 10 days' treatment with RANKL and M-CSF in BMMCs culture. Most wild type bone marrow cells differentiated into mature osteoclasts

(Fig.20, D). However, osteoclastogenesis of AMBN$^{\Delta 5\text{-}6}$ bone marrow was suppressed. The expression level of *Nfatc, c-fos, TRAP* and *RANK* were markedly reduced in AMBN$^{\Delta 5\text{-}6}$ bone marrow cell cultures compared with control (Fig.20 E).

In addition, the chondrogenic differentiation potential of AMBN$^{\Delta 5\text{-}6}$ BMSCs was tested in BMSC pellet cultures. After 21 days of induction, proteoglycan secretion in AMBN$^{\Delta 5\text{-}6}$ BMSCs was substantially reduced as revealed by less intense alcian blue and purple/red Safranin O staining when compared to WT BMSCs. In support of this finding, chondrogenesis related marker genes (*Sox9, ColX, Acan, Ihh*) were expressed at lower levels in AMBN$^{\Delta 5\text{-}6}$ BMSCs compared with wild type counterparts after 14 days of induction (Fig.20 F). In summary, this data demonstrates that AMBN mutation affects osteogenesis, osteoclastogenesis and chondrogenesis differentiation of bone marrow cells.

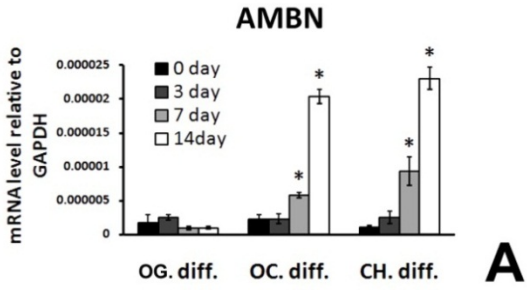
AMBN
mRNA level relative to GAPDH
0.000025
0.00002
0.000015
0.00001
0.000005
0
0 day
3 day
7 day
14day
*
OG. diff.
OC. diff.
CH. diff.

A

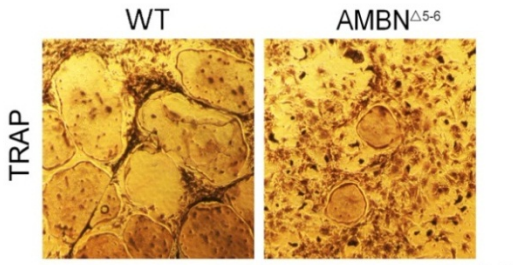
WT
AMBN△5-6
TRAP

D

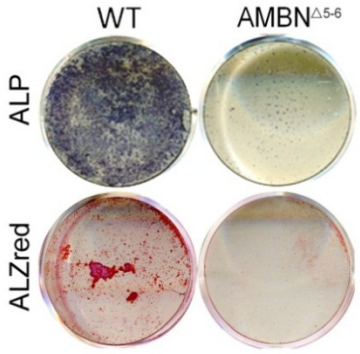
WT
AMBN△5-6
ALP
ALZred

B

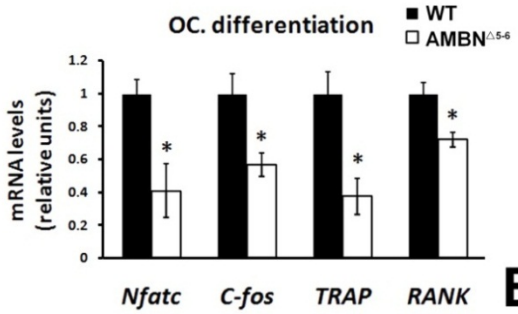
OC. differentiation
WT
AMBN△5-6
mRNA levels (relative units)
1.2
1
0.8
0.6
0.4
0.2
0
*
Nfatc
C-fos
TRAP
RANK

E

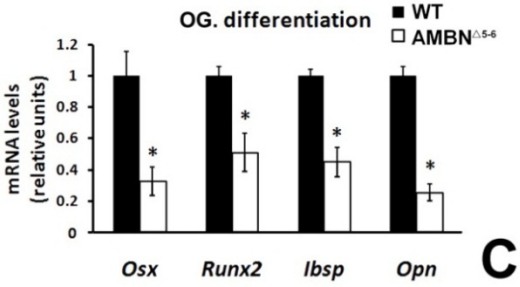
OG. differentiation
WT
AMBN△5-6
mRNA levels (relative units)
1.2
1
0.8
0.6
0.4
0.2
0
*
Osx
Runx2
Ibsp
Opn

C

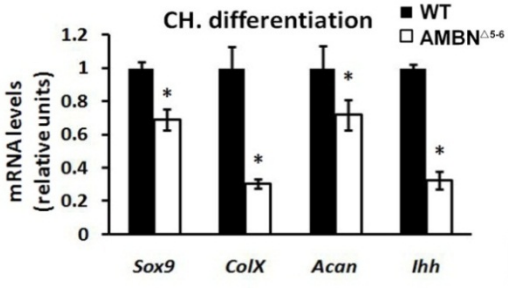
CH. differentiation
WT
AMBN△5-6
mRNA levels (relative units)
1.2
1
0.8
0.6
0.4
0.2
0
*
Sox9
ColX
Acan
Ihh

F

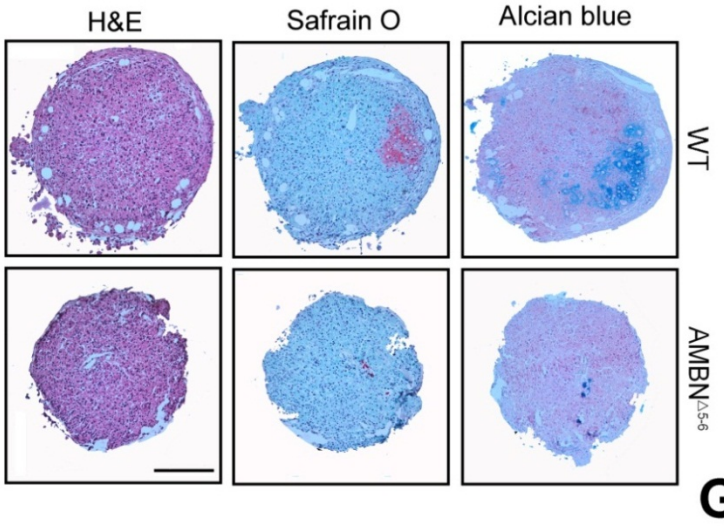
H&E
Safrain O
Alcian blue
WT
AMBN△5-6

G

Figure 20. AMBN mutation affected osteogenesis, osteoclastogenesis and chondrogenesis of bone marrow cells. (A) AMBN expression during osteogenic (OG) and chondrogenic (CH) differentiation of BMSCs, and osteoclastogenic (OC) of BMMCs. Total RNA was isolated after 3,7 and 14 days of culture. AMBN mRNA level were determined by real-time PCR analysis using SYBR Green and normalized to GAPDH. Data were obtained from triplicate PCRs using RNA from three different cultures, and values are presented as means ± SD. * = $p<0.05$ versus 0 day culture. (B) Osteoblastic differentiation of BMSCs from WT and $AMBN^{\Delta 5\text{-}6}$ mice. ALP activity staining was performed after 15 days of osteogenesis induction. Matrix mineralization was verified by alizarin red staining after 21 days of induction. (C) Real-time PCR analysis of osteoblastic markers on day 7 during osteoblastic differentiation of BMSCs. Expression of each targeted gene was normalized to GAPDH and calculated as relative expression over WT expression level. Data are mean ± SD. * = $p<0.05$ homozygous mutant verse WT expression. (D) Osteoclastic formation in the culture of BMMCs obtained from wild-type and AMBN mutant mice. $TRAP^{+}$ multinucleated cells were induced by M-CSF and RANKL treatment for 10 days. (E) Real-time PCR analysis of *c-fos, Nfatc1, RANK* and *TRAP* expression. Real-time PCR analysis was performed using SYBR Green and normalized to the levels of GAPDH. Data were obtained from 4 different cell cultures, and values are expressed as mean ±SD.* = $p<0.05$ $AMBN^{\Delta 5\text{-}6}$ verse WT expression. (F) Real-time PCR analysis of chondrocytes differentiation markers on day 7 after induction. Expression of each target gene was normalized to GAPDH and calculated as relative expression over WT expression level. Data are mean ±SD. * = $p<0.05$ verse WT expression. (G) The histological section of primary BMSC chondrogenic aggregated culture from WT and $AMBN^{\Delta 5\text{-}6}$mice on day 21, using H&E staining (upper panels), Alcian Blue staining (middle) and Safrain O staining (lower panels). Bar=200μm.

C.10. Reduced expression of osteogenesis- and chondrogenesis-related growth factors in AMBN$^{\Delta 5\text{-}6}$ mice

In order to identify target genes affected by truncated of full lenght AMBN during osteogenic differentiation of BMSCs, mRNA isolated from WT and AMBN mutant BMSCs were screened for the expression of 84 genes linked to osteoblast differentiation and bone metabolism using PCR array as described (*140*). In total, expression of 27 genes from AMBN$^{\Delta 5\text{-}6}$ mice was either up- or down-regulated (fold change > 2.0 or <-2.0) (data not show) after treatment with osteogeneic medium for 7 days compared with wild type controls. Several osteogenesis-related growth factors were significantly decreased in AMBN$^{\Delta 5\text{-}6}$ mutant BMSCs (Fig.21 A). Compared with wild type BMSCs, AMBN mutant BMSCs displayed a 12.9-fold downregulation of *Bmp7* and 5.2-fold downregulation of *Igf1*. Expression levels of *Fgfr1, Bmp6, Ihh, Bmp2* and *Csf-1* were also down regulated.

To confirm the PCR array results, real-time PCR was performed independently and in duplicate from 3 different animal samples in each genotype group (Fig.21 B). After 7 days of osteogenic stimulation, *Bmp7* expression in AMBN mutant BMSCs was 80% ($p<0.05$) lower than in wild type controls, and *Igf1, Csf-1* and *Ihh* expression levels were significantly ($p<0.05$) decreased (41%, 50% and 22% respectively) compared with controls.

Subsequently, immunohistochemistry was used to verify our PCR array and real-time PCR results, and to qualitatively illustrate the presence of the genes products involved in long bone growth (Fig.21 C-E). In postnatal day 21 littermates, osteoblasts reacted positively for IGF1 on the trabecular bone surface of the distal femur metaphysis (Fig.8 C) of AMBN mutant and wild type control mice. The number of brownish stained IGF1 expressing osteoblast was significantly reduced by 32% ($p<0.05$) compared to that of WT mice as documented by semiquantification

histological analysis (Fig.21 E). Similarly, the number of brownish-stained BMP7 expressing osteoblast was 21% less ($p<0.05$) in the AMBN mutants when compared with WT littermates (Fig.21, D, E). These data indicate that disruption of the full length AMBN impairs the expression of osteogenesis-related growth factors such as IGF1 and BMP7, adding another potential mechanism by which AMBN might affect long bone growth.

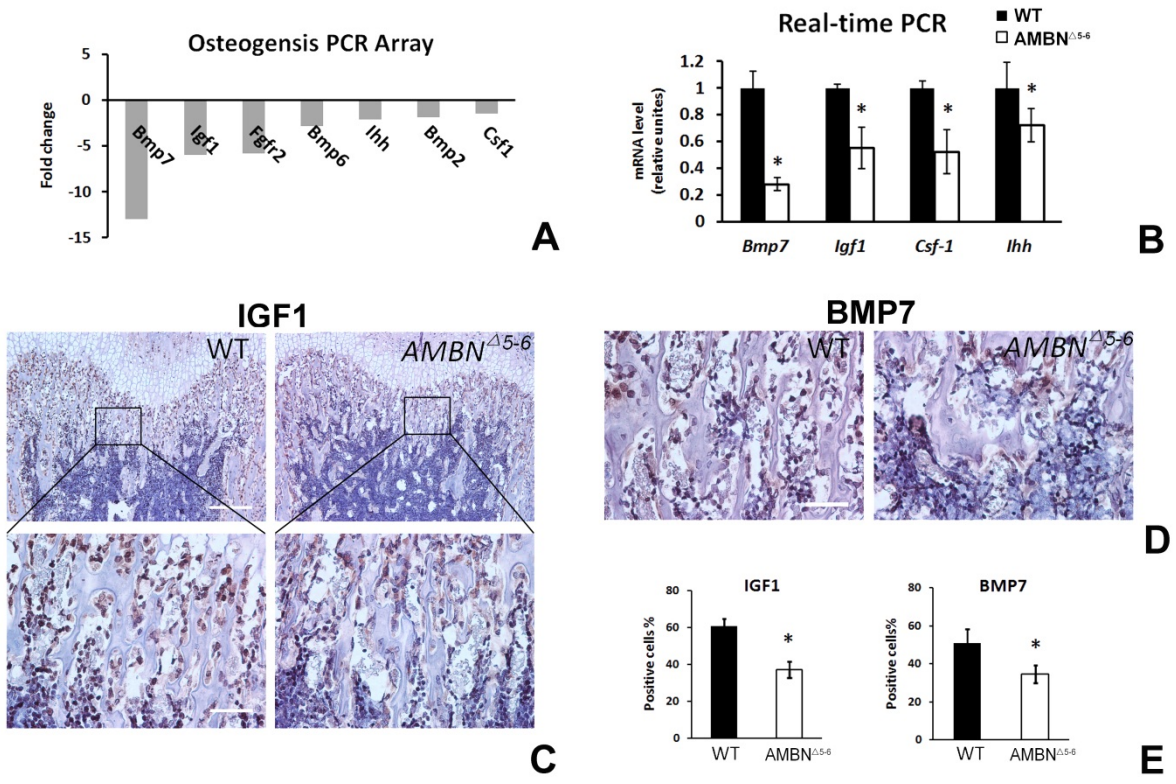

Figure 21. Expression of osteogenesis- and chondrogenesis- related growth factors were reduced in AMBN$^{\Delta 5\text{-}6}$ mice. (A) Selected down-regulated genes (<2.5 fold) after 7 days osteogenic induction of BMSCs from AMBN$^{\Delta 5\text{-}6}$ mice compare with WT cells. (B) Real-time PCR analysis confirmed the down-regulated osteogenesis-related growth factors from WT and AMBN$^{\Delta 5\text{-}6}$ in 4 mice in each group. Expression of each gene was normalized to GAPDH and calculated as relative with WT expression level. Data are mean ± SD. * = $p<0.05$ verse WT expression. (C) Immunohistochemistry staining localized the IGF1 expression in femurs of 3-week-old WT and AMBN mutant litters. Lower panels is the high magnification of inset box from upper panels. Bar=200μm upper, and =50μm lower. (D) BMP7 expression in same samples of WT and AMBN mutant litters as (C). Bar=50μm. (E) Histomorphometry analysis showed the ratio of IGF1 (left) and BMP7 (right) positive cell verse total nucleated cell. Data were obtained from 3 different mice in each group expressed as the mean ±SD. * = $p<0.05$ mutant verse WT.

C.11. Fracture healing was delayed in AMBN$^{\Delta 5\text{-}6}$ mice

Bone fracture healing is a specialized wound healing process important for the survival of organisms and similar in nature to skeletal development (*141*). Endochondral fracture healing requires primary cartilage formation and a subsequent replacement of the cartilaginous soft callus by hard bony callus (*142*). This process involved numerous growth factors such as BMPs, IGFs, and FGFs, as well as extracellular matrix proteins such as fibronectin, collagen, and osteopontin (*98*). To ask the question whether AMBN plays a role in long bone fracture healing, AMBN mutant mice and WT controls were subjected to a lower leg fracture procedure. Following bone fracture, there were no skeletal malformations in mice from all groups as revealed by X-ray analysis (Fig.22 A). All groups displayed a similar fracture pattern involving both tibia and fibula with a consistent transverse gap in the center of the tibia diaphysis. The fracture gap remained clear without indication of bridging by day 7 post-operatively, both in WT and AMBN$^{\Delta 5\text{-}6}$ mutant mice. By day 21, a blurred gap with more consolidated bridging was observed and the bridging was almost complete on the last time point (D28) in this study.

Micro-CT data revealed an unbridged large callus in 3D images of the control mouse fracture on D7. On D14, the fracture displayed a large and bridged callus with well-defined areas of mineralized tissue. On D21, control fractures formed a fully bridged, solid bony callus and also contained porous bony structures on the surface. On D28 the bony callus united with cortical bone forming a smooth surface (Fig.22 B, upper panels). In contrast, the 3D reconstruction AMBN$^{\Delta 5\text{-}6}$fracture callus appeared smaller than that of the control animals on D7 and D14 and did not bridge the fracture gap (Fig.22 B, lower panels). On D21 and D28, the fracture gap was bridged in AMBN$^{\Delta 5\text{-}6}$ animals, but contained extensive porous structures not detected in wild type control animals. The callus bone volume/total volume (BV/TV) ratio at fracture sites was

significantly decreased in AMBN$^{\Delta 5\text{-}6}$ mice compared to WT control mice by D7, D14, D21 and D28 post-operatively ($p<0.05$) (Fig.22 C). Callus bone mineral density values (BMD) in AMBN$^{\Delta 5\text{-}6}$ were also decreased by D7 and D14, but almost matched those of wild type control levels by D21 and D28 (Fig.22 D).

Histologic analysis was performed using Safranin O staining (Fig.23 A). By D7, the control group displayed a small cartilaginous callus with periosteal ossification starting adjacent to the cartilage borders. By D14, the differentiated cartilage was decreased in size, and ossification center were detected on both sides of the cortical bone. By D21 and D28, the control callus was fully bridged and the cartilage was almost undetectable by Safranin O staining. At this stage, the cortical bone was largely remodeled. Compared to the normal fracture repair process, cartilaginous callus formation in AMBN$^{\Delta 5\text{-}6}$ mice was distinctly different (Fig.23 A, right panels). The cartilaginous area in the callus on D7 and D14 was much larger than in controls, indicative of the unbridged bone fracture. By D21 and D28, the cartilage was almost undetectable and the fracture gap was closed, however, cortical bone continuity at the fracture site was interrupted. Histomorphometric analysis demonstrated a significant increase in the cartilage area/periosteal callus area (Cg.Ar./Ps.Cl.Ar.%) of D10 and D14 mice, while the mineralized area/periosteal callus area (Md.Ar./Ps.Cl.Ar.%) was reduced by D7 to D28 post-operatively ($p<0.05$) in AMBN$^{\Delta 5\text{-}6}$ mutant mice compared to wild type controls. By D28, the cartilage area in both WT and AMBN mutant animals was almost undetectable.

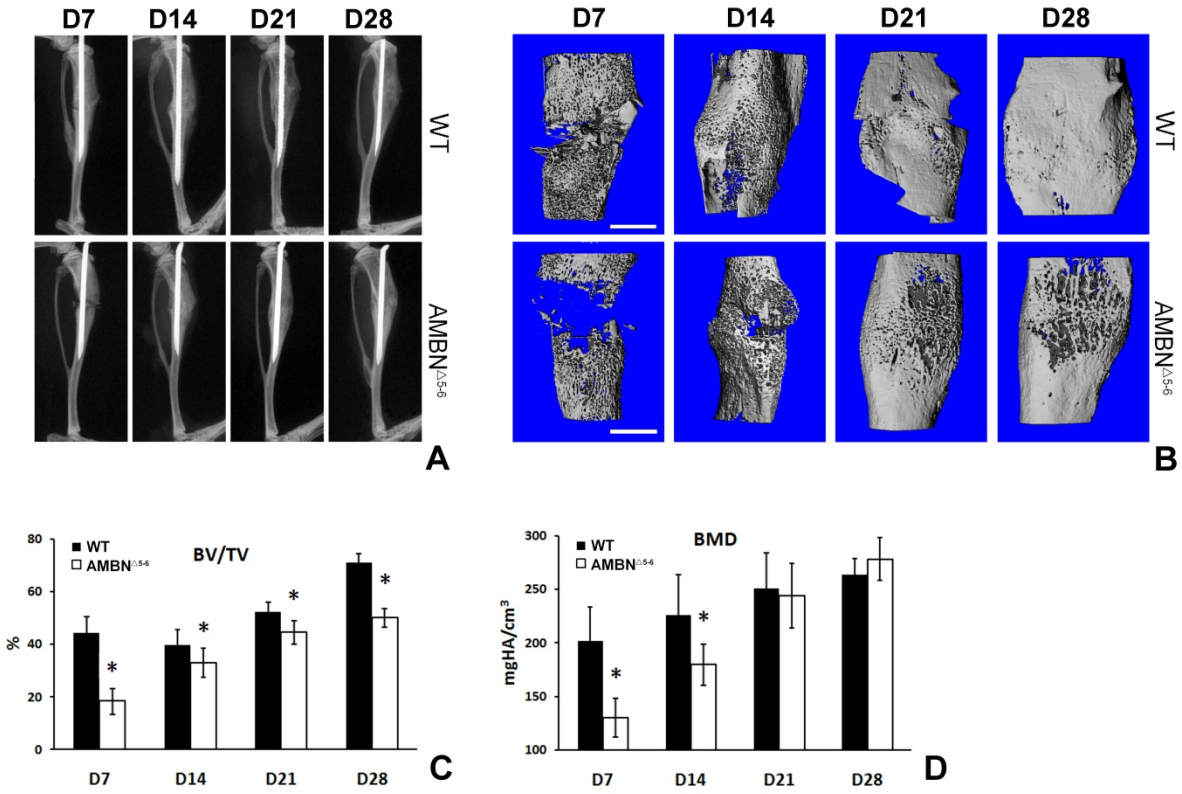

Figure 22. Representative X-ray and 3D μ-CT images of the fracture callus in the WT and AMBN$^{\Delta 5-6}$ mice. (A) X-ray radiographic evaluation of the fracture sites at 7, 14, 21 and 28 days post-surgery between WT and AMBN mutant mice. (B) The μ-CT reconstruction of fracture callus showed the morphological structure and mineralization of callus tissue 7-28 days post-operative. Bar=1mm. (C, D) The bone volume (BV/TV) (C) and bone mineral density (BMD) (D) were analysis between WT and AMBN mutant group. * = $p<0.05$ verse WT

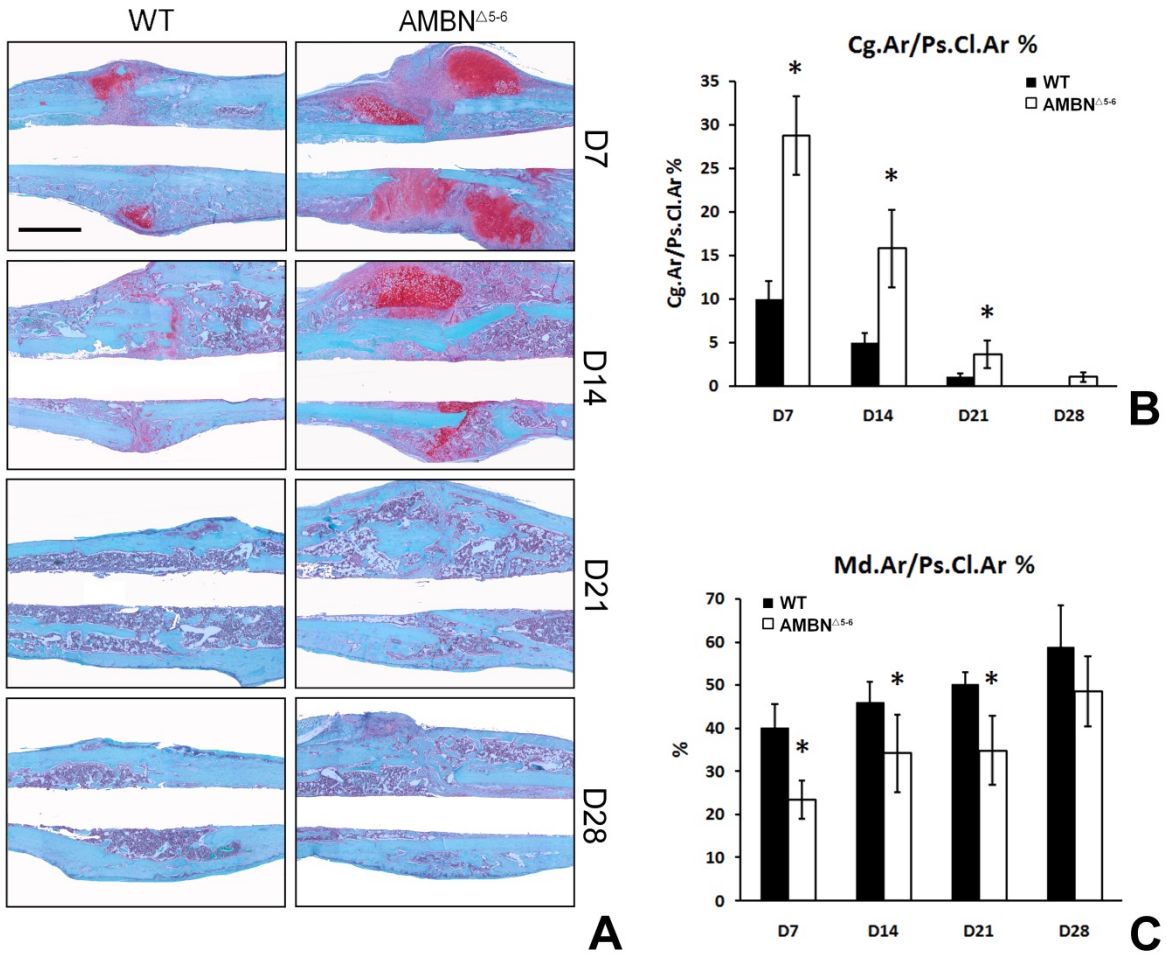

Figure 23. Histological analysis of AMBN$^{\Delta 5\text{-}6}$ and WT mice during healing stages. (A)The sections were stained by Safrain O to mark cartilage (red) and mineralized tissue (green) of AMBN$^{\Delta 5\text{-}6}$ and WT mice at different time points. Bar=1mm. (B, C) Histomorphometric quantification of cartilage area verse periosteal callus area (Cg.Ar./Ps.Cl.Ar.%) (B) and mineralized area verse periosteal callus area (Md.Ar./Ps.Cl.Ar.%) (C) between WT and AMBN mutant group during fracture healing stage. Data are presented as mean and ± SD. Statistical significance was evaluated by one way ANOVA, *$p<0.05$.

TABLE III

LIST OF PRIMERS

GENOTYPE PCR PRIMERS

Forward 1 (*Ambn*^{WT})	5'-CAAGTTGCCTTACCCCAAGA-3'
Reward 1 (*Ambn*^{WT})	5'-TTGGGGTTATTGGAGTGGAG-3'
Reward 2 (*Ambn*$^{\triangle 5\text{-}6}$)	5'-AAGCGAAGGAGCAAAGCTGCTATT-3'
K14 Forward	5'-GCTTAGCCAGGGTGACAGAG-3'
K14 Reward	5'-CACAGAGGCGTAAATGCAGA-3'

REAL TIME PCR PRIMERS

AMBN	NM_009664.1	Forward	5'-TTTTGATTGGCATCATCAGG-3'
		Reward	5'-TAGCAGTGGCTGCTGAGTGT-3'
ACAN	NC_000073	Forward	5'-AGGTTGCTATGGTGACAAGG-3'
		Reward	5'-TGGAAGGTGAATTTCTCTGGG-3'
BMP7	NM_007557	Forward	5'-ACTACATCCGGGAGCGATTTGACA-3'
		Reward	5'-TATCAAACACCAACCAGCCCTCCT-3'
C-FOS	NM_010234	Forward	5'-CCGTGTCAGGAGGCAGAGC-3'
		Reward	5'-GCAGCCATCTTATTCCGTTCCC-3'
COL 1a1	NM_007742	Forward	5'-AAGACCTCCCGCCTGCCCAT-3'
		Reward	5'-CACGAAGCAGGCAGGCAGGGCCAA-3'
COL 2a1	NM_031163	Forward	5'-TGTCTGCAGAATGGGCAGAGGTAT-3'
		Reward	5'-AGGACATTCCCAGTGTCACACACA-3'
COL X	NM_009925	Forward	5'-GCAGCATTACGACCCAAGAT-3'
		Reward	5'-TGAGTCCCTTTCACATGCAC-3'
CSF-1	NM_007778	Forward	5'-TTTTCCTGGGCATTGTGGTCT-3'
		Reward	5'-AGGAGGTTCAGGGCTTCTTTG-3'
GAPDH	NM_008084	Forward	5'-GGGTGTGAACCACGAGAAAT-3'
		Reward	5'-CCTTCCACAATGCCAAAGTT-3'
IBSP	NM_008318	Forward	5'-GCCTCAGTTGAATAAACATGAAA-3'
		Reward	5'-TCCTCACCCTTCAATTAAATCCCACAA-3'
IGF1	NM_010512	Forward	5'-TGAGCTGGTGGATGCTCTTCAGTT-3'
		Reward	5'-TCATCCACAATGCCTGTCTGAGGT-3'
IHH	NM_010544	Forward	5'-GAGCTCACCCCCAACTACAA-3'
		Reward	5'-TGACAGAGATGGCCAGTGAG-3'
NFATC1	NM_001164109	Forward	5'-AGCCCAAGTCTCACCACAGG-3'
		Reward	5'-CAGCCGTCCCAATGAACAGC-3'
OPN	NM_001204201	Forward	5'-TCTGATGAGACCGTCACTGC-3'
		Reward	5'-CCTCAGTCCATAAGCCAAGC-3'
OSX	NC_000081.6	Forward	5'-TTCTGTCCCCTGCTCCTTCTAG-3'
		Reward	5'-CGTCAACGACGTTATGCTCTTC-3'

TABLE III

LIST OF PRIMERS(continued)

REAL TIME PCR PRIMERS (continued)

PTHrP	NM_008970	Forward	5'-ACAAGGTGGAGACGTACAAAG-3'
		Reward	5'-TTCTCCTGTTCTCTGCGTTTC-3'
RANK	NM_009399	Forward	5'-TCGTCCACAGACAAATGCAAAC-3'
		Reward	5'-TGGAAGAGCTGCAGACCACAT-3'
RUNX2	NM_009820	Forward	5'-GCCTCACAAACAACCACAGA-3'
		Reward	5'-TTAAACGCCAGAGCCTTCTT-3'
SOX9	NM_011448	Forward	5'-GGGCTGGTACTTGTAATCGG-3'
		Reward	5'-CAAGACTCTGGGCAAGCTC-3'
TRAP	NM_001102404	Forward	5'-AACACCACGAGAGTCCTGCT-3'
		Reward	5'-GTACCAGGGCAGAGAAGCTG-3'

IV. DISCUSION

A. The function of AMBN in enamel.

In the present study transmission electron microscopy and scanning electron microscopy were used to study the influence of the enamel matrix protein AMBN on enamel crystal growth in transgenic mouse models. According to western blot analysis, the K14 promoter-driven AMBN construct resulted in strong AMBN over- expression in developing teeth, while the cross with AMELX null mice successfully removed the AMELX background. The expression of K14 in developing ameloblasts was confirmed in earlier studies (*143*) and the robust K14 promoter has been used successfully to drive transgene expression in epithelial tissues (*144*). The cross of a strong AMBN overexpressor with an AMEL null mouse resulted in the generation of a unique enamel matrix highly enriched in AMBN and devoid of AMELX, according to western blotting.

Evaluation of transmission electron micrographs demonstrated that enamel crystals in the AMBN-enriched enamel matrix devoid of AMELX were short and randomly oriented compared with the long and parallel oriented crystals in controls. These data suggest that among enamel proteins, AMBN is not involved in enamel apatite crystal elongation along the *c*-axis and perhaps plays other roles in enamel crystal growth. Unlike AMBN, there have been numerous studies suggesting that AMELX is associated with *c*-axis crystal growth (*145-148*) especially as a result of its elongated PXX tripeptide repeats. This hypothesis was confirmed here by the presence of long and parallel crystals in the wild-type control and in the AMBN overexpressor, both of which expressed AMELX. The data presented here also revealed an unexpected growth of elongated and parallel enamel crystals in the AMELX null mouse. The AMELX null rudimentary enamel matrix contains both enamelin and AMBN among major enamel proteins,

but no AMELX, suggesting that apart from AMELX, enamelin might play a role in crystal elongation, as suggested earlier (*149, 150*).

Compared with an earlier study in which the AMELX promoter was used to drive the AMBN transgene (*23*), the enamel generated in our K14 promoter-driven AMBN overexpressors featured enamel prisms of half the diameter of their wild-type counterparts. At an ultrastructural level, individual crystals were sharply delineated from inter crystal line protein matrix, a finding that was only exaggerated in the AMBN overexpressors lacking AMELX. These data were somewhat in contrast with the reduction in rod architecture, the increase in inter-rod enamel crystal patterns, and the reduction in crystal length reported in an earlier study based on an AMELX promoter-driven AMBN overexpressor (*23*). Neither the AMELX promoter of the previous study nor the K14 promoter employed here represent the gene-specific promoter that naturally controls AMBN expression, the AMBN promoter. The K14 promoter model used in the present study certainly benefits from AMBN overexpression during an extended period of amelogenesis, and significant AMBN overexpression was demonstrated by western blotting. At least for the purpose of the present study, and in tandem with the cross with AMELX null mice, our K14-driven AMBN overexpressor proved to be a highly suitable model system for testing the effect of an AMBN-enriched matrix on hydroxyapatite crystal growth.

Comparative studies with developing *Iguana* enamel revealed that the short and randomly oriented crystals in the AMBN-rich enamel matrix exhibited remarkable similarity with the short and randomly oriented enamel crystals of the squamate reptile *I. iguana*. The short and randomly oriented enamel crystals of AMBN overexpressors and the thin enamel layer of *Iguana* were representative of the enamel crystal organization found in the development enamel of many squamates (*27, 151*). Based on earlier hypotheses on the relationship between ameloblasts and

secreted matrix during enamel prism growth (*152*), it is likely that both cellular and biochemical factors play a role in the rapid change in crystal orientation and structure during the reptilian–mammalian transition. Biochemical factors include an increase of the percentage of AMELX in the enamel matrix or a change in enamel protein processing and alternative splicing (*153*). Cellular factors involved in prism shape and growth may include Tomes' processes (*154*) and the mechanisms that control its extension. As suggested earlier (*152*), biochemical and cellular factors may influence each other and depend on each other. Here we explain the similarities in enamel crystal structure between the developing *Iguana* enamel and the AMBN-rich enamel as a result of a higher percentage of AMBN in the developing *Iguana* matrix compared with its mammalian counterpart. Such an explanation is bolstered by the previously reported gradual increase of AMELX in the developing enamel matrix at the expense of other enamel proteins during vertebrate evolution (*149, 150*).

B. The function of AMBN in periodontal ligament

In the present study we have used a number of model systems to examine the relationship between the ECM protein AMBN and osteoclast mediated resorption of mineralized tissues such as bone and cementum. AMBN function was tested using both an overexpressing transgenic mouse line and an *in vitro* system in which BMMCs were exposed to AMBN surface coatings. For our transgenic approach we took advantage of naturally occurring AMBN expression levels in Hertwig's Epithelial Root Sheath (HERS) and in the Epithelial Rests of Malassez (ERM), a network of odontogenic epithelial cells remaining in the periodontal ligament after tooth eruption (*143*, *155*). The human Keratin 14 promoter was used to overexpress the AMBN protein in mouse HERS and ERM cells. Keratin 14 is commonly known as an epithelial protein encoded by the KRT14 gene. Here we have further confirmed K14 expression in HERS and ERM by β-gal staining for the K14 LacZ transgene in K14 LacZ transgenic mice using whole mount staining. AMBN and K14 co-localized both in HERS cells and in alveolar bone osteoblasts. In the present study, K14-driven overexpression of AMBN in mouse molars resulted in a robust 5-fold enhancement of AMBN levels compared to controls, confirming the effectiveness of our epithelium-driven AMBN overexpression approach in mouse periodontal tissues. For our *in vitro* studies, we exploited AMBN's putative role as an extracellular matrix protein, using surface coating of culture plates as a well-established method (*156*, *157*, *158*) to examine the effect of AMBN on osteoclast attachment and differentiation. Together, these studies indicated that AMBN significantly altered osteoclast activity, both *in vivo* and *in vitro*.

In developing tooth roots, AMBN was expressed in HERS, ERM, and PDL, as demonstrated by *in situ* hybridization and immunoreactions. Our data on AMBN expression in HERS and ERM match previous findings (*53, 54, 58, 120*). Evidence of AMBN expression in HERS and

ERM contributes to an expanded understanding of a group of proteins previously called “enamel proteins”, including AMELX, ENAM, AMBN, and others. In addition to ameloblasts and HERS (*159*), AMBN has now also been identified in pulp cells (*52, 120, 160*), osteoblasts, CD34 + cells and osteoclasts (*125, 57*). AMBN's function in bone remodeling involves homing and recruitment of CD34 + cells and commitment to an osteoblast or osteoclast pathway (*125, 57*). Thus, AMBN function may go beyond its role as cell adhesion modulator in ameloblast differentiation and enamel formation (*60, 17, 159, 161, 162*), and also include a role in bone formation and periodontal regeneration (*125, 159, 163, 116*).

Enforced AMBN expression in our mouse model resulted in bone loss and tooth root resorption, and these defects were accompanied by higher osteoclast activity, actin ring and podosome belt formation, and increased number of TRAP positive cells. Enhanced osteoclast activity in our AMBN overexpressors occurred without inflammatory stimuli, indicating that AMBN affects osteoclast activation directly and without inflammatory mediators. The effect of AMBN as it relates to bone, root, and tooth resorption suggests that AMBN activates classic mechanisms of osteoclastogenesis through modulation of attachment and RANKL activation. In support of this concept, our data indicated that AMBN increased BMMC adhesion and multinucleated osteoclast number through integrins and RhoA. Moreover, AMBN also directly enhanced the effect of RANKL and CSF-1 on osteoclastogenesis, suggesting that AMBN has the ability to trigger key mechanisms of osteoclast induction.

Supportive of a potential involvement of integrins in the effect of AMBN on mineralized tissue homeostasis, our study revealed that the AMBN-induced increase in osteoclast count was significantly reduced when antibodies against integrin α2β1 or an inhibitor against ERK-1 were applied to the culture medium. It has been well-documented that αvβ3 and α2β1 are the most

prominent integrins expressed in BMMCs and osteoclasts (*47*). These integrins mediate osteoclast adhesion to bone matrix proteins and regulate cytoskeleton reorganization (*164*). Other integrins αvβ5 and α9β1 are found in osteoclast precursors and regulate osteoclast formation and function (*165*, *46*). Antibodies against integrin α2β1 only resulted in a partial block of osteoclastogenesis in our study, leaving the possibility open that other isoforms or surface receptors may also be involved in the interaction between AMBN protein and BMMCs.

Our study demonstrated that AMBN treatment enhanced RhoA protein expression and resulted in ERK and AKT phosphorylation. Moreover, blocking ERK and PI3K pathways inhibited AMBN-induced formation of podosome and osteoclast differentiation after BMMCs attached on an AMBN-containing substrate, suggesting that that extracellular matrix signaling pathways play a crucial role in mediating the effect of AMBN on osteoclast differentiation. Cell adhesion to the extracellular matrix, especially through integrins, activates various protein kinases such as focal adhesion kinase, mitogen-activated protein kinase, extracellular signal-regulated kinase, and GTPases of the Rho-family (*166*, *167*). These signaling pathways also play distinct roles in osteoclast differentiation and function (*168*, *169*). Cross-talk between pathways and positive/negative feedback loops are therefore likely to be involved in AMBN-mediated osteoclast dynamics.

Further examination of the mechanism by which AMBN regulates osteoclastogenesis illustrated that expression levels of NFATc1, a key transcription factor of osteoclast differentiation, was increased during RANKL-stimulated osteoclast differentiation following AMBN treatment. AMBN addition to BMMCs resulted in increased expression of the osteoclastogenic transcription factor NFATc1 and this effect once more was blocked using the anti-α2β1 integrin antibody and the ERK-1/2 antagonist U0126. NFATc1 plays a pivotal role in

osteoclast fusion and activation through regulation of various genes responsible for osteoclast adhesion, migration, acidification and degradation of inorganic and organic matrix (*170*). Transcriptional up-regulation of the NFATc1 gene may therefore contribute to enhanced osteoclastogenesis by the AMBN protein. Based on the findings of the present study, we thus propose a model of AMBN-associated osteoclastogenesis by which the AMBN protein enhances BMMC adhesion, induces formation of cell attachment structures, and upregulates Rho A and NFATc1 gene expression, resulting in BMMCs differentiation toward an osteoclast lineage through integrin and MEK/ERK pathways.

C. The function of AMBN in long bone formation

During the recent decade, a number of studies have enhanced the concept of AMBN as an enamel protein and either reported AMBN expression in bones or proposed possible functional intermediaries by which AMBN might affect osteoblasts. The present study was designed to determine whether AMBN expression outside of the craniofacial region was of physiological relevance for the life of an organism. We focused on the femur of developing mice as the subject of analysis, and included other bones of the skeletal system where applicable. Our analysis contained four major aspects, (i) a comprehensive map of AMBN expression during postnatal bone development as revealed by immunohistochemistry and Western blots, (ii) a thorough analysis of the entire skeleton of developing and mature ameloblastin deficient mice ($AMBN^{\Delta 5\text{-}6}$) and especially of their femurs, (iii) a comparison of lower leg long bone fracture healing parameters in wild-type and ameloblastin deficient mice ($AMBN^{\Delta 5\text{-}6}$), and (iv) a series of cellular and mechanistic studies based on bone marrow stem cells (BMSCs) from WT and $AMBN^{\Delta 5\text{-}6}$ mutant mice. Much of our analysis relied on ameloblastin mutant mice, in which the full length AMBN is replaced by a truncated isoform lacking exons 5 and 6 (*124*), effectively eliminating important self-assembly and polyprolin-rich domains, as well as the casein kinase II phosphorylation site in exon 5 (*117-119*). Defects in enamel and periodontal tissues (*124*) in these mice have already been reported, but the dispute over the role of AMBN in bone remodeling and repair remains. Together, our data reveal significantly delayed long bone growth, decreased bone mass, and delayed fracture healing in $AMBN^{\Delta 5\text{-}6}$ femurs, and we attributed this finding to the downregulation of osteogensis-related growth factors, IGF1 and BMP7, in $AMBN^{\Delta 5\text{-}6}$ mesenchymal progenitor cells and their effect on the decrease in proliferation and differentiation potential.

AMBN mRNA and protein were found to be expressed in femur during long bone development. Immunohistochemistry detected AMBN protein, which expressed in chondrocytes, epiphyseal bone cells and differentiated cell layers of the epiphyseal growth plate in the primary ossification center, secondary ossification center and growth plate during postnatal development stage (Fig.14). The epiphyseal growth plate is responsible for elongation and growth of long bones through endochondral ossification (*71*). Spahr et al. showed that AMBN mRNA and protein expression were observed within the hyaline cartilage template, perichondrium and proliferative zone of the cartilage but reduced in the hypertrophic zone (*53*). Their discoveries together with our finding indicate that during endonchondral bone formation, AMBN may play a role in the cartilage formation and/or in its transition into trabecular bone. Moreover, AMBN is also expressed in the long bone periosteum, which composed of progenitor cells, suggesting that AMBN may also function during cortical bone formation.

Since AMBN has been verified to be expressed in many different tissue of mesenchymal origin (*53, 120, 121*), and its potential mechanism related with osteogenesis has been examined (*66*), it is worth to characterize the bone phenotype in the AMBN deficient mice ($AMBN^{\Delta 5\text{-}6}$) (*124*). For this consideration, we collected embryos subject to whole mount staining and examined adults by X-ray scanning to check skeleton (Fig. 15). Our results demonstrated that $AMBN^{\Delta 5\text{-}6}$ exhibited smaller skeleton and mild patterning defects with delayed ossification in phalange and metatarsal at E18.5-day-old. Also compared within 2-month-old adult littermates, AMBN deficient mice appeared morphologically normal but smaller skeleton. During 16-week development, AMBN mutant mice showed a lower growth rate although they took same amount of food compared with wild-type control mice. Previous studies have been shown AMBN expression during craniofacial bone formation from embryonic to postnatal stage and in the bone

formation and remodeling related cells (*53*). In addition, the AMBN gene upstream region contains more than 50 different potential regulatory elements, which relate to embryonic development, mesenchymal differentiation, haematopoietic differentiation and cell cycle control, regulating transcriptional activity (*126*). Taken together, it indicates AMBN may function during the long bone development from embryonic to postnatal stage.

Our data show that the femurs from AMBN$^{\Delta 5\text{-}6}$mice exhibited delayed growth in 6 month development stage associated with the shorten growth plate and decreased proliferating chondrocytes in proliferation zone (Fig. 16, 18).The orderly progression of the growth plate is critical for proper development of the endochondral skeleton during postnatal bone growth (*72*). The proliferation of the less mature chondrocytes at the epiphysis , followed by their hypertrophy and their eventual replacement by trabecular bone near the diaphysis, results in a distal displacement of the growth plate and longitudinal growth of each skeletal element (*95*). The abnormal length or organization of growth plate will cause endonchondral bone defects (*171*). Chondrocytes in the growth plate are influenced by various regulatory factors that together determine the rate of proliferation and maturation (*171*). Paracrine regulators like parathyroid hormone-related protein (PTHrP) and Indian hedgehog (Ihh) are considered key factors in the regulation of the growth plate. These secreted growth factors coordinate endochondral ossification by regulating chondrocyte proliferation and differentiation as well as osteoblast differentiation (*172, 173*). We found the BMSCs from AMBN mutant mice decreased the expression of *Ihh* both during osteogenesis and chondrogenesis differentiation (Fig.20, 21). *Ihh* is primarily synthesized by chondrocytes leaving the proliferative pool (prehypertrophic chondrocytes) and by early hypertrophic chondrocytes (*72*), and promotes chondrocytes proliferation (*174*). It infers AMBN function during bone longitudinal growth by regulating

chondrocytes proliferation mediated by *Ihh.*

Our μ-CT and histology analysis results demonstrated that AMBN$^{\Delta 5\text{-}6}$ mice exhibit low bone mass phenotype and deteriorated bone architecture. We observed that the decrease bone mass appeared both in the trabecular bone and cortical bone compartments (Fig.17). Trabecular bone is formed by osteoblast derived from mesenchymal progenitors first occurs within the perichondrium and continues within the marrow cavity following vascularization of the hypertrophic cartilage (*32*). Cortical bone forming by periosteum is composed of osteoblastic progenitor cells. We observed AMBN protein presented in the trabecular bone surface at the mineralization front of long bones as well as in the periosteum. The serum biochemistry analysis showed that serum ALP activity was decreased in the AMBN mutant mice. Serum ALP is a group of enzymes found primarily in bone tissue. The primary importance of measuring ALP is to check the possibility of bone disease such as fracture and bone loss (*175, 176*). We hold the view that osteoblast activity is impaired by missing full length AMBN. Furthermore, by our histmorphometric study, we found AMBN mutant mice exhibited decreased number of osteoblast on bone area (No. Ob/bone area). Impaired osteoblast bone formation suggests that absence of full-length functional AMBN could lead to impaired attachment, differentiation or function of osteoblastic progenitors. These phenomenons are support by some *in vivo* and *in vitro* studies. Tamburstuen et al. evidenced that AMBN promotes bone growth *in vitro* and stimulates bone healing *in vivo* (*125*). From another aspect, AMBN contains several binding domains to some matrix proteins (*32, 65*), including heparin and fibronectin, and function as an adhesion molecule in extracellular matrix. The long bone defects without functional AMBN are also associated with femur biomechanical parameters changing examined by femur 3-point-bending test (Table I). It suggests AMBN could affect bone mineral matrix composition. This presumed involvement of

AMBN in bone mineralization is supported by several other studies indicating the calcium-binding capability of this protein (*17, 21*).

Decreased *in vivo* bone formation in AMBN$^{\Delta 5\text{-}6}$ mice can result from several defects in osteoblast cell populations, including impaired cell proliferation and differentiation. We found decreased CD105^{+} and CD106^{+} (vascular cell adhesion molecule 1 ,VCAM1) positive stem cell populations (Fig.19), as well as decreased numbers of CFU-F and CFU-ALP, which are surrogate markers for *in vivo* osteogenic stem cells, suggesting the presence of stem cell atrophy in AMBN$^{\Delta 5\text{-}6}$ mice. It is plausible that sufficient numbers of osteogenic progenitors and stem cell proliferating abilities are need for proper bone formation, and this becomes limiting in the context of AMBN deficient function. AMBN is expressed in many mesenchymal origin tissues and cells, including osteoblasts, PDL cells and human mesenchymal stem cells (*57*). And it could promote bone growth by enhance proliferation of progenitor cells (*125*) and regulate osteogenic differentiation (*66*). In our study, we found AMBN expression in the BMSCs during osteogenic differentiation and the bone marker genes (Fig. 20), including *Osx, Runx2*, *Ibsp* and *Opn* were decreased in the AMBN$^{\Delta 5\text{-}6}$ BMSCs cultured in osteoblastogenic differentiation medium. Conversely, in previous studies (*123*) we found overexpression of AMBN inhibits cranial suture closure by reducing Msx2 down-stream target genes. It is thus plausible that AMBN might function as osteogenic balancing molecule, either upregulating or downregulating expression causing bone formation defects. There are a few other examples of a single protein either over- or lower- expression leading to suppression of osteoblast cell differentiation (*78, 177*). In all case where an amount of portion expression in the cell and tissue is important to maintain the proper bone mass.

Our findings reveal that AMBN also acts as an intrinsic regulator of osteoclast

differentiation (Fig. 20). During osteoclast differentiation, AMBN expression significantly increased after 7 days treated by osteoclastic induction medium. The number and surface area of osteoclasts were reduced in Ambn$^{\Delta 5\text{-}6}$ mice consistent with decreased serum TRAP activity, which is a bone resorption marker related to osteoclast activity. In addition, AMBN$^{\Delta 5\text{-}6}$ precursor cells, when cultured in the presence of RANKL and M-CSF, showed a markedly reduced number of mature osteoclasts after 10-day culture. Our findings also revealed that osteoclasts marker genes, including *Nfatc1, c-fos, TRAP* and *RANK*, were significantly downregulated in AMBN$^{\Delta 5\text{-}6}$ osteoclasts. Therefore, it is possible that mature osteoclast numbers are reduced in AMBN mutant owing to the loss of AMBN function in osteoclast precursors resulting in inhibition of osteoclast differentiation. This discovery is supported by our previous study which confirmed AMBN modulates osteoclastogenesis through ERK/integrin pathway (*178*). During BMSCs differentiated to chondrocytes, AMBN expression also significant increased after 7 days treatment by chondrogeneic medium (Fig.20). And in the absence of full length AMBN less secreted proteoglycans in BMSCs were present in BMSCs pellet culture. Thus, AMBN may function during chondrocytes differentiation.

We found that AMBN$^{\Delta 5\text{-}6}$ mice exhibited a low bone mass phenotype possibly associated with decreased expression of several osteogenesis-related growth factores, including BMP7, BMP2, IGF1, IHH and CSF-1 (Fig.21). IGF1 is the most abundant growth factor produced by osteoblasts (*179, 180*) and stored in bone matrix. *In vitro* studies showed that IGF1 increases osteoblast proliferation, matrix synthesis and mineralization (*32, 181*). *Igf1* null mice exhibit impaired postnatal growth and defect in longitudinal bone growth (*107, 182*). Our AMBN mutant mice showed delayed femur growth and decreased proliferation ability of BMSCs, these phenotypes might be associated with decreased IGF1 expression both in the cell and bone. BMPs

have a central role in bone development and osteoblast differentiation (*183*), which in turn regulate the bone marker gene expression. In PDL cells, AMBN and AMELX showed growth factor like activity and promoted PDL cells to express BMP2 and BMP4 (*56, 116*). Following experiments showed that BMSCs treated by AMBN protein led to enhance BMP2 expression (*125*). By loss-of-function studies, we found not only BMP2, but also BMP7 were down-regulated in $AMBN^{\Delta 5\text{-}6}$ BMSCs. BMP7 plays a pivotal role in the development of bone and kidney, and is also crucially involved in differentiation of brown adipose tissue (*98*). Clinically, BMP7 is used in orthopedics to treat bone fracture healing defects that could not be healed with autologous bone (*184*). In our research, we evaluated bone fracture healing process in $AMBN^{\Delta 5\text{-}6}$ mice by μ-CT and histomorphometry (Fig. 22, 23). Compared with wild-type mice, the bone healing process was delayed in AMBN mutants that showed significant decreases in BV/TV and BMD. Furthermore, large cartilage volume and smaller bone volume were detected in AMBN mutant mice compare with wild-type control, suggesting that AMBN may lead to a prolonged cartilage phase and delayed osteogenic phase in fracture callus. This finding further verified AMBN function might relate with chondrogenesis differentiation and endochondral ossification.

In conclusion, our findings provide evidences that AMBN expressed during long bone development and mutated AMBN cause delayed femur growth and low bone mass phenotypes. Less bone content in AMBN mutant results from BMSCs impaired proliferation and osteogenic differentiation potentials which is associate with down regulated osteogenesis-related growth factors, IGF1 and BMP7. Moreover, our finding also showed AMBN plays roles in osteoclastogenic differentiation suggesting that AMBN not only relate s to bone formation but is also involve in bone remodeling. Finally, the bone fracture healing deficiency in $Ambn^{\Delta 5\text{-}6}$ mutant further verified AMBN function in chondrocytes differentiation and could potentially

explain the growth plate defects in the AMBN mutant.

V. CITED LITERATURE

(1) Kawasaki, K., Suzuki, T., and Weiss, K.M. (2004) Genetic basis for the evolution of vertebrate mineralized tissue. *Proceedings of the National Academy of Sciences of the United States of America*. **101**, 11356-11361

(2) Kawasaki, K., and Weiss, K.M. (2006) Evolutionary genetics of vertebrate tissue mineralization: the origin and evolution of the secretory calcium-binding phosphoprotein family. *Journal of experimental zoology. Part B, Molecular and developmental evolution*. **306**, 295-316

(3) Kawasaki, K., and Weiss, K.M. (2003) Mineralized tissue and vertebrate evolution: the secretory calcium-binding phosphoprotein gene cluster. *Proceedings of the National Academy of Sciences of the United States of America*. **100**, 4060-4065

(4) Kawasaki, K., and Weiss, K.M. (2008) SCPP gene evolution and the dental mineralization continuum. *Journal of dental research*. **87**, 520-531

(5) Fisher, L.W., Torchia, D.A., Fohr, B., Young, M.F., and Fedarko, N.S. (2001) Flexible structures of SIBLING proteins, bone sialoprotein, and osteopontin. *Biochemical and biophysical research communications*. **280**, 460-465

(6) Sire, J.Y., Davit-Beal, T., Delgado, S., and Gu, X. (2007) The origin and evolution of enamel mineralization genes. *Cells, tissues, organs*. **186**, 25-48

(7) Lau, E.C., Mohandas, T.K., Shapiro, L.J., Slavkin, H.C., and Snead, M.L. (1989) Human and mouse amelogenin gene loci are on the sex chromosomes. *Genomics*. **4**, 162-168

(8) Salido, E.C., Yen, P.H., Koprivnikar, K., Yu, L.C., and Shapiro, L.J. (1992) The human enamel protein gene amelogenin is expressed from both the X and the Y chromosomes. *American journal of human genetics*. **50**, 303-316

(9) Hart, P.S., Hart, T.C., Simmer, J.P., and Wright, J.T. (2002) A nomenclature for X-linked amelogenesis imperfecta. *Archives of oral biology*. **47**, 255-260

(10) Wright, J.T., Hart, P.S., Aldred, M.J., Seow, K., Crawford, P.J., Hong, S.P., Gibson, C.W., and Hart, T.C. (2003) Relationship of phenotype and genotype in X-linked amelogenesis imperfecta. *Connective tissue research*. **44 Suppl 1**, 72-78

(11) Gibson, C.W., Yuan, Z.A., Hall, B., Longenecker, G., Chen, E., Thyagarajan, T., Sreenath, T., Wright, J.T., Decker, S., Piddington, R., Harrison, G., and Kulkarni, A.B. (2001) Amelogenin-deficient mice display an amelogenesis imperfecta phenotype. *The Journal of biological chemistry*. **276**, 31871-31875

(12) Lyngstadaas, S.P., Risnes, S., Sproat, B.S., Thrane, P.S., and Prydz, H.P. (1995) A synthetic, chemically modified ribozyme eliminates amelogenin, the major translation

product in developing mouse enamel in vivo. *The EMBO journal*. **14**, 5224-5229

(13) Brookes, S.J., Robinson, C., Kirkham, J., and Bonass, W.A. (1995) Biochemistry and molecular biology of amelogenin proteins of developing dental enamel. *Archives of oral biology*. **40**, 1-14

(14) Moradian-Oldak, J., and Goldberg, M. (2005) Amelogenin supra-molecular assembly in vitro compared with the architecture of the forming enamel matrix. *Cells, tissues, organs*. **181**, 202-218

(15) Fincham, A.G., Moradian-Oldak, J., Simmer, J.P., Sarte, P., Lau, E.C., Diekwisch, T., and Slavkin, H.C. (1994) Self-assembly of a recombinant amelogenin protein generates supramolecular structures. *Journal of structural biology*. **112**, 103-109

(16) Fincham, A.G., and Simmer, J.P. (1997) Amelogenin proteins of developing dental enamel. *Ciba Foundation symposium*. **205**, 118-130; discussion 130-114

(17) Krebsbach, P.H., Lee, S.K., Matsuki, Y., Kozak, C.A., Yamada, K.M., and Yamada, Y. (1996) Full-length sequence, localization, and chromosomal mapping of ameloblastin. A novel tooth-specific gene. *The Journal of biological chemistry*. **271**, 4431-4435

(18) Mardh, C.K., Backman, B., Simmons, D., Golovleva, I., Gu, T.T., Holmgren, G., MacDougall, M., and Forsman-Semb, K. (2001) Human ameloblastin gene: genomic organization and mutation analysis in amelogenesis imperfecta patients. *European journal of oral sciences*. **109**, 8-13

(19) Fukumoto, S., Yamada, A., Nonaka, K., and Yamada, Y. (2005) Essential roles of ameloblastin in maintaining ameloblast differentiation and enamel formation. *Cells, tissues, organs*. **181**, 189-195

(20) Hu, C.C., Fukae, M., Uchida, T., Qian, Q., Zhang, C.H., Ryu, O.H., Tanabe, T., Yamakoshi, Y., Murakami, C., Dohi, N., Shimizu, M., and Simmer, J.P. (1997) Cloning and characterization of porcine enamelin mRNAs. *Journal of dental research*. **76**, 1720-1729

(21) Yamakoshi, Y., Tanabe, T., Oida, S., Hu, C.C., Simmer, J.P., and Fukae, M. (2001) Calcium binding of enamel proteins and their derivatives with emphasis on the calcium-binding domain of porcine sheathlin. *Archives of oral biology*. **46**, 1005-1014

(22) Uchida, T., Murakami, C., Wakida, K., Satoda, T., Dohi, N., and Takahashi, O. (1997) Synthesis, Secretion, Degradation, and Fate of Ameloblastin During the Matrix Formation Stage of the Rat Incisor as Shown by Immunocytochemistry and Immunochemistry Using Region-specific Antibodies. *Journal of Histochemistry & Cytochemistry*. **45**, 1329-1340

(23) Paine, M.L., Wang, H.J., Luo, W., Krebsbach, P.H., and Snead, M.L. (2003) A transgenic

animal model resembling amelogenesis imperfecta related to ameloblastin overexpression. *The Journal of biological chemistry*. **278**, 19447-19452

(24) Kim, J.W., Simmer, J.P., Lin, B.P., Seymen, F., Bartlett, J.D., and Hu, J.C. (2006) Mutational analysis of candidate genes in 24 amelogenesis imperfecta families. *European journal of oral sciences*. **114 Suppl 1**, 3-12; discussion 39-41, 379

(25) Donoghue, P.C., and Sansom, I.J. (2002) Origin and early evolution of vertebrate skeletonization. *Microscopy research and technique*. **59**, 352-372

(26) Sire, J.Y., Delgado, S., Fromentin, D., and Girondot, M. (2005) Amelogenin: lessons from evolution. *Archives of oral biology*. **50**, 205-212

(27) Diekwisch, T.G., Berman, B.J., Anderton, X., Gurinsky, B., Ortega, A.J., Satchell, P.G., Williams, M., Arumugham, C., Luan, X., McIntosh, J.E., Yamane, A., Carlson, D.S., Sire, J.Y., and Shuler, C.F. (2002) Membranes, minerals, and proteins of developing vertebrate enamel. *Microscopy research and technique*. **59**, 373-395

(28) C. B. Wood, E.R.D., A. W. Crompton. (1999) New Studies of Enamel Microstructure in Mesozoic Mammals: A Review of Enamel Prisms as a Mammalian Synapomorphy. *Journal of Mammalian Evolution*. **Volume 6**, pp 177-213

(29) Teitelbaum, S.L. (2000) Bone resorption by osteoclasts. *Science*. **289**, 1504-1508

(30) Nakagawa, N., Kinosaki, M., Yamaguchi, K., Shima, N., Yasuda, H., Yano, K., Morinaga, T., and Higashio, K. (1998) RANK is the essential signaling receptor for osteoclast differentiation factor in osteoclastogenesis. *Biochemical and biophysical research communications*. **253**, 395-400

(31) Lacey, D.L., Timms, E., Tan, H.L., Kelley, M.J., Dunstan, C.R., Burgess, T., Elliott, R., Colombero, A., Elliott, G., Scully, S., Hsu, H., Sullivan, J., Hawkins, N., Davy, E., Capparelli, C., Eli, A., Qian, Y.X., Kaufman, S., Sarosi, I., Shalhoub, V., Senaldi, G., Guo, J., Delaney, J., and Boyle, W.J. (1998) Osteoprotegerin ligand is a cytokine that regulates osteoclast differentiation and activation. *Cell*. **93**, 165-176

(32) John P. Bilezikian, L.G.R.a.T.J.M. (2008) *Principles of bone biology* pp. 342, UK: Oxford

(33) Rodriguez-Pato, R.B. (2004) Root resorption in chronic periodontitis: a morphometrical study. *Journal of periodontology*. **75**, 1027-1032

(34) Hartsfield, J.K., Jr. (2009) Pathways in external apical root resorption associated with orthodontia. *Orthodontics & craniofacial research*. **12**, 236-242

(35) McCauley, L.K., and Nohutcu, R.M. (2002) Mediators of periodontal osseous destruction and remodeling: principles and implications for diagnosis and therapy. *Journal of*

periodontology. **73**, 1377-1391

(36) Page, R.C., and Schroeder, H.E. (1976) Pathogenesis of inflammatory periodontal disease. A summary of current work. *Laboratory investigation; a journal of technical methods and pathology*. **34**, 235-249

(37) Nakamura, I., Rodan, G.A., and Duong le, T. (2003) Regulatory mechanism of osteoclast activation. *Journal of electron microscopy*. **52**, 527-533

(38) Takahashi, N., Ejiri, S., Yanagisawa, S., and Ozawa, H. (2007) Regulation of osteoclast polarization. *Odontology / the Society of the Nippon Dental University*. **95**, 1-9

(39) Saltel, F., Destaing, O., Bard, F., Eichert, D., and Jurdic, P. (2004) Apatite-mediated actin dynamics in resorbing osteoclasts. *Molecular biology of the cell*. **15**, 5231-5241

(40) Jurdic, P., Saltel, F., Chabadel, A., and Destaing, O. (2006) Podosome and sealing zone: specificity of the osteoclast model. *European journal of cell biology*. **85**, 195-202

(41) Barkalow, K., and Hartwig, J.H. (1995) Actin Cytoskeleton - Setting the Pace of Cell-Movement. *Curr Biol*. **5**, 1000-1002

(42) Chellaiah, M.A., Soga, N., Swanson, S., McAllister, S., Alvarez, U., Wang, D., Dowdy, S.F., and Hruska, K.A. (2000) Rho-A is critical for osteoclast podosome organization, motility, and bone resorption. *The Journal of biological chemistry*. **275**, 11993-12002

(43) Bhadriraju, K., Yang, M., Alom Ruiz, S., Pirone, D., Tan, J., and Chen, C.S. (2007) Activation of ROCK by RhoA is regulated by cell adhesion, shape, and cytoskeletal tension. *Experimental cell research*. **313**, 3616-3623

(44) Del Fattore, A., Teti, A., and Rucci, N. (2008) Osteoclast receptors and signaling. *Archives of biochemistry and biophysics*. **473**, 147-160

(45) Nesbitt, S., Nesbit, A., Helfrich, M., and Horton, M. (1993) Biochemical characterization of human osteoclast integrins. Osteoclasts express alpha v beta 3, alpha 2 beta 1, and alpha v beta 1 integrins. *The Journal of biological chemistry*. **268**, 16737-16745

(46) Rao, H., Lu, G., Kajiya, H., Garcia-Palacios, V., Kurihara, N., Anderson, J., Patrene, K., Sheppard, D., Blair, H.C., Windle, J.J., Choi, S.J., and Roodman, G.D. (2006) Alpha9beta1: a novel osteoclast integrin that regulates osteoclast formation and function. *Journal of bone and mineral research : the official journal of the American Society for Bone and Mineral Research*. **21**, 1657-1665

(47) Teitelbaum, S.L. (2007) Osteoclasts: what do they do and how do they do it? *The American journal of pathology*. **170**, 427-435

(48) Spinardi, L., and Marchisio, P.C. (2006) Podosomes as smart regulators of cellular

adhesion. *European journal of cell biology*. **85**, 191-194

(49) Duong, L.T., Lakkakorpi, P., Nakamura, I., and Rodan, G.A. (2000) Integrins and signaling in osteoclast function. *Matrix biology : journal of the International Society for Matrix Biology*. **19**, 97-105

(50) Kagami, S., Urushihara, M., Kondo, S., Loster, K., Reutter, W., Tamaki, T., Yoshizumi, M., and Kuroda, Y. (2001) Requirement for tyrosine kinase-ERK1/2 signaling in alpha 1 beta 1 integrin-mediated collagen matrix remodeling by rat mesangial cells. *Experimental cell research*. **268**, 274-283

(51) Nagano, T., Oida, S., Ando, H., Gomi, K., Arai, T., and Fukae, M. (2003) Relative levels of mRNA encoding enamel proteins in enamel organ epithelia and odontoblasts. *Journal of dental research*. **82**, 982-986

(52) Hao, J., He, G., Narayanan, K., Zou, B., Lin, L., Muni, T., Ramachandran, A., and George, A. (2005) Identification of differentially expressed cDNA transcripts from a rat odontoblast cell line. *Bone*. **37**, 578-588

(53) Spahr, A., Lyngstadaas, S.P., Slaby, I., and Pezeshki, G. (2006) Ameloblastin expression during craniofacial bone formation in rats. *European journal of oral sciences*. **114**, 504-511

(54) Nunez, J., Sanz, M., Hoz-Rodriguez, L., Zeichner-David, M., and Arzate, H. (2010) Human cementoblasts express enamel-associated molecules in vitro and in vivo. *Journal of periodontal research*. **45**, 809-814

(55) Hasegawa, N., Kawaguchi, H., Ogawa, T., Uchida, T., and Kurihara, H. (2003) Immunohistochemical characteristics of epithelial cell rests of Malassez during cementum repair. *Journal of periodontal research*. **38**, 51-56

(56) Kitagawa, M., Kitagawa, S., Nagasaki, A., Miyauchi, M., Uchida, T., and Takata, T. (2011) Synthetic ameloblastin peptide stimulates differentiation of human periodontal ligament cells. *Archives of oral biology*. **56**, 374-379

(57) Tamburstuen, M.V., Reseland, J.E., Spahr, A., Brookes, S.J., Kvalheim, G., Slaby, I., Snead, M.L., and Lyngstadaas, S.P. (2011) Ameloblastin expression and putative autoregulation in mesenchymal cells suggest a role in early bone formation and repair. *Bone*. **48**, 406-413

(58) Zeichner-David, M., Oishi, K., Su, Z., Zakartchenko, V., Chen, L.S., Arzate, H., and Bringas, P., Jr. (2003) Role of Hertwig's epithelial root sheath cells in tooth root development. *Developmental dynamics : an official publication of the American Association of Anatomists*. **228**, 651-663

(59) Hirose, N., Shimazu, A., Watanabe, M., Tanimoto, K., Koyota, S., Sugiyama, T., Uchida,

T., and Tanne, K. (2013) Ameloblastin in Hertwig's epithelial root sheath regulates tooth root formation and development. *PloS one*. **8**, e54449

(60) Fukumoto, S., Kiba, T., Hall, B., Iehara, N., Nakamura, T., Longenecker, G., Krebsbach, P.H., Nanci, A., Kulkarni, A.B., and Yamada, Y. (2004) Ameloblastin is a cell adhesion molecule required for maintaining the differentiation state of ameloblasts. *The Journal of cell biology*. **167**, 973-983

(61) Zhang, Y., Zhang, X., Lu, X., Atsawasuwan, P., and Luan, X. (2011) Ameloblastin regulates cell attachment and proliferation through RhoA and p27. *European journal of oral sciences*. **119 Suppl 1**, 280-285

(62) Staatz, W.D., Fok, K.F., Zutter, M.M., Adams, S.P., Rodriguez, B.A., and Santoro, S.A. (1991) Identification of a tetrapeptide recognition sequence for the alpha 2 beta 1 integrin in collagen. *The Journal of biological chemistry*. **266**, 7363-7367

(63) Yamada, Y., and Kleinman, H.K. (1992) Functional domains of cell adhesion molecules. *Current opinion in cell biology*. **4**, 819-823

(64) Sonoda, A., Iwamoto, T., Nakamura, T., Fukumoto, E., Yoshizaki, K., Yamada, A., Arakaki, M., Harada, H., Nonaka, K., Nakamura, S., Yamada, Y., and Fukumoto, S. (2009) Critical role of heparin binding domains of ameloblastin for dental epithelium cell adhesion and ameloblastoma proliferation. *The Journal of biological chemistry*. **284**, 27176-27184

(65) Beyeler, M., Schild, C., Lutz, R., Chiquet, M., and Trueb, B. (2010) Identification of a fibronectin interaction site in the extracellular matrix protein ameloblastin. *Experimental cell research*. **316**, 1202-1212

(66) Iizuka, S., Kudo, Y., Yoshida, M., Tsunematsu, T., Yoshiko, Y., Uchida, T., Ogawa, I., Miyauchi, M., and Takata, T. (2011) Ameloblastin regulates osteogenic differentiation by inhibiting Src kinase via cross talk between integrin beta1 and CD63. *Molecular and cellular biology*. **31**, 783-792

(67) Karsenty, G. (2003) The complexities of skeletal biology. *Nature*. **423**, 316-318

(68) Thorogood, P.V., and Hinchliffe, J.R. (1975) An analysis of the condensation process during chondrogenesis in the embryonic chick hind limb. *Journal of embryology and experimental morphology*. **33**, 581-606

(69) Bruder, S.P., and Caplan, A.I. (1989) Cellular and molecular events during embryonic bone development. *Connective tissue research*. **20**, 65-71

(70) Lian, J.B., and Stein, G.S. (1992) Concepts of osteoblast growth and differentiation: basis for modulation of bone cell development and tissue formation. *Critical reviews in oral biology and medicine : an official publication of the American Association of Oral*

Biologists. **3**, 269-305

(71) Long, F., and Ornitz, D.M. (2013) Development of the endochondral skeleton. *Cold Spring Harbor perspectives in biology*. **5**, a008334

(72) Kronenberg, H.M. (2003) Developmental regulation of the growth plate. *Nature*. **423**, 332-336

(73) Bianco, P., Cao, X., Frenette, P.S., Mao, J.J., Robey, P.G., Simmons, P.J., and Wang, C.Y. (2013) The meaning, the sense and the significance: translating the science of mesenchymal stem cells into medicine. *Nature medicine*. **19**, 35-42

(74) Phinney, D.G. (2012) Functional heterogeneity of mesenchymal stem cells: implications for cell therapy. *Journal of cellular biochemistry*. **113**, 2806-2812

(75) Deng, Z.L., Sharff, K.A., Tang, N., Song, W.X., Luo, J., Luo, X., Chen, J., Bennett, E., Reid, R., Manning, D., Xue, A., Montag, A.G., Luu, H.H., Haydon, R.C., and He, T.C. (2008) Regulation of osteogenic differentiation during skeletal development. *Frontiers in bioscience : a journal and virtual library*. **13**, 2001-2021

(76) Ducy, P., Zhang, R., Geoffroy, V., Ridall, A.L., and Karsenty, G. (1997) Osf2/Cbfa1: a transcriptional activator of osteoblast differentiation. *Cell*. **89**, 747-754

(77) Komori, T. (2006) Regulation of osteoblast differentiation by transcription factors. *Journal of cellular biochemistry*. **99**, 1233-1239

(78) Komori, T., Yagi, H., Nomura, S., Yamaguchi, A., Sasaki, K., Deguchi, K., Shimizu, Y., Bronson, R.T., Gao, Y.H., Inada, M., Sato, M., Okamoto, R., Kitamura, Y., Yoshiki, S., and Kishimoto, T. (1997) Targeted disruption of Cbfa1 results in a complete lack of bone formation owing to maturational arrest of osteoblasts. *Cell*. **89**, 755-764

(79) Mundlos, S., Otto, F., Mundlos, C., Mulliken, J.B., Aylsworth, A.S., Albright, S., Lindhout, D., Cole, W.G., Henn, W., Knoll, J.H., Owen, M.J., Mertelsmann, R., Zabel, B.U., and Olsen, B.R. (1997) Mutations involving the transcription factor CBFA1 cause cleidocranial dysplasia. *Cell*. **89**, 773-779

(80) Otto, F., Thornell, A.P., Crompton, T., Denzel, A., Gilmour, K.C., Rosewell, I.R., Stamp, G.W., Beddington, R.S., Mundlos, S., Olsen, B.R., Selby, P.B., and Owen, M.J. (1997) Cbfa1, a candidate gene for cleidocranial dysplasia syndrome, is essential for osteoblast differentiation and bone development. *Cell*. **89**, 765-771

(81) Otto, F., Kanegane, H., and Mundlos, S. (2002) Mutations in the RUNX2 gene in patients with cleidocranial dysplasia. *Human mutation*. **19**, 209-216

(82) Nakashima, K., Zhou, X., Kunkel, G., Zhang, Z., Deng, J.M., Behringer, R.R., and de Crombrugghe, B. (2002) The novel zinc finger-containing transcription factor osterix is

required for osteoblast differentiation and bone formation. *Cell*. **108**, 17-29

(83) Zhou, X., Zhang, Z., Feng, J.Q., Dusevich, V.M., Sinha, K., Zhang, H., Darnay, B.G., and de Crombrugghe, B. (2010) Multiple functions of Osterix are required for bone growth and homeostasis in postnatal mice. *Proceedings of the National Academy of Sciences of the United States of America*. **107**, 12919-12924

(84) Kurata, H., Guillot, P.V., Chan, J., and Fisk, N.M. (2007) Osterix induces osteogenic gene expression but not differentiation in primary human fetal mesenchymal stem cells. *Tissue engineering*. **13**, 1513-1523

(85) Ma, L., Golden, S., Wu, L., and Maxson, R. (1996) The molecular basis of Boston-type craniosynostosis: the Pro148-->His mutation in the N-terminal arm of the MSX2 homeodomain stabilizes DNA binding without altering nucleotide sequence preferences. *Human molecular genetics*. **5**, 1915-1920

(86) Sabatakos, G., Sims, N.A., Chen, J., Aoki, K., Kelz, M.B., Amling, M., Bouali, Y., Mukhopadhyay, K., Ford, K., Nestler, E.J., and Baron, R. (2000) Overexpression of DeltaFosB transcription factor(s) increases bone formation and inhibits adipogenesis. *Nature medicine*. **6**, 985-990

(87) Satokata, I., Ma, L., Ohshima, H., Bei, M., Woo, I., Nishizawa, K., Maeda, T., Takano, Y., Uchiyama, M., Heaney, S., Peters, H., Tang, Z., Maxson, R., and Maas, R. (2000) Msx2 deficiency in mice causes pleiotropic defects in bone growth and ectodermal organ formation. *Nature genetics*. **24**, 391-395

(88) Cheng, S.L., Shao, J.S., Charlton-Kachigian, N., Loewy, A.P., and Towler, D.A. (2003) MSX2 promotes osteogenesis and suppresses adipogenic differentiation of multipotent mesenchymal progenitors. *The Journal of biological chemistry*. **278**, 45969-45977

(89) Dodig, M., Tadic, T., Kronenberg, M.S., Dacic, S., Liu, Y.H., Maxson, R., Rowe, D.W., and Lichtler, A.C. (1999) Ectopic Msx2 overexpression inhibits and Msx2 antisense stimulates calvarial osteoblast differentiation. *Developmental biology*. **209**, 298-307

(90) Cook, D., and Genever, P. (2013) Regulation of mesenchymal stem cell differentiation. *Advances in experimental medicine and biology*. **786**, 213-229

(91) Canalis, E. (2009) Growth factor control of bone mass. *Journal of cellular biochemistry*. **108**, 769-777

(92) Chen, G., Deng, C., and Li, Y.P. (2012) TGF-beta and BMP signaling in osteoblast differentiation and bone formation. *International journal of biological sciences*. **8**, 272-288

(93) Giuliani, N., Lisignoli, G., Magnani, M., Racano, C., Bolzoni, M., Dalla Palma, B., Spolzino, A., Manferdini, C., Abati, C., Toscani, D., Facchini, A., and Aversa, F. (2013)

New insights into osteogenic and chondrogenic differentiation of human bone marrow mesenchymal stem cells and their potential clinical applications for bone regeneration in pediatric orthopaedics. *Stem cells international*. **2013**, 312501

(94) Chen, D., Zhao, M., and Mundy, G.R. (2004) Bone morphogenetic proteins. *Growth factors*. **22**, 233-241

(95) Long, F. (2012) Building strong bones: molecular regulation of the osteoblast lineage. *Nature reviews. Molecular cell biology*. **13**, 27-38

(96) Bandyopadhyay, A., Tsuji, K., Cox, K., Harfe, B.D., Rosen, V., and Tabin, C.J. (2006) Genetic analysis of the roles of BMP2, BMP4, and BMP7 in limb patterning and skeletogenesis. *PLoS genetics*. **2**, e216

(97) Tsuji, K., Bandyopadhyay, A., Harfe, B.D., Cox, K., Kakar, S., Gerstenfeld, L., Einhorn, T., Tabin, C.J., and Rosen, V. (2006) BMP2 activity, although dispensable for bone formation, is required for the initiation of fracture healing. *Nature genetics*. **38**, 1424-1429

(98) Boon, M.R., van der Horst, G., van der Pluijm, G., Tamsma, J.T., Smit, J.W., and Rensen, P.C. (2011) Bone morphogenetic protein 7: a broad-spectrum growth factor with multiple target therapeutic potency. *Cytokine & growth factor reviews*. **22**, 221-229

(99) Giannoudis, P.V., and Tzioupis, C. (2005) Clinical applications of BMP-7: the UK perspective. *Injury*. **36 Suppl 3**, S47-50

(100) Westendorf, J.J., Kahler, R.A., and Schroeder, T.M. (2004) Wnt signaling in osteoblasts and bone diseases. *Gene*. **341**, 19-39

(101) Glass, D.A., 2nd, Bialek, P., Ahn, J.D., Starbuck, M., Patel, M.S., Clevers, H., Taketo, M.M., Long, F., McMahon, A.P., Lang, R.A., and Karsenty, G. (2005) Canonical Wnt signaling in differentiated osteoblasts controls osteoclast differentiation. *Developmental cell*. **8**, 751-764

(102) Holmen, S.L., Zylstra, C.R., Mukherjee, A., Sigler, R.E., Faugere, M.C., Bouxsein, M.L., Deng, L., Clemens, T.L., and Williams, B.O. (2005) Essential role of beta-catenin in postnatal bone acquisition. *The Journal of biological chemistry*. **280**, 21162-21168

(103) Mohan, S., and Kesavan, C. (2012) Role of insulin-like growth factor-1 in the regulation of skeletal growth. *Current osteoporosis reports*. **10**, 178-186

(104) Crane, J.L., and Cao, X. (2013) Function of matrix IGF-1 in coupling bone resorption and formation. *Journal of molecular medicine*.

(105) Giustina, A., Mazziotti, G., and Canalis, E. (2008) Growth hormone, insulin-like growth factors, and the skeleton. *Endocrine reviews*. **29**, 535-559

(106) Zhao, G., Monier-Faugere, M.C., Langub, M.C., Geng, Z., Nakayama, T., Pike, J.W., Chernausek, S.D., Rosen, C.J., Donahue, L.R., Malluche, H.H., Fagin, J.A., and Clemens, T.L. (2000) Targeted overexpression of insulin-like growth factor I to osteoblasts of transgenic mice: increased trabecular bone volume without increased osteoblast proliferation. *Endocrinology*. **141**, 2674-2682

(107) Liu, J.P., Baker, J., Perkins, A.S., Robertson, E.J., and Efstratiadis, A. (1993) Mice carrying null mutations of the genes encoding insulin-like growth factor I (Igf-1) and type 1 IGF receptor (Igf1r). *Cell*. **75**, 59-72

(108) Powell-Braxton, L., Hollingshead, P., Warburton, C., Dowd, M., Pitts-Meek, S., Dalton, D., Gillett, N., and Stewart, T.A. (1993) IGF-I is required for normal embryonic growth in mice. *Genes & development*. **7**, 2609-2617

(109) Woods, K.A., Camacho-Hubner, C., Savage, M.O., and Clark, A.J. (1996) Intrauterine growth retardation and postnatal growth failure associated with deletion of the insulin-like growth factor I gene. *The New England journal of medicine*. **335**, 1363-1367

(110) Lin, G.L., and Hankenson, K.D. (2011) Integration of BMP, Wnt, and notch signaling pathways in osteoblast differentiation. *Journal of cellular biochemistry*. **112**, 3491-3501

(111) Grandin, H.M., Gemperli, A.C., and Dard, M. (2012) Enamel matrix derivative: a review of cellular effects in vitro and a model of molecular arrangement and functioning. *Tissue engineering. Part B, Reviews*. **18**, 181-202

(112) Rathe, F., Junker, R., Chesnutt, B.M., and Jansen, J.A. (2009) The effect of enamel matrix derivative (Emdogain) on bone formation: a systematic review. *Tissue engineering. Part B, Reviews*. **15**, 215-224

(113) Sculean, A., Schwarz, F., Becker, J., and Brecx, M. (2007) The application of an enamel matrix protein derivative (Emdogain) in regenerative periodontal therapy: a review. *Medical principles and practice : international journal of the Kuwait University, Health Science Centre*. **16**, 167-180

(114) Fukae, M., Kanazashi, M., Nagano, T., Tanabe, T., Oida, S., and Gomi, K. (2006) Porcine sheath proteins show periodontal ligament regeneration activity. *European journal of oral sciences*. **114 Suppl 1**, 212-218; discussion 254-216, 381-212

(115) Kanazashi, M., Gomi, K., Nagano, T., Tanabe, T., Arai, T., and Fukae, M. (2006) The 17-kDa sheath protein in enamel proteins induces cementum regeneration in experimental cavities created in a buccal dehiscence model of dogs. *Journal of periodontal research*. **41**, 193-199

(116) Zeichner-David, M., Chen, L.S., Hsu, Z., Reyna, J., Caton, J., and Bringas, P. (2006) Amelogenin and ameloblastin show growth-factor like activity in periodontal ligament

cells. *European journal of oral sciences*. **114 Suppl 1**, 244-253; discussion 254-246, 381-242

(117) Vymetal, J., Slaby, I., Spahr, A., Vondrasek, J., and Lyngstadaas, S.P. (2008) Bioinformatic analysis and molecular modelling of human ameloblastin suggest a two-domain intrinsically unstructured calcium-binding protein. *European journal of oral sciences*. **116**, 124-134

(118) Dosztanyi, Z., Meszaros, B., and Simon, I. (2010) Bioinformatical approaches to characterize intrinsically disordered/unstructured proteins. *Briefings in bioinformatics*. **11**, 225-243

(119) Zhang, X., Diekwisch, T.G., and Luan, X. (2011) Structure and function of ameloblastin as an extracellular matrix protein: adhesion, calcium binding, and CD63 interaction in human and mouse. *European journal of oral sciences*. **119 Suppl 1**, 270-279

(120) Fong, C.D., Cerny, R., Hammarstrom, L., and Slaby, I. (1998) Sequential expression of an amelin gene in mesenchymal and epithelial cells during odontogenesis in rats. *European journal of oral sciences*. **106 Suppl 1**, 324-330

(121) Spahr, A., Lyngstadaas, S.P., Slaby, I., Haller, B., Boeckh, C., Tsoulfidou, F., and Hammarstrom, L. (2002) Expression of amelin and trauma-induced dentin formation. *Clinical oral investigations*. **6**, 51-57

(122) Atsawasuwan, P., Lu, X., Ito, Y., Chen, Y., Gopinathan, G., Evans, C.A., Kulkarni, A.B., Gibson, C.W., Luan, X., and Diekwisch, T.G. (2013) Expression and function of enamel-related gene products in calvarial development. *Journal of dental research*. **92**, 622-628

(123) Atsawasuwan, P., Lu, X., Ito, Y., Zhang, Y., Evans, C.A., and Luan, X. (2013) Ameloblastin inhibits cranial suture closure by modulating MSX2 expression and proliferation. *PloS one*. **8**, e52800

(124) Wazen, R.M., Moffatt, P., Zalzal, S.F., Yamada, Y., and Nanci, A. (2009) A mouse model expressing a truncated form of ameloblastin exhibits dental and junctional epithelium defects. *Matrix biology : journal of the International Society for Matrix Biology*. **28**, 292-303

(125) Tamburstuen, M.V., Reppe, S., Spahr, A., Sabetrasekh, R., Kvalheim, G., Slaby, I., Syversen, U., Lyngstadaas, S.P., and Reseland, J.E. (2010) Ameloblastin promotes bone growth by enhancing proliferation of progenitor cells and by stimulating immunoregulators. *European journal of oral sciences*. **118**, 451-459

(126) Tamburstuen, M.V., Snead, M.L., Reseland, J.E., Paine, M.L., and Lyngstadaas, S.P. (2011) Ameloblastin upstream region contains structural elements regulating transcriptional activity in a stromal cell line derived from bone marrow. *European journal of oral sciences*. **119 Suppl 1**, 286-292

(127) Bouxsein, M.L., Boyd, S.K., Christiansen, B.A., Guldberg, R.E., Jepsen, K.J., and Muller, R. (2010) Guidelines for assessment of bone microstructure in rodents using micro-computed tomography. *Journal of bone and mineral research : the official journal of the American Society for Bone and Mineral Research*. **25**, 1468-1486

(128) Ferguson, V.L., Ayers, R.A., Bateman, T.A., and Simske, S.J. (2003) Bone development and age-related bone loss in male C57BL/6J mice. *Bone*. **33**, 387-398

(129) Margolis, D.S., Kim, D., Szivek, J.A., Lai, L.W., and Lien, Y.H. (2006) Functionally improved bone in calbindin-D28k knockout mice. *Bone*. **39**, 477-484

(130) Zhu, H., Guo, Z.K., Jiang, X.X., Li, H., Wang, X.Y., Yao, H.Y., Zhang, Y., and Mao, N. (2010) A protocol for isolation and culture of mesenchymal stem cells from mouse compact bone. *Nature protocols*. **5**, 550-560

(131) Mi, M., Jin, H., Wang, B., Yukata, K., Sheu, T.J., Ke, Q.H., Tong, P., Im, H.J., Xiao, G., and Chen, D. (2013) Chondrocyte BMP2 signaling plays an essential role in bone fracture healing. *Gene*. **512**, 211-218

(132) Talic, N.F., Evans, C.A., Daniel, J.C., and Zaki, A.E. (2003) Proliferation of epithelial rests of Malassez during experimental tooth movement. *American journal of orthodontics and dentofacial orthopedics : official publication of the American Association of Orthodontists, its constituent societies, and the American Board of Orthodontics*. **123**, 527-533

(133) Lu, X., Ito, Y., Kulkarni, A., Gibson, C., Luan, X., and Diekwisch, T.G. (2011) Ameloblastin-rich enamel matrix favors short and randomly oriented apatite crystals. *European journal of oral sciences*. **119 Suppl 1**, 254-260

(134) Pullikuth, A.K., and Catling, A.D. (2010) Extracellular signal-regulated kinase promotes Rho-dependent focal adhesion formation by suppressing p190A RhoGAP. *Molecular and cellular biology*. **30**, 3233-3248

(135) Lakkakorpi, P.T., Wesolowski, G., Zimolo, Z., Rodan, G.A., and Rodan, S.B. (1997) Phosphatidylinositol 3-kinase association with the osteoclast cytoskeleton, and its involvement in osteoclast attachment and spreading. *Experimental cell research*. **237**, 296-306

(136) Martin, K.H., Slack, J.K., Boerner, S.A., Martin, C.C., and Parsons, J.T. (2002) Integrin connections map: to infinity and beyond. *Science*. **296**, 1652-1653

(137) Vielkind, S., Gallagher-Gambarelli, M., Gomez, M., Hinton, H.J., and Cantrell, D.A. (2005) Integrin regulation by RhoA in thymocytes. *Journal of immunology*. **175**, 350-357

(138) Prince, C.W., Oosawa, T., Butler, W.T., Tomana, M., Bhown, A.S., Bhown, M., and

Schrohenloher, R.E. (1987) Isolation, characterization, and biosynthesis of a phosphorylated glycoprotein from rat bone. *The Journal of biological chemistry*. **262**, 2900-2907

(139) Qin, C., Brunn, J.C., Cook, R.G., Orkiszewski, R.S., Malone, J.P., Veis, A., and Butler, W.T. (2003) Evidence for the proteolytic processing of dentin matrix protein 1. Identification and characterization of processed fragments and cleavage sites. *The Journal of biological chemistry*. **278**, 34700-34708

(140) Liu, J., Wang, X., Jin, Q., Jin, T., Chang, S., Zhang, Z., Czajka-Jakubowska, A., Giannobile, W.V., Nor, J.E., and Clarkson, B.H. (2012) The stimulation of adipose-derived stem cell differentiation and mineralization by ordered rod-like fluorapatite coatings. *Biomaterials*. **33**, 5036-5046

(141) Ferguson, C., Alpern, E., Miclau, T., and Helms, J.A. (1999) Does adult fracture repair recapitulate embryonic skeletal formation? *Mechanisms of development*. **87**, 57-66

(142) Claes, L., Recknagel, S., and Ignatius, A. (2012) Fracture healing under healthy and inflammatory conditions. *Nature reviews. Rheumatology*. **8**, 133-143

(143) Luan, X., Ito, Y., and Diekwisch, T.G. (2006) Evolution and development of Hertwig's epithelial root sheath. *Developmental dynamics : an official publication of the American Association of Anatomists*. **235**, 1167-1180

(144) Seitz, C.S., Lin, Q., Deng, H., and Khavari, P.A. (1998) Alterations in NF-kappaB function in transgenic epithelial tissue demonstrate a growth inhibitory role for NF-kappaB. *Proceedings of the National Academy of Sciences of the United States of America*. **95**, 2307-2312

(145) Diekwisch, T., David, S., Bringas, P., Jr., Santos, V., and Slavkin, H.C. (1993) Antisense inhibition of AMEL translation demonstrates supramolecular controls for enamel HAP crystal growth during embryonic mouse molar development. *Development*. **117**, 471-482

(146) Diekwisch, T.G., Jin, T., Wang, X., Ito, Y., Schmidt, M., Druzinsky, R., Yamane, A., and Luan, X. (2009) Amelogenin evolution and tetrapod enamel structure. *Frontiers of oral biology*. **13**, 74-79

(147) Fincham, A.G., Moradian-Oldak, J., Diekwisch, T.G., Lyaruu, D.M., Wright, J.T., Bringas, P., Jr., and Slavkin, H.C. (1995) Evidence for amelogenin "nanospheres" as functional components of secretory-stage enamel matrix. *Journal of structural biology*. **115**, 50-59

(148) Yang, X., Wang, L., Qin, Y., Sun, Z., Henneman, Z.J., Moradian-Oldak, J., and Nancollas, G.H. (2010) How amelogenin orchestrates the organization of hierarchical elongated microstructures of apatite. *The journal of physical chemistry. B*. **114**, 2293-2300

(149) Herold, R., Rosenbloom, J., and Granovsky, M. (1989) Phylogenetic distribution of enamel proteins: immunohistochemical localization with monoclonal antibodies indicates the evolutionary appearance of enamelins prior to amelogenins. *Calcified tissue international*. **45**, 88-94

(150) Satchell, P.G., Anderton, X., Ryu, O.H., Luan, X., Ortega, A.J., Opamen, R., Berman, B.J., Witherspoon, D.E., Gutmann, J.L., Yamane, A., Zeichner-David, M., Simmer, J.P., Shuler, C.F., and Diekwisch, T.G. (2002) Conservation and variation in enamel protein distribution during vertebrate tooth development. *The Journal of experimental zoology*. **294**, 91-106

(151) Wang, X., Fan, J.L., Ito, Y., Luan, X., and Diekwisch, T.G. (2006) Identification and characterization of a squamate reptilian amelogenin gene: Iguana iguana. *Journal of experimental zoology. Part B, Molecular and developmental evolution*. **306**, 393-406

(152) Osborn, J.W. (1970) The mechanism of prism formation in teeth: a hypothesis. *Calcified tissue research*. **5**, 115-132

(153) Ajay Kishore Mathur, P.D.P. (Mar 2000) The Evolution of Enamel Microstructure: How Important Is Amelogenin? *Journal of Mammalian Evolution*. **Volume 7**, pp 23-42

(154) Hanaizumi, Y., Yokota, R., Domon, T., Wakita, M., and Kozawa, Y. (2010) The initial process of enamel prism arrangement and its relation to the Hunter-Schreger bands in dog teeth. *Archives of histology and cytology*. **73**, 23-36

(155) Hamamoto, Y., Nakajima, T., and Ozawa, H. (1989) Ultrastructural and histochemical study on the morphogenesis of epithelial rests of Malassez. *Archives of histology and cytology*. **52**, 61-70

(156) Fujii, D.K., Massoglia, S.L., Savion, N., and Gospodarowicz, D. (1982) Neurite outgrowth and protein synthesis by PC12 cells as a function of substratum and nerve growth factor. *The Journal of neuroscience : the official journal of the Society for Neuroscience*. **2**, 1157-1175

(157) Kleinman, H.K., Luckenbill-Edds, L., Cannon, F.W., and Sephel, G.C. (1987) Use of extracellular matrix components for cell culture. *Analytical biochemistry*. **166**, 1-13

(158) Cooke, M.J., Phillips, S.R., Shah, D.S., Athey, D., Lakey, J.H., and Przyborski, S.A. (2008) Enhanced cell attachment using a novel cell culture surface presenting functional domains from extracellular matrix proteins. *Cytotechnology*. **56**, 71-79

(159) Fong, C.D., Slaby, I., and Hammarstrom, L. (1996) Amelin: an enamel-related protein, transcribed in the cells of epithelial root sheath. *Journal of bone and mineral research : the official journal of the American Society for Bone and Mineral Research*. **11**, 892-898

(160) Begue-Kirn, C., Krebsbach, P.H., Bartlett, J.D., and Butler, W.T. (1998) Dentin

sialoprotein, dentin phosphoprotein, enamelysin and ameloblastin: tooth-specific molecules that are distinctively expressed during murine dental differentiation. *European journal of oral sciences*. **106**, 963-970

(161) Lee, S.K., Krebsbach, P.H., Matsuki, Y., Nanci, A., Yamada, K.M., and Yamada, Y. (1996) Ameloblastin expression in rat incisors and human tooth germs. *The International journal of developmental biology*. **40**, 1141-1150

(162) Lee, S.K., Kim, S.M., Lee, Y.J., Yamada, K.M., Yamada, Y., and Chi, J.G. (2003) The structure of the rat ameloblastin gene and its expression in amelogenesis. *Molecules and cells*. **15**, 216-225

(163) Kakegawa, A., Oida, S., Gomi, K., Nagano, T., Yamakoshi, Y., Fukui, T., Kanazashi, M., Arai, T., and Fukae, M. (2010) Cytodifferentiation activity of synthetic human enamel sheath protein peptides. *Journal of periodontal research*. **45**, 643-649

(164) McHugh, K.P., Hodivala-Dilke, K., Zheng, M.H., Namba, N., Lam, J., Novack, D., Feng, X., Ross, F.P., Hynes, R.O., and Teitelbaum, S.L. (2000) Mice lacking beta3 integrins are osteosclerotic because of dysfunctional osteoclasts. *The Journal of clinical investigation*. **105**, 433-440

(165) Inoue, M., Namba, N., Chappel, J., Teitelbaum, S.L., and Ross, F.P. (1998) Granulocyte macrophage-colony stimulating factor reciprocally regulates alphav-associated integrins on murine osteoclast precursors. *Molecular endocrinology*. **12**, 1955-1962

(166) Clark, E.A., and Brugge, J.S. (1995) Integrins and signal transduction pathways: the road taken. *Science*. **268**, 233-239

(167) Howe, A.K., and Juliano, R.L. (1998) Distinct mechanisms mediate the initial and sustained phases of integrin-mediated activation of the Raf/MEK/mitogen-activated protein kinase cascade. *The Journal of biological chemistry*. **273**, 27268-27274

(168) Blair, H.C., Robinson, L.J., and Zaidi, M. (2005) Osteoclast signalling pathways. *Biochemical and biophysical research communications*. **328**, 728-738

(169) Feng, X. (2005) RANKing intracellular signaling in osteoclasts. *IUBMB life*. **57**, 389-395

(170) Zhao, Q., Wang, X., Liu, Y., He, A., and Jia, R. (2010) NFATc1: functions in osteoclasts. *The international journal of biochemistry & cell biology*. **42**, 576-579

(171) Emons, J., Chagin, A.S., Savendahl, L., Karperien, M., and Wit, J.M. (2011) Mechanisms of growth plate maturation and epiphyseal fusion. *Hormone research in paediatrics*. **75**, 383-391

(172) Karp, S.J., Schipani, E., St-Jacques, B., Hunzelman, J., Kronenberg, H., and McMahon, A.P. (2000) Indian hedgehog coordinates endochondral bone growth and morphogenesis

via parathyroid hormone related-protein-dependent and -independent pathways. *Development*. **127**, 543-548

(173) van der Eerden, B.C., Karperien, M., Gevers, E.F., Lowik, C.W., and Wit, J.M. (2000) Expression of Indian hedgehog, parathyroid hormone-related protein, and their receptors in the postnatal growth plate of the rat: evidence for a locally acting growth restraining feedback loop after birth. *Journal of bone and mineral research : the official journal of the American Society for Bone and Mineral Research*. **15**, 1045-1055

(174) Long, F., Zhang, X.M., Karp, S., Yang, Y., and McMahon, A.P. (2001) Genetic manipulation of hedgehog signaling in the endochondral skeleton reveals a direct role in the regulation of chondrocyte proliferation. *Development*. **128**, 5099-5108

(175) Mora, S., Cafarelli, L., Erba, P., Puzzovio, M., Zamproni, I., Giacomet, V., and Vigano, A. (2009) Differential effect of age, gender and puberty on bone formation rate assessed by measurement of bone-specific alkaline phosphatase in healthy Italian children and adolescents. *Journal of bone and mineral metabolism*. **27**, 721-726

(176) Garnero, P., and Delmas, P.D. (1993) Assessment of the serum levels of bone alkaline phosphatase with a new immunoradiometric assay in patients with metabolic bone disease. *The Journal of clinical endocrinology and metabolism*. **77**, 1046-1053

(177) Liu, W., Toyosawa, S., Furuichi, T., Kanatani, N., Yoshida, C., Liu, Y., Himeno, M., Narai, S., Yamaguchi, A., and Komori, T. (2001) Overexpression of Cbfa1 in osteoblasts inhibits osteoblast maturation and causes osteopenia with multiple fractures. *The Journal of cell biology*. **155**, 157-166

(178) Lu, X., Ito, Y., Atsawasuwan, P., Dangaria, S., Yan, X., Wu, T., Evans, C.A., and Luan, X. (2013) Ameloblastin modulates osteoclastogenesis through the integrin/ERK pathway. *Bone*. **54**, 157-168

(179) Seck, T., Scheppach, B., Scharla, S., Diel, I., Blum, W.F., Bismar, H., Schmid, G., Krempien, B., Ziegler, R., and Pfeilschifter, J. (1998) Concentration of insulin-like growth factor (IGF)-I and -II in iliac crest bone matrix from pre- and postmenopausal women: relationship to age, menopause, bone turnover, bone volume, and circulating IGFs. *The Journal of clinical endocrinology and metabolism*. **83**, 2331-2337

(180) Bikle, D.D., and Wang, Y. (2012) Insulin like growth factor-I: a critical mediator of the skeletal response to parathyroid hormone. *Current molecular pharmacology*. **5**, 135-142

(181) Hill, P.A., Tumber, A., and Meikle, M.C. (1997) Multiple extracellular signals promote osteoblast survival and apoptosis. *Endocrinology*. **138**, 3849-3858

(182) Wang, J., Zhou, J., and Bondy, C.A. (1999) Igf1 promotes longitudinal bone growth by insulin-like actions augmenting chondrocyte hypertrophy. *FASEB journal : official publication of the Federation of American Societies for Experimental Biology*. **13**, 1985-

1990

(183) Li, X., and Cao, X. (2006) BMP signaling and skeletogenesis. *Annals of the New York Academy of Sciences*. **1068**, 26-40

(184) Nauth, A., Ristiniemi, J., McKee, M.D., and Schemitsch, E.H. (2009) Bone morphogenetic proteins in open fractures: past, present, and future. *Injury*. **40 Suppl 3**, S27-31

VI. VITA

PERSONAL INFORMATION

Name: Xuanyu Lu

Citizenship: P.R. China

EDUCATION

2009.8 – 2013.12 **Doctor of Philosophy, Oral Science**

University of Illinois at Chicago, College of Dentistry, Chicago, US

Advisor: Xianghong Luan

2007.7 - 2009.6 **Master of Stomatology, Oral Pathology**

Jilin University, School of Stomatology, Changchun, China

Advisor: Hongchen Sun

2002.9 - 2007.6 **Bachelor of Dentistry Surgery**

Jilin University, School of Stomatology, Changchun, China

RESEARCH EXPERIENCE

2009.8 –2013.12 **GraduateResearch Assistant,**

Brodie Laboratory for Craniofacial Genetics

University of Illinois at Chicago, Collage of Dentistry, Chicago,US

2007.12- 2009.7 **Graduate Researcher,**

Oral Biomedical Engineering Laboratory of Jilin Province

Jilin University, School of Stomatology, Changchun, China

2005.6- 2005.12 **Intership Researcher,**

Laboratory of Cellular Biology

Jilin University, Norman Bethune College of Medicine, Changchun, China

CLINIC EXPERIENCE

2007.5- 2008.6 **Internship, General Dentistry**

Jilin University, TheStomatological hospital of Jilin University, Changchun, China

2006.6 - 2006.10 **Internship, General Medicine**

Jilin University, The Second Hospital of Jilin University, Changchun

PROFESSIONAL MEMBERSHIP

2012-present Member, The American Society for Bone and Mineral Research (ASBMR)

2011-present Member, The International and American Association for Dental Research (IADR/AADR)

2008-present Member, The Chinese Stomatological Association (CSA)

PUBLICATIONS

(1) Atsawasuwan, P., Lu, X., Ito, Y., Chen, Y., Gopinathan, G., Evans, C. A., Kulkarni, A.B., Gibson, C.W., Luan, X., Diekwisch, T.G..(2013) Expression and Function of Enamel-related Gene Products in Calvarial Development. *Journal of Dental Research*. **92**, 622-628.

(2) Lu, X., Ito,Y., Atsawasuwan, P., Dangaria, S., Yan, X., Wu, T., Evans, C.A., Luan, X. (2013)Ameloblastin Modulates Osteoclastogenesis Through the Integrin/ERK Pathway. *Bone*.**54**, 157-68.

(3) Pan, S., Dangaria, S., Gopinathan, G., Yan, X., Lu, X., Kolokythas, A., Niu, Y., Luan,X..(2013) SCF Promotes Dental Pulp Progenitor Migration, Neovascularization, and Collagen Remodeling-potential Applications as a Homing Factor in Dental Pulp Regeneration. *Stem Cell Reviews and Reports*.**9**, 655-67.

(4) Atsawasuwan, P., Lu, X., Ito, Y., Zhang, Y., Evans, C.A., and Luan, X. (2013) Ameloblastin inhibits cranial suture closure by modulating MSX2 expression and proliferation. *PloS one*. **8**, e52800

(5) Lu, X., Ito, Y., Kulkarni, A., Gibson, C., Luan, X., Diekwisch,T.G.. Ameloblastin-rich Enamel Matrix Favors Short and Randomly Oriented Apatite Crystals. *European Journal of Oral Science*. 2011 Dec; **119 Suppl 1**:254-60.

(6) Zhang, Y., Zhang, X., Lu, X., Atsawasuwan, P., Luan, X..(2011) Ameloblastin Regulates Cell Attachment and Proliferation ThroughRhoA and p27. *European Journal of Oral Science.***119 Suppl 1**, 280-285.

(7) Yu, L., Sun, H., Shen, Y., Lu, X..(2009) Study the Osteogenic Effect of TWEAK Gene on Rats Bone Marrow Mesenchymal Stem Cells Induced by Adenovirus. *Journal of Oral Science*. **25**, 12-15. In Chinese.